T H E U N I V E R S I T Y O F M I C H I G A N

COLLEGE OF ENGINEERING
Department of Mechanical Engineering

Technical Report No. 6

FILM BOILING ON VERTICAL SURFACES IN TURBULENT REGIME

Narasipur V. Suryanarayana

Herman Merte, Jr.
Project Supervisor

ORA Project 07461

under contract with:

NATIONAL AERONAUTICS AND SPACE ADMINISTRATION
GEORGE C. MARSHALL SPACE FLIGHT CENTER
CONTRACT NO. NAS-8-20228
HUNTSVILLE, ALABAMA

administered through:

OFFICE OF RESEARCH ADMINISTRATION ANN ARBOR

September 1970

TABLE OF CONTENTS

TABLE OF CONTENTS (Continued)

TABLE OF CONTENTS (Concluded

LIST OF TABLES

LIST OF FIGURES

LIST OF FIGURES (Continued)

LIST OF FIGURES (Concluded)

NOMENCLATURE

Normal units used are indicated; when other units are used, they are indicated as such in the text.

A	area, ft^2
a	amplitude of interfacial oscillations, ft
b	amplitude of interfacial oscillations = $a/\delta(s)$, dimensionless
C	heat transfer enhancement coefficient Eq. (5.5a)
C_p	specific heat, Btu/lbm °R
g	gravitational acceleration, ft/sec^2
h_{fg}	enthalpy of vaporization, Btu/lbm
h_{fg}'	modified enthalpy of vaporization, Btu/lbm
h	heat transfer coefficient, Btu/hr ft^2 °R
h_x	local heat transfer coefficient at height x, Btu/hr ft^2 °R
h_L	average heat transfer coefficient over height L, Btu/hr ft^2 °R
k	thermal conductivity, Btu/hr ft °R
k	wave number
L	height of heating surface, ft
m	mass, lbm
Nu_x	local Nusselt number, dimensionless
Nu_L	average Nusselt number, dimensionless
P	pressure, psi
Pr	Prandtl number, dimensionless

q	heat transfer rate, Btu/hr
q'	heat flux = q/A, Btu/hr ft^2
Re	Reynolds number, dimensionless
T	vapor temperature, °R
T_w	heater surface temperature, °R
T_s	liquid saturation temperature, °R
t	time, hr
u	velocity, ft/hr
u^*	friction velocity = $\sqrt{\tau_w/\rho}$, ft/hr
u^+	velocity = u/u^* dimensionless
v	velocity, ft/hr
x	height along heater surface, ft
y	distance perpendicular to heater surface, ft
y^+	distance = yu^*/ν, dimensionless
α	thermal diffusivity, ft^2/hr
Γ	mass rate of flow, lbm/hr
δ	vapor film thickness, ft
ΔT	surface superheat = $T_w - T_s$, °R
η	vapor film thickness = y/δ, dimensionless
θ	temperature = $T/\Delta T$, dimensionless
θ^+	$\frac{\rho c u^*(T_w - T)}{q'}$, dimensionless
λ	wavelength, ft
μ	viscosity, lbm/hr ft

ν	kinematic viscosity μ/ρ, ft^2/hr
ρ	density, lbm/ft^3
σ	surface tension, lbf/ft
τ	shear stress, lbf/ft^2
Φ	velocity u/u_{max}, dimensionless
Φ	temperature $(T_w-T)/\Delta T$, dimensionless

In general the following subscripts are used. When there is no subscript, the quantities refer to the vapor.

ℓ	liquid
s	saturation
v	vapor
w	heater surface

ABSTRACT

The purpose of this study was to (1) determine the local heat flux values in film boiling in a saturated liquid on a plane vertical surface in the turbulent regime, (ii) extend the region of laminar vapor flow through the use of a drop tower, (iii) gain an understanding of the nature and influence of liquid-vapor interfacial oscillations on heat transfer rates, and (iv) model and analyze the phenomenon of film boiling on a vertical surface to predict heat transfer rates as a function of height and surface superheat.

The variables studied in the determination of the local heat flux values were the height of the heating surface and heater surface superheat in two cryogenic liquids, nitrogen, and hydrogen. To avoid edge effects in a finite plane vertical surface, cylindrical heating surfaces were used. Heat flux values at 11 locations over a total height of 6 in. at four values of surface superheat were determined, employing a transient technique. A warm cylindrical heating surface with thermally insulated instrumented sections was immersed in the cryogenic fluid, inducing film boiling, and the rate of cooling was recorded. From this rate of cooling and properties of the test sections, heat transfer rates were computed.

The region of laminar vapor film was extended by reducing gravity forces in a drop tower. Local heat flux values at six locations in a height of 4 in. were determined for one value of surface superheat each in liquid nitrogen and liquid hydrogen at $a/g \cong 0.008$. Additional heat flux values were obtained under subcooled conditions.

Motion pictures of film boiling on a vertical cylindrical surface in liquid nitrogen were taken at four different heights of the surface and three values of surface superheat. Analyses of these motion pictures indicating the variation of vapor film thickness as a function of time, and the extent of interfacial oscillations, are presented.

Film boiling was modelled on the assumption that the universal velocity profile of Spalding is valid everywhere in the vapor region. It is shown that interfacial oscillations increase heat transfer rates and the effect of such increase is taken into account in the solution of the resulting equations. Solutions are presented based on the effect of such oscillations being constant at all heights and also considering the variation of the extent of interfacial oscillations.

The data presented show an initial decrease in the heat flux with height and a gradual increase after reaching a minimum value. These experimental values show considerable deviation, both quantitatively and qualitatively, from the laminar analysis predictions of heat transfer rates. These departures are explained on the basis of onset of turbulence and interfacial oscillations. The solution to the set of equations taking these effects into account are shown to predict heat transfer rates within $\pm$ 15% in the turbulent regime. The heat transfer rates under reduced gravity forces show the same behavior as laminar predictions but are consistently higher.

CHAPTER I

INTRODUCTION

A. Purpose and Scope

Boiling has been known for centuries, but it is only in the past few decades that serious studies are being made to understand this phenomenon.

Surface boiling is generally classified as nucleate boiling where the liquid surrounding the heating surface makes repeated contact with the surface. This is characterized by vapor bubbles emanating from the surface. In film boiling the heating surface is blanketed by a vapor film and, in general, no bubbles emanate from the surface. In the third regime—the transition regime—there is partial nucleate boiling and partial film boiling, both taking place alternately or simultaneously at different parts in the surface. This transition boiling is unstable for an imposed heat flux and either nucleate or film boiling is established.

Nucleate boiling is the more attractive mode of heat transfer in boiling as it is characterized by large rates of heat transfer (relative to film boiling) at low degrees of superheat of the heating surface. There exists an immense amount of literature on different aspects of nucleate boiling, both analytic and experimental.

While in the majority of applications, nucleate boiling is the desired mode, there are important applications, particularly with the increasing use of cryogenic fluids in space applications, where film boiling occurs. It occurs during cool down of cryogenic containers and in quenching of metals.

Failure of nuclear reactor fuel elements may also lead to film boiling. Thus there are some technically important areas where film boiling occurs but relatively little work has been done on this aspect of boiling. Most of the experimental data reported on film boiling are for small diameter horizontal tubes or spheres.

The purpose of the present study is to determine experimentally the local heat transfer rates in film boiling on a vertical surface. A transient technique is employed and local heat transfer rates are determined as a function of height and $\Delta T = (T_{wall}-T_{sat})$ in liquid nitrogen and liquid hydrogen. It was observed that most available correlations based on a laminar vapor film with a smooth interface predicted heat transfer rates which were much too low, particularly with increasing height. Visual observation of film boiling indicated that the interface was far from being steady and had oscillations of considerable amplitude. To obtain data on the nature of the interface and the vapor film thickness, motion pictures are taken with a high-speed camera. Although predictions based on a laminar vapor film are found to be too low, it may be expected that there is some region near the leading edge where the conditions of laminar vapor film with a steady interface are satisfied. In order to examine the validity of such an expectation, the region of validity of laminar flow is extended by reducing gravity forces in a drop tower and local heat transfer rates determined. Additional limited data are obtained on heat transfer rates in film boiling in subcooled liquid nitrogen and liquid hydrogen.

There are two aspects of film boiling which render modelling of the phenomenon difficult—the possible onset of turbulence in the vapor film and the oscillations at the liquid-vapor interface, both of which tend to increase the heat transfer rates compared with film boiling in laminar flow with a steady interface. Some researchers have attempted to define a parameter to characterize the transition from laminar to turbulent flow. However, there is no evidence to support the value of the parameter so used. Moreover, it is to be expected that such a transition is gradual and not sudden. In the present analysis, no attempt is made to define, in precise terms, the extent of the laminar region and any parameter to indicate transition to turbulence. Instead, the velocity field throughout the region is approximated by Spalding's universal velocity profile which gives a linear velocity distribution for thin films and a logarithmic velocity profile for thick films when it can be expected to be turbulent. With the assumption of unchanging temperature profile, it will be shown that any oscillations in the vapor-liquid interface will increase the average heat flux. From the motion pictures, it is established that considerable oscillations do exist and hence the heat transfer rates are higher than is expected for the case with a smooth, steady interface. The extent of such increase in heat transfer will be shown to be dependent on the ratio of the amplitude of oscillation to the mean vapor film thickness. No known method exists to predict the extent of such oscillations. However, two different approaches will be taken to find the value of the ratio of the heat transfer with interfacial oscillations so that with a steady interface, (1) an empirical one wherein the value of this ratio which best fits the experimental

data is used in the solution of equations obtained in the present analysis, and (2) a semi-empirical one whereby the value of this ratio is assumed to vary with the local Reynolds number and an attempt made to find this variation from the results of the photographic studies.

B. LITERATURE SURVEY

The phenomenon of film boiling on vertical surfaces is, in many respects, similar to that of film condensation and hence references to some of the works on condensation relevant to the present study are included.

Nusselt (1)* developed an expression for heat transfer in film condensation on vertical surfaces, assuming laminar flow of the condensate film. Neglecting the acceleration terms in the momentum equation and assuming zero shear stress at the condensate-vapor interface, he obtained a parabolic velocity distribution for the condensate film. Again neglecting the convective terms and conduction parallel to the surface in the energy equation, a linear temperature distribution was obtained; with these assumptions the following expressions for the local and average heat transfer coefficients were obtained.

$$h_x = \left[\frac{\rho_\ell^2 \, g \, h_{fg} \, k_\ell^3}{4\mu_\ell \, x \, (T_s - T_w)} \right]^{1/4} \tag{1.1}$$

$$h_L = 0.94 \left[\frac{\rho_\ell^2 \, g \, h_{fg} \, k_\ell^3}{\mu_\ell \, L \, (T_s - T_w)} \right]^{1/4} \tag{1.2}$$

*Numbers in parentheses refer to references in the Bibliography.

$$Nu_L = \frac{h_L L}{k_\ell} = 0.94 \left[\frac{\rho_\ell^2 \, g \, h_{fg} \, k_\ell^3 \, L^3}{\mu_\ell \, (T_s - T_w)} \right]^{1/4} \tag{1.3}$$

Rohsenow (2) improved Nusselt's model by considering the nonlinearity of temperature distribution but retaining the same flow model. The calculation is based on an iterative process and the expressions for the heat transfer coefficient differs from that given by Nusselt only in that the enthalpy of vaporization is corrected to

$$h_{fg}' = h_{fg} \left(1 + \frac{3}{8} \frac{C_p \, \Delta T}{h_{fg}} \right) \tag{1.4}$$

in the first iteration and to

$$h_{fg}'' = h_{fg}' \left[1 - \frac{1}{10} \frac{C_p \Delta T}{h_{fg}'} - 0.328 \left(\frac{C_p \Delta T}{h_{fg}'} \right)^2 \right] \tag{1.5}$$

in the second iteration process.

Sparrow and Gregg (3) further improved the solution by considering the acceleration and convective terms in the momentum and energy equations; the boundary layer equations are numerically solved after first reducing them to ordinary differential equations through similarity transformations; zero interfacial shear was assumed. Their results are in agreement with those of Rohsenow (2) and show that for $Pr_\ell > 1$, the effect of neglecting the acceleration terms is very small. However, the departure from Nusselt's solution becomes significant for $Pr_\ell < 0.003$ and values of the parameter $C_p \, \Delta T/h_{fg} > 0.001$. Koh (4) has given a solution to the condensate problem using integral methods; it is shown that this solution is within 5% of that obtained by solving the boundary layer

equations. Koh, Sparrow, and Hartnett (5) further improved the solutions by solving the boundary layer equations for both the condensate and the vapor with appropriate boundary conditions at the interface, viz., compatibility of u, v, and $\partial u/\partial y$ for both the liquid and the vapor at the interface. Similarity techniques reduce the set of nonlinear partial differential equations to ordinary differential equations, which are solved numerically. Results of the solution for the local Nusselt number are tabulated as a function of the parameters Pr_ℓ, $\left[(\rho\mu)_\ell/(\rho\mu)_v\right]^{1/2}$, and $C_p\Delta T/h_{fg}$. It is shown that (i) interfacial shear has almost no effect on heat transfer for $Pr_\ell > 10$, (ii) interfacial shear is important for liquid metals which have very low $Pr_\ell < 0.01$, and (iii) the heat transfer is relatively unaffected by the magnitude of the parameter $\left[(\rho\mu)_\ell/(\rho\mu)_v\right]^{1/2}$.

Bromley (6) assumed a model for laminar film boiling on vertical surfaces similar to that of Nusselt for condensation and obtained the following expressions for the average heat transfer coefficient

$$h_L = \text{const.} \left[\frac{k_v^2 \rho_v (\rho_\ell-\rho_v) g h_{fg}' C_p}{L(T_w-T_s) Pr}\right]^{1/4}, \qquad (1.6)$$

and

$$\frac{h_L L}{k_v} = \text{const.} \left[\frac{k_v^3 \rho_v(\rho_\ell-\rho_v) g h_{fg}' C_p L^3}{(T_w-T_s) Pr}\right]^{1/4}. \qquad (1.7)$$

The value of the constant depends on whether zero interfacial velocity or zero interfacial shear is assumed. Experimental data obtained from horizontal tubes were given in support of the hypothesized model. Agreement between the predictio

and experimental results is reasonably good for small diameters. Allowance for radiation effects were made. In a subsequent work Bromley (7) has given a derivation for the use of modified enthalpy of vaporization in the above equation. The modified enthalpy of vaporization is given as

$$h_{fg}' = h_{fg}\left[1 + 0.4\,\frac{C_p \Delta T}{h_{fg}}\right]^2 . \qquad (1.8)$$

Following the pattern of development of the film condensation problem, McFadden and Grosh (8) improved this solution by solving the boundary layer equations for the vapor , with the approximation of zero interfacial velocity. Koh (9) has shown that this approximation is satisfactory, for values of the parameter $\left[(\rho\mu)_v/(\rho\mu)_\ell\right]^{1/2} \ll 1$, which is satisfied under most conditions. Cess (10) solved the same problem by employing integral methods. Koh (9) treated it as a two-domain problem, applying the boundary layer equations to both the vapor film and the adjacent saturated liquid. The boundary conditions for velocity and shear stress for the two domains were matched at the liquid-vapor interface. Using similarity transformation, a set of ordinary differential equations were obtained and these were solved numerically to obtain the dimensionless velocity

$$u/\left[2\left\{\frac{g(\rho_\ell-\rho_v)x}{\rho_v}\right\}^{1/2}\right]$$

and dimensionless temperature $(T-T_s)/(T_w-T_s)$ for various values of the parameters $[(\rho\mu)_v/(\rho\mu)_\ell]^{1/2}$, $C_p\Delta T/h_{fg}$ and Pr. From the results of these calculations, it is concluded that (i) a decrease in the value of the parameter $[(\rho\mu)_v/(\rho\mu)_\ell]^{1/2}$ decreases the heat transfer rate. (ii) The assumption of zero interfacial velocity is valid for a fluid with small $[(\rho\mu)_v/(\rho\mu)_\ell]^{1/2}$. (iii) The effect of

vapor Prandtl number on heat transfer is small for thin vapor films but significant for thick films. Vapor film thickness is denoted by the parameter $C_p \Delta T/h_{fg}$. (iv) The heat transfer drops gradually to a minimum value and then rises again as $C_p \Delta T/h_{fg}$ increases. (v) The temperature profile is quite linear for a thin vapor film and the nonlinearity increases as the vapors film thickness increases.

The effect of a subcooled liquid with film boiling has been studied by several workers. Sparrow and Cess (11) employed the same techniques as Koh (9) in the solution of the boundary layer equations. However, they assumed zero interfacial velocity. This was subsequently improved by Nishikawa and Ito (12) who dropped the assumption of zero interfacial velocity and used matching boundary conditions at the interface. This solution and that given by Koh (9) are essentially similar, and the main difference is in the addition of one more energy equation for the subcooled liquid. The results show that with an increase in the degree of subcooling, the rate of heat transfer rises; the percentage increase of heat flux is greater for a lower degree of heater surface superheat. Frederking (13) approximates vapor and liquid velocity profiles and the vapor temperature profile with polynomials, employing integral methods to obtain the heat transfer rate. Similar methods have been employed by Frederking and Hopenfield (14) for the subcooled case. The effect of variable properties has been included in the analysis of McFadden and Grosh (15), who solved the boundary layer equation through similarity transformations. Tachibana and Fukui (16) have given a solution to film boiling in subcooled liquids using integral methods. Lubin (17) includes effects of radiation in his analysis.

It has been recognized (13) that laminar film boiling occurs rather infrequently as compared with turbulent film boiling. It occurs at leading edges, stagnation points and on small objects under normal conditions. The experimental data of Bromley (6) and others, obtained mainly for small horizontal diameter tubes, are sometimes used in support of analytical solutions. Where experimental data are available, these solutions do not show any significant improvement in the predictions over the solution of Bromley (6); where these solutions show noticeable departure from that of Bromley (6) no experimental data are available.

Merte and Clark (18) obtained experimental data for both the film and nucleate boiling in liquid nitrogen at standard and fractional gravity using 1 in. and 1/2 in. dia copper spheres. Rhea and Nevins (19) studied the effects of oscillations of a sphere in film boiling. Hendricks and Baumeister (20) have given an analytical solution for film boiling on submerged spheres.

Chang (21,22) has attempted to use the wave theory, to predict heat transfer rates in film boiling on horizontal and vertical surfaces. The concept of Taylor-Helmholtz instabilities has been applied to film boiling on a horizontal surface by Berenson (23). The effect of the diameter of horizontal tubes on film boiling heat transfer was studied by Breen and Westwater (24). From their experimental data they show that for a given ΔT, heat transfer rates rapidly decrease with increase in diameter, reach a minimum, then slowly increase with diameter. They also infer that this critical diameter (having the minimum heat flux) is independent of the ΔT. Hosler and Westwater (24) have applied Taylor instability approach to film boiling on horizontal plates.

Experimental studies of the effects of increasing gravity on film boiling on a horizontal tube have been reported by Pomerantz (26) who concludes that the film boiling mechanism for a horizontal tube is dependent on the ratio of the diameter to the critical wavelength, and reports nominal 1/3 power dependency of heat flux on local gravity. An analysis of laminar flow of film boiling from a horizontal wire has been given by Baumeister and Hamill (27). They conclude that the heat transfer coefficient is a function of gravitational acceleration to the 0.375 power for large wires and to the zero power for very small wires.

A number of other studies deal with particular aspects of film boiling, such as film boiling in a forced convection boundary layer flow by Cess and Sparrow (28), film boiling of liquid nitrogen from porous surfaces with vapor suction by Pai and Bankoff (29), film boiling of saturated nitrogen flowing in a vertical tube by Laverty and Rohsenow (30), slug flow and film boiling of hydrogen by Chi (31), effects of interfacial instability on film boiling of saturated liquid helium I above a horizontal surface by Frederking, Wu and Clement (32), radiation effects by Sparrow (33) and Yeh and Yang (34), stability of film boiling two-phase flow in cryogenic systems by Frederking (35).

From the above references, it is seen that there are a number of analyses for film boiling from vertical surfaces. However, there is very little or no data in support of such analyses. As has already been pointed out earlier, the phenomena of laminar film boiling with a smooth interface is rarely observed, and in the majority of cases the interface is oscillating and the

flow apparently not laminar. Considerable deviation has been observed between such predictions and experimental results. However, to date there appears to be very little reported work which takes into account the effects of turbulence and interfacial oscillations.

Rohsenow, Weber, and Ling (36) made a study of heat transfer coefficients for film condensation in the turbulent regime, hypothesizing that the onset of turbulence would occur at a given value of $4\Gamma/\mu$. McAdams (37) gives a critical Reynolds number of 1800 for the onset of turbulence, but much lower values of 200-300 have been reported. Using the following model, similar to the three-layer model of Karman-Martinelli-Boelter,

$$
\begin{aligned}
u^+ &= y^+ && 0 \le y^+ \le 5 \\
u^+ &= -3.05 + 5.0 \ln y^+ && 5 \le y^+ \le 30 \\
u^+ &= 5.5 + 2.5 \ln y^+ && 30 \le y^+ \le y_o^+
\end{aligned}
\qquad (1.9)
$$

$$
\text{with } u^+ = u/\sqrt{\tau_\omega/\rho_\ell}, \qquad y^+ = \frac{y\sqrt{\tau_\omega/\rho_\ell}}{\nu_\ell}
$$

y_o = liquid film thickness

and a transition criterion of $4\Gamma/\mu_\ell = 1800$ and assuming that the eddy diffusivities for momentum and heat are equal, Rohsenow (36) obtained

$$
\frac{(T_s - T_w)}{q'_w} \cdot \rho_\ell C_{p\ell} \sqrt{\frac{g(1-\rho_v/\rho_\ell)y_o}{M}} = F_2 . \qquad (1.10)
$$

Here F_2 is defined as,

For $y_o^+ < 30$,

$$F_2 = 5\,Pr_\ell + 5\ln(1 + 5\,Pr_\ell) + \frac{2.5}{\sqrt{1 + \frac{10M}{Pr_\ell y_o^+}}}$$

$$\ln\left[\frac{2M - 1 + \sqrt{1 + \frac{10M}{Pr_\ell y_o^+}}\;\frac{60M}{y_o^+} - 1 - \sqrt{1 + \frac{10M}{Pr_\ell y_o^+}}}{2M - 1 - \sqrt{1 + \frac{10M}{Pr_\ell y_o^+}}\;\frac{60M}{y_o^+} - 1 + \sqrt{1 + \frac{10M}{Pr_\ell y_o^+}}}\right] \qquad (1.11)$$

For $5 < y_o^+ < 30$ $\quad F_2 = 5\,Pr_\ell + 5\ln\left[1 + Pr_\ell\left(\frac{y_o^+}{5} - 1\right)\right]$

and $\quad M = 1/\left\{g_o\,\tau_v/g(\rho_\ell - \rho_v) + 1\right\}.$ (1.12)

Lee (38) took a slightly different approach. Using Diessler's expression for eddy viscosity (53), he assumed that the eddy thermal diffusivity is a constant multiple of eddy kinematic viscosity. Bradfield, Barkdoll, and Byrne (42) report some data on natural convection film boiling in liquid nitrogen on the surface of torpedo shaped body at a height of 2.69 in. These results are shown to agree within ± 32% of the prediction of Hsu and Westwater (39). However, no details are given as to how the local heat flux measurements were made, nor on the manner of isolating that section from adjoining parts of the body.

Hsu (39) reported analytical and experimental studies on turbulent film boiling on a vertical surface. He postulated a two-layer model which was essentially a simplified version of Karman's three-layer model referred to above with a viscous sublayer where $u^+ = y^+$ for $y^+ \leq 10$ and beyond this a uniform velocity in the turbulent core. The temperature profile was linear in the

viscous sublayer and uniform in the turbulent core. For the two-layer model it was assumed that $u^+ = y^+$ for $y^+ = 10$. Because of the relationship between u^+ and y^+ at the transition from viscous sublayer to turbulent core we have $(y^+)^2 = (y^+u^+) = uy/\nu$; then $(y^+)^2$ evaluated at $y^+ = 10$ is the local Reynolds number based on the maximum velocity and the sublayer thickness. It was hypothesized that, since the Reynolds number based on the sublayer thickness determines the boundary between the viscous sublayer and the turbulent core, using an arbitrary critical Reynolds number of 100, the flow would become turbulent when the Reynolds number formed by taking the maximum velocity and the film thickness in the laminar region, near the leading edge, became 100. With this assumption, a force balance was made on an element of turbulent core, taking into account the gravity forces, the shear forces on the sublayer and approximating the shear force at the interface by the use of a friction factor. As adequate data on such friction factors are not available values of friction factors for vapor-liquid interface for water and air given by Henratty and Engen (40) were used. Solution to the resulting momentum and energy equations give

$$\left(\frac{1}{y_s}\right)^2 = \frac{2}{3}\left(\frac{3A}{3B+1}\right)(x-L_o) + \left(\frac{1}{y^*}\right)^2 \tag{1.13}$$

$$A = \frac{g(\rho_\ell-\rho_v)}{\rho_v}\left(\frac{\overline{\rho_v}}{\mu_v Re^*}\right)^2 \tag{1.14}$$

$$B = \left(\mu_v + \frac{f\,\rho_v\mu_v\,Re^*}{2\,\overline{\rho_v}} + \frac{k_v\Delta T}{h_{fg}}\right)\Big/\left(\frac{k_v\Delta T}{h_{fg}}\right) \tag{1.15}$$

$$q' = \frac{k_v \Delta T}{y_s} \tag{1.16}$$

$$h_x = \frac{q'}{\Delta T} = \frac{k_v}{y_s} \tag{1.17}$$

The average heat transfer coefficient over the entire height of the heating surface is then obtained by integrating the local heat transfer coefficient, using Bromley's results for the laminar region. The resulting expression is

$$\frac{h_L L}{k_v} = \frac{2 h_{fg}' \mu_v Re^*}{3 k_v \Delta T} + \frac{B + 1/3}{A}\left[\left\{\frac{2A}{3(B + 1/3)}(L-L_o) + \left(\frac{1}{y^*}\right)^2\right\}^{3/2} - \left(\frac{1}{y^*}\right)^3\right] \tag{1.18}$$

Here L_o is the height over which laminar vapor film prevails. Experimental data were obtained using tubes of length from 2 in. to 6-1/4 in. and 1/2 in. O.D. to 3/4 in. O.D. in methenol, benzene, carbon tetrachloride, nitrogen, and argon. The data so obtained are shown to agree within ± 32% of the predicted values.

Borishansky and Fokin (41) arrived at the following expressions based on dimensional reasoning:

Film Thickness:

$$\delta = \text{const.} \frac{\sigma}{\rho_\ell - \rho_v} F\left[\frac{q'\mu}{h_{fg} \rho_v \sigma}\right] \tag{1.19}$$

using experimental results from other sources, a value of 31 was assigned to the constant in the above equation and the form of the function F as

$$F = \left[\frac{q'\mu}{h_{fg} \rho_v \sigma}\right]^{0.53} \tag{1.20}$$

Nusselt Number based on film thickness:

The following empirical expressions were given for the Nusselt number:

$$Nu_\delta = 0.28 \left[Ga_\delta \frac{\rho_\ell - \rho_v}{\rho_\ell} \right]^{0.33} \tag{1.21}$$

$$\text{for } 2 \times 10^4 < Ga_\delta \frac{\rho_\ell - \rho_v}{\rho_v} < 1.6 \times 10^6$$

and

$$Nu_\delta = 0.0094 \left[Ga_\delta \frac{\rho_\ell - \rho_v}{\rho_v} \right]^{0.57} \tag{1.22}$$

$$\text{for } 1.4 \times 10^6 < Ga_\delta \frac{\rho_\ell - \rho_v}{\rho_v} < 1.5 \times 10^7$$

where

$$Ga_\delta \frac{\rho_\ell - \rho_v}{\rho_\ell} = \frac{g\delta^3}{\nu_v^2} \frac{\rho_\ell - \rho_v}{\rho_v} \; . \tag{1.23}$$

This parameter corresponds to Grashoff number in natural convection.

CHAPTER II

EXPERIMENTAL APPARATUS

The data to be obtained for the present study were local heat flux values at different values of surface superheat both under normal and reduced gravity conditions, and values of vapor film thickness as a function of time for an understanding of the nature of the vapor film.

To obtain local heat transfer rates, it was decided to employ a transient technique. The general nature of the technique adopted was to immerse a warm body in a relatively cold liquid so that film boiling was induced, and measure the time rate of change of temperature of the immersed body. If the temperature distribution of the body is known as a function of time, the rate of change of enthalpy gives the heat transfer rates.

This transient technique has several advantages, as compared with steady state techniques. The main advantage of the transient technique is its simplicity. By installing thermocouples as needed in the test pieces, the rate of cooling can be recorded as a function of time. Steady state techniques to determine the local heat flux values would require, in addition to thermocouples to monitor the temperatures, comparatively elaborate set up of individual heating elements in every section of the test piece. The transient technique would enable data to be obtained even in the transition regime from film to nucleate boiling where steady state techniques have proved difficult because of the unstable nature of the transition regime. To obtain data under

reduced gravity conditions in a drop tower, where the drop usually takes a few seconds, transient techniques are preferred as steady states can be achieved only with test surfaces of negligibly small heat capacity. This transient technique has been successfully employed for obtaining boiling data under different conditions of gravity forces, pressures and subcooling in liquid nitrogen and liquid hydrogen (18,54).

To determine the local heat flux values as a function of temperature, in film boiling in cryogenic liquids, a suitably instrumented test surface with thermally isolated test sections was used, along with appropriate dewars for the cryogenic liquids. For measuring the vapor film thickness as a function of time, it was decided to adopt photographic methods which would produce motion pictures at a high speed. A test surface with a constant, and uniform controlled surface temperature was used for experimental simplification. For this it was necessary to have a high-speed camera with associated auxiliaries and a dewar with plane transparent windows.

The test surfaces, the dewars, and photographic equipment used for the present study are described in the succeeding paragraphs.

A. Heating Surfaces

To obtain heat flux versus wall superheat data, test surfaces were constructed of oxygen-free high-conductivity copper. The choice of this material was based on its high thermal diffusivity which would permit using lumped analysis (Appendix D) in the calculation of heat flux, thus permitting the use of

just one thermocouple in each test section, and its well documented properties at low temperatures. For photographic studies, it was necessary to have a steady state test surface; tellurium copper was chosen for this test surface because of its easy machinability.

1. HEAT FLUX MEASURING TEST SURFACES

In order to avoid edge effects, cylindrical test surfaces were used to simulate plane vertical surfaces. A test piece assembly is shown in Figure 1, and the details are shown in Figure 2. The test piece, Figure 1, consisted of three test sections, each 1/4 in. thick with a hole in the center to pass the thermocouple wires. Each test section was insulated from the adjoining spacer pieces with 0.005 in. thick Teflon washers. Heat leakage to the adjoining sections was further reduced by cutting a recess such that only a circular section of 1/16 in. radial width would bear in between the sections. The sections were held together by two 3/32 in. diameter stainless steel through bolts, insulated from the copper by winding a 0.001 in. Teflon tape around the bolts. Boiling from the top and the bottom of the test piece was prevented by mounting an additional cylindrical piece constructed of 0.001 in. stainless steel shim stock. The thermocouple wires from the test sections were passed through the central holes, through a 1/4 in. diameter stainless steel tube soldered to the top section and out of the tube through a Conax bare wire thermocouple gland. The stainless steel bolts holding the test pieces together also served to attach the test piece to the cables which raised and lowered the test surfaces in the dewar.

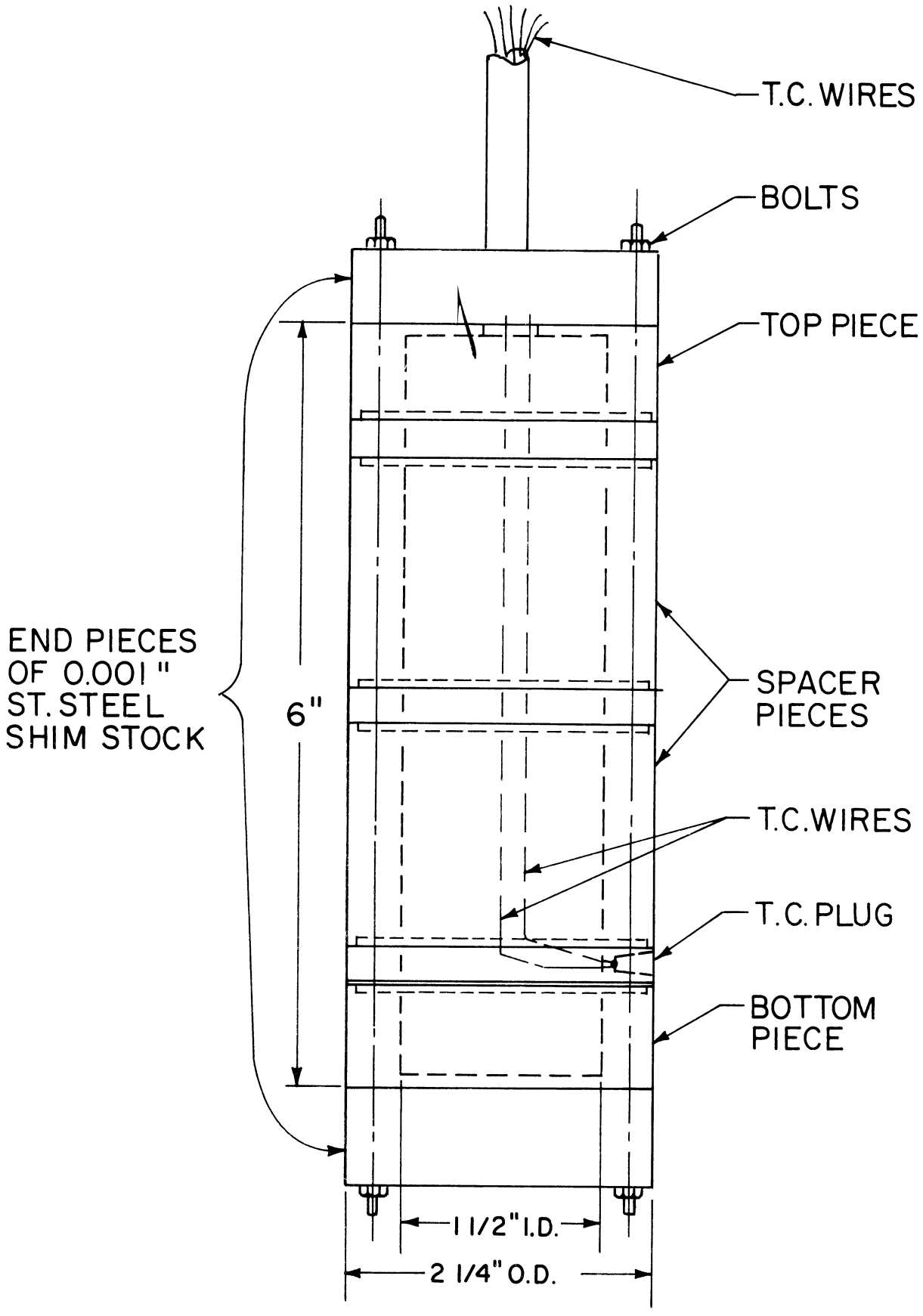

Figure 1. 2-1/4 in. diameter test surface.

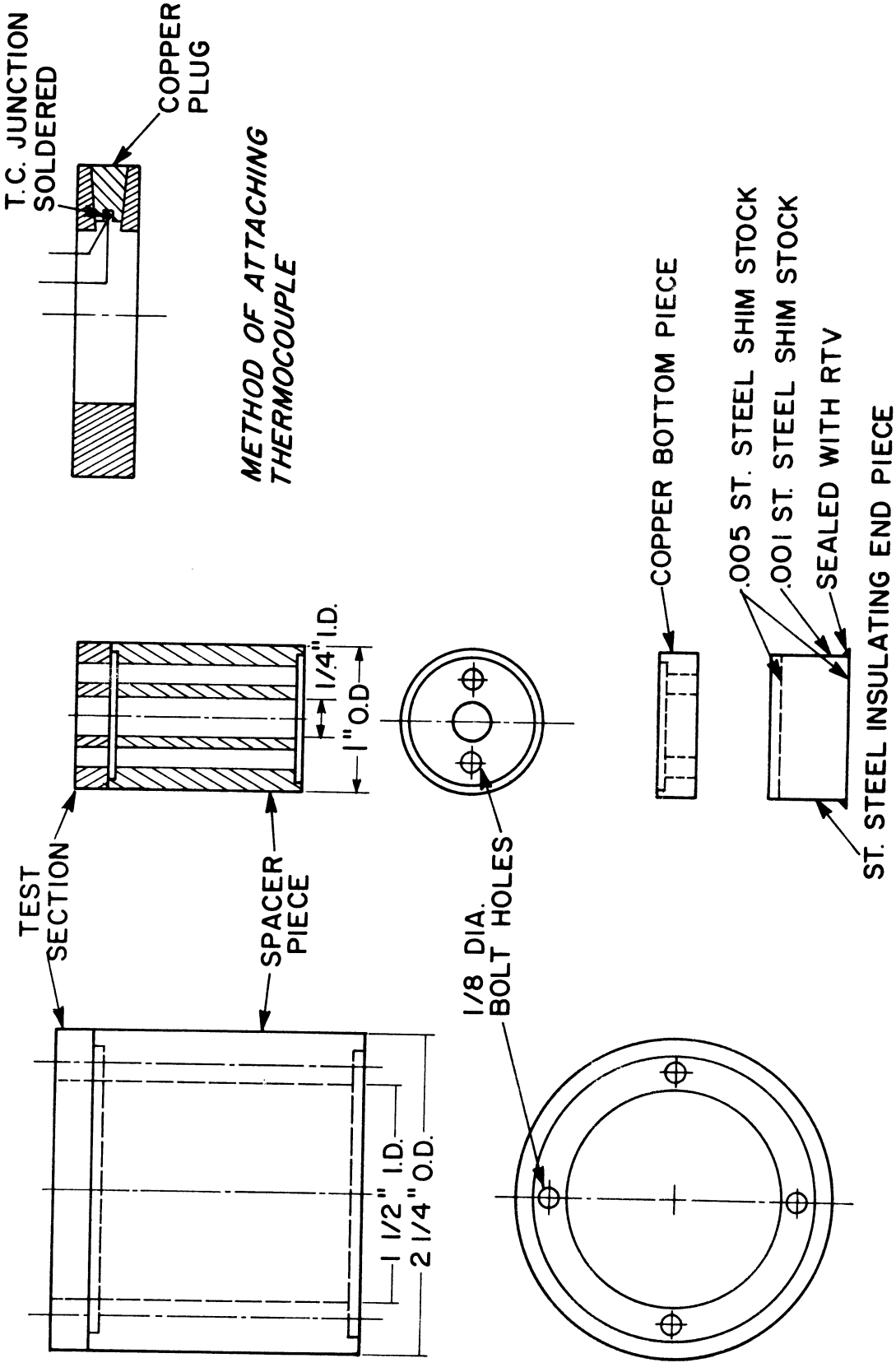

Figure 2. Test section build up.

The sections of the test piece were assembled to check the alignment of the different sections. The heating surfaces were then sandpapered with 400-grit emery tape and smoothened with crocus cloth. The surfaces were finally polished with jeweler's polish to obtain a smooth mirror-like finish. No attempt was made to quantitatively measure the surface roughness, as it has been established that film boiling is relatively insensitive to surface finish.

a. Method of Attaching Thermocouples

In previous work with spheres, thermocouples were attached to the sphere by drilling a 0.040 in. diameter hole in the sphere to the required depth and soldering the welded thermocouple junction at the bottom of this hole. In the present study this method of attaching thermocouples proved inconvenient as it required drilling a small diameter hole from the inside of the ring shaped test section.

In order to find the most convenient way of attaching thermocouples consistent with acceptable response, six thermocouples of copper constantan were installed in different ways in a test block of OFHC copper measuring 2-1/4 in. wide x 1-1/2 in. high x 3/4 in. thick as shown in Figure 3. Thermocouples 1 and 2 were made by welding 30-gauge copper and constantan wires. These were

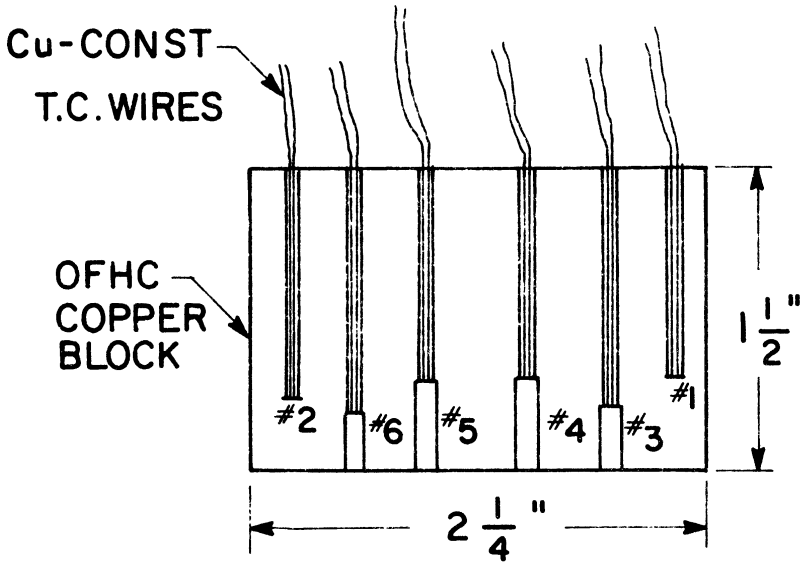

Figure 3. Different methods of attaching thermocouples.

then inserted in a hole of 0.055 in. diameter x 1 in. deep in the copper block and attached to the block with 50-50 soft solder. Thermocouples 3 and 4 were identical and were made by welding the junctions and soldering these to similar copper plugs of 1/16 in. diameter x 3/8 in. long. Thermocouple 5 was made by welding the junction, slitting the edge of a 1/16 in. diameter plug, sandwiching the thermocouple junction between the slit ends and mechanically pressing them. Thermocouple 6 was made by electrically welding the wires to one end of an OFHC plug. It was found that this was mechanically weak; to provide the necessary mechanical strength, a thin coating of soft solder was applied to the junction after welding. These plugs were driven into hole at the bottom of the copper block, the wires coming out of the top through corresponding holes as shown.

The responses of the various thermocouples were compared by immersing the copper block in liquid nitrogen and recording the output of the thermocouples on a Sanborn Recorder. The temperature level at which these runs were made was 255°R (-205°F). It was found that Thermocouple 4 had the best response and the responses of all other thermocouples were compared with that of Thermocouple 4: Thermocouples 1 and 6 lagged by 5μv (0.35°R), Thermocouple 2 by 2μv (0.15°R), and Thermocouples 3 and 5 by 10μv (0.7°R). The time rate of change of temperature as measured by Thermocouple 1 was lower by 0.5-1% compared with that of Thermocouple 2. There were no differences in the measured time rate of change of temperatures as recorded by Thermocouples 2, 3, 4, and 6. Thermocouple 5 measured 4% too low. These results indicate that there was an uncertainty of about 0.7°F in the measurement of the temperature and less than 0.5% in the heat flux measurement due to thermocouple responses.

In the test pieces the thermocouple junctions were made by welding the thermocouple wires, soldering the junction to a tapered copper plug of approximately 1/16 in. diameter and driving the plugs into holes in the test section.

Excess length of the plug was filed off and the plug end peened over and polished.

b. Thermal Insulation of Test Sections

The local heat transfer rates from the test surfaces to the surrounding liquid was determined by equating them to the rates of enthalpy change of the test sections in the test surfaces. For this technique to be satisfactory, test sections had to be thermally insulated from the adjoining spacer pieces.

Before deciding to use cylindrical heating surfaces, attempts were made to use rectangular copper blocks as plane vertical heating surfaces. With some of the methods of insulating the sides of rectangular block to reduce end effects, interesting results were observed. With Teflon strips as insulation on the sides of blocks, higher heat flux values were observed than without the insulation strips.

To avoid such edge effects, cylindrical heating surfaces were used instead of plane vertical surfaces. To insulate the test sections from the spacer pieces, attempts were made to introduce an air gap of 0.005 in. between them but this was not practicable because of difficulty in properly aligning the different sections.

It was established that no adverse effects were introduced by using a 0.005 in. Teflon washer between the sections (Appendix B). To minimize the area of heat leakage from the test section to the adjoining sections due to temperature differential in the various sections during the cool down period, a recess was cut in the spacer pieces so that only a circular section of 1/16 in. radial thickness was in contact with the test section.

c. Test Piece Dimensions

As has been mentioned earlier, to avoid possible edge effects, it was decided to use cylindrical test surfaces to simulate plane vertical surfaces. This would then require establishing that using a cylindrical test surface would give the same results as plane surfaces. It was proposed to establish this fact by using test surfaces of different diameters so that if the results obtained from these surfaces agreed within themselves, it could be concluded that the curvature had no effect. For the smaller test surface, it was arbitrarily decided to use a 1 in. diameter test surface. The selection of the largest diameter depended on the size of dewars available. To find the largest diameter test surface that could be used in the available dewar without introducing any effects due to the container size several tests were conducted and the results showed (Appendix C) that with the 4 in. diameter dewar, a maximum diameter of 3 in. for the test surface could be used. To be sure that the container size had no effect on the results obtained, it was decided to limit the diameter of test surfaces to 2-1/4 in. Hence, test pieces of 1 in. diameter and 2-1/4 in. diameter were constructed. Earlier reported results (24,39) indicated that turbulence effects would become apparent at relatively short heights from the leading edge—of the order of a fraction of an inch. It was, therefore, decided to construct test surfaces of 6 in. height to obtain data under normal gravity conditions. However, because of dimensional limitations imposed by the dewar in the drop package, the height of test pieces to be used in the drop package was limited to 4 in. and a diameter of 1 in.

To obtain local heat flux data under normal gravity conditions, five test surfaces were constructed as shown in Table I. It might be noted that each of the five test surfaces constructed contains one section located at the same height of 3 in. from the leading edge, for purposes of comparison of data obtained with the different test surfaces.

TABLE I

DETAILS OF TEST SURFACE: a/g=1

Test Surface Identification Number	Diameter of Test Surface, in.	Test Section Locations Above Leading Edge, in.
2	1	3/8, 3, 4-1/2
4	1	5/8, 3, 5-5/8
5	1	1/4, 1-1/2, 3
6	2-1/4	7/8, 3, 3-1/2
7	2-1/4	2, 3, 4

Because of the shorter heights of test surfaces that could be accommodated in the drop package for studies under reduced gravity conditions, it was decided to limit the number of test sections to two in each surface. Details of test surface dimension and test section locations for reduced gravity studies are given in Table II.

TABLE II

DETAILS OF TEST SURFACES: $a/g \cong 0.008$

Test Surface Identification Number	Diameter of Test Surface, in.	Test Section Locations Above Leading Edge, in.
8	1	3/8, 2
9	1	5/8, 3
10	1	1-1/8, 3-1/2

2. TEST SURFACE FOR PHOTOGRAPHIC STUDIES

While all heat flux measurements were made by employing a transient technique, it was desirable to have steady state conditions available for photographic measurements of vapor film thickness. For this purpose a test surface as shown in Figure 4 was constructed of free machining telurium copper. A 1/2 in. hole was drilled in a 1 in. diameter cylinder x 6-1/2 in. height to receive a 1/2 in. diameter cartridge heater of 1000 watts capacity. To avoid the possibility of noise pick up by thermocouples, D.C. power supply was used for the cartridge heater. Two thermocouples were installed in drilled holes at the top to measure the temperature of the test piece. The ends of the surface were closed by threaded copper end pieces. To prevent boiling from top and bottom ends of the test surfaces, end pieces of 0.001 in. stainless steel shimstock, similar to those used for the other pieces, were attached to the test surface. For photographic studies only a part of the cylinder was seen and hence a reference was necessary for quantitative measurements for film

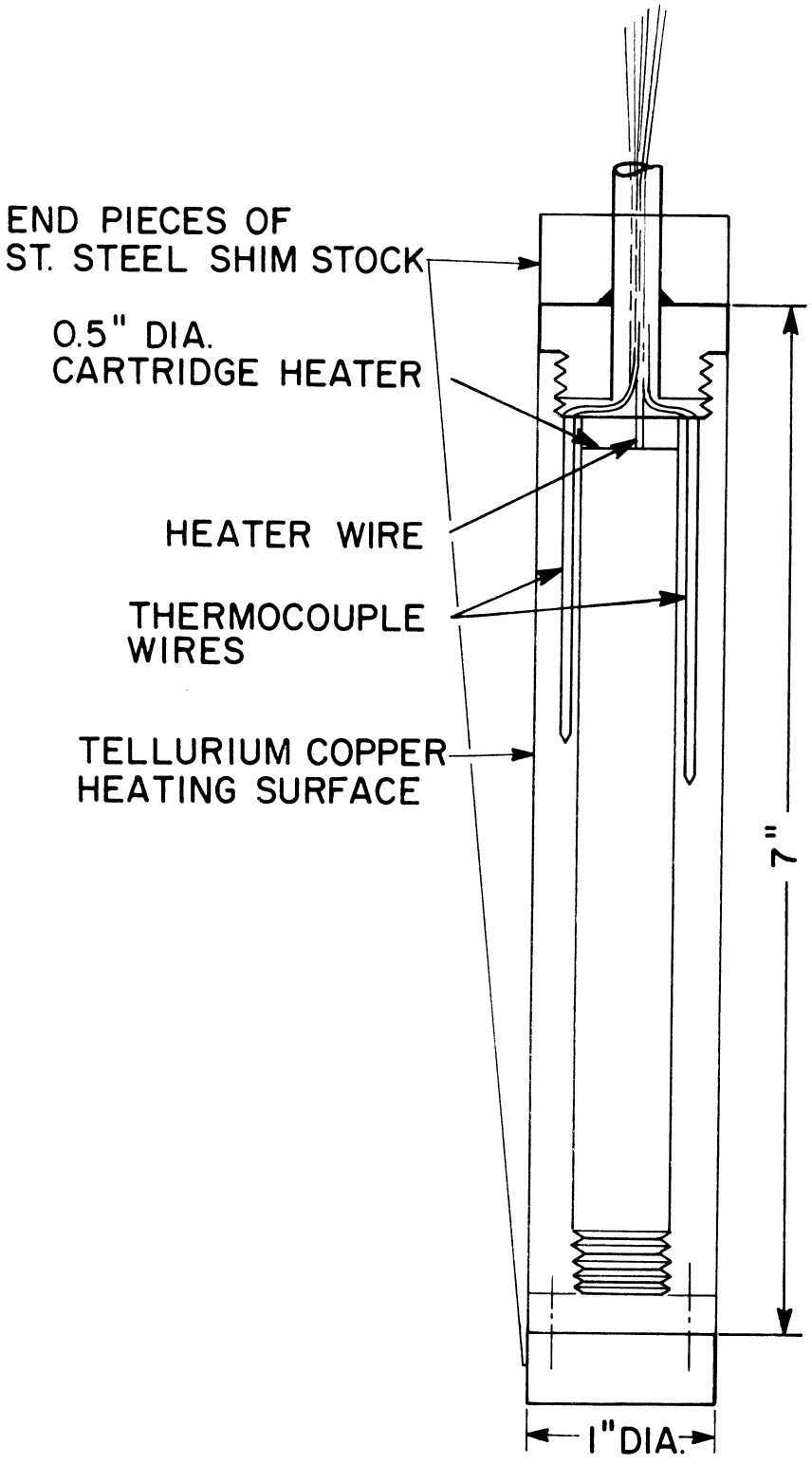

Figure 4. Test surface for photographic studies.

thickness. For this purpose, an 18-gauge wire (0.040 in. diameter) was stretched parallel to the test surface at a distance of 1/2 in. from the cylinder. Pinch marks were made at intervals of 1 in., the first one approximately to coincide with the leading edge of the test surface. In the photographic films only about 3/4 in. along the axis was visible and these pinch marks served to identify the distance from the leading edge at which photographs were taken.

B. Dewars

Three different dewars were used—a deep Pyrex glass dewar for obtaining local heat flux values under normal gravity conditions, a cylindrical stainless steel dewar for local heat flux measurements under reduced gravity conditions, and a rectangular stainless steel dewar with Pyrex glass windows for photographic studies. In the glass dewar and the drop package dewar, the instrumented test surfaces were immersed in a pool of liquid nitrogen or liquid hydrogen and the temperatures of the test section monitored by the thermocouples attached to them and recorded on an eight-channel Sanborn Recorder. The test piece for photographic studies was heated by a cartridge-type electric heater. Pressures in the dewars were held constant by the use of pressure relief valves.

1. PYREX GLASS DEWAR

To obtain the local heat flux values a Pyrex glass dewar as shown in Figure 5 was used. This dewar was double walled, vacuum insulated with an upper part

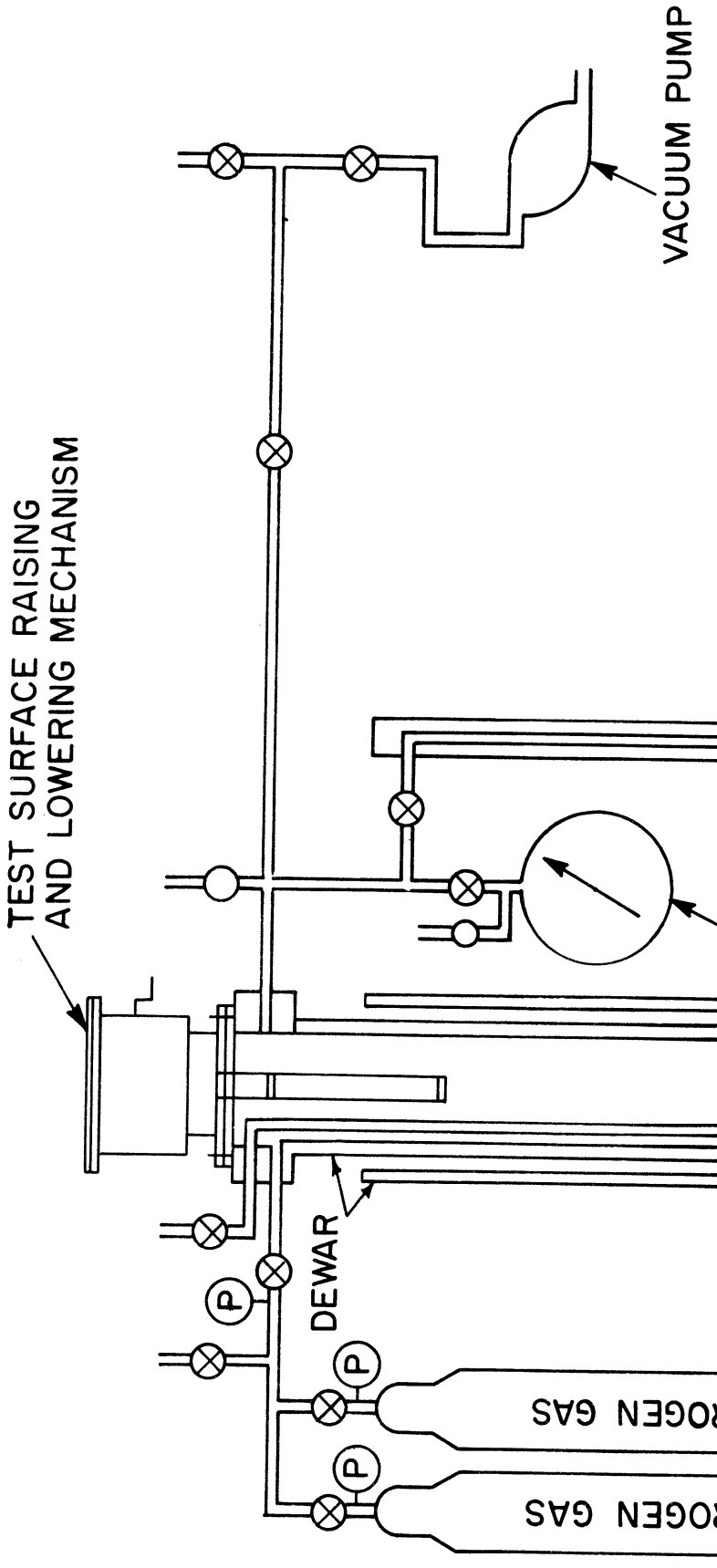

Figure 5. Schematic of Pyrex dewar and associated equipment.

made of single walled section which terminated with a metal flange via a Kovar intermediate metal flange. The dewar was silvered except for two 1 in. wide diametrically opposite strips which permitted visual observation of boiling. The dewar had an I.D. of 10 cm, a height of 65 cm, and had a capacity of 5 liters. The dewar itself was surrounded by a second double walled, vacuum insulated dewar which was used to surround the inner dewar with liquid nitrogen. This liquid nitrogen acted as a heat shield for the test liquid contained in the inner dewar.

In previous works with spheres, the test object was attached to a stainless steel tube which passed through a gland on the flange mounted on top of the dewar. The sphere was introduced into the test liquid by sliding the tube in the gland. It was observed that small quantities of moisture adhering to this sliding tube found its way into the glass dewar where it was vaporized. When the sphere was withdrawn from the test liquid, this moisture condensed on the sphere and if the sphere was immersed with this coating of condensed moisture on it, heat flux values higher than that with a clean sphere were obtained. The problem was solved by raising the temperature of the sphere to levels above the dew point and then introducing it in the test liquid. However, the same procedure could not be adopted with the present cylindrical test surfaces to obtain data at temperature levels lower than 32°F; in such cases starting with a temperature above 32°F and cooling the test surfaces to much lower temperatures would result in considerable temperature differentials being established between the different sections that make up a test surface, thus producing a nonisothermal surface. It was desired to maintain an

isothermal surface. This was accomplished by precooling the test surface to the vicinity of the desired temperature level by immersion in the liquid, removing the test surface, suitably warming it up to establish an isothermal surface and introducing it in the test liquid. For this technique to be successful, it was necessary to prevent the ingress of moisture, and hence a lifting and lowering device with a rotary seal instead of a sliding seal was designed and used.

A manifold flange mounted on the top of the glass dewar provided all permanent connections such as vent lines, pressurization lines, etc., and also served as a base for the upper chamber assembly which supported the test piece. Figure 6 shows details of this assembly. The upper chamber contained a shaft one end of which was supported on a bearing on the inside of the chamber and the other end came out of the chamber through a gland. This shaft had two pulleys which housed sufficient lengths of stainless steel cables. The test piece was suspended from these cables. The shaft extension had a handle and an automatic stop to prevent the lowering of the test surface by its own weight. To the top flange of the chamber, a smaller flange with a bare wire thermocouple gland was attached. All the thermocouple wires from the test sections passed through this gland. The top flange also carried two 1/2 in. relief valves set to open at 1/2 psig, and a fitting for filling the dewar with liquid hydrogen. A dump tube extending to the bottom of the dewar was used to evacuate the liquid by pressurizing the dewar. The dump tube was connected to a heat exchanger made of copper tubing, whose outlet was led into

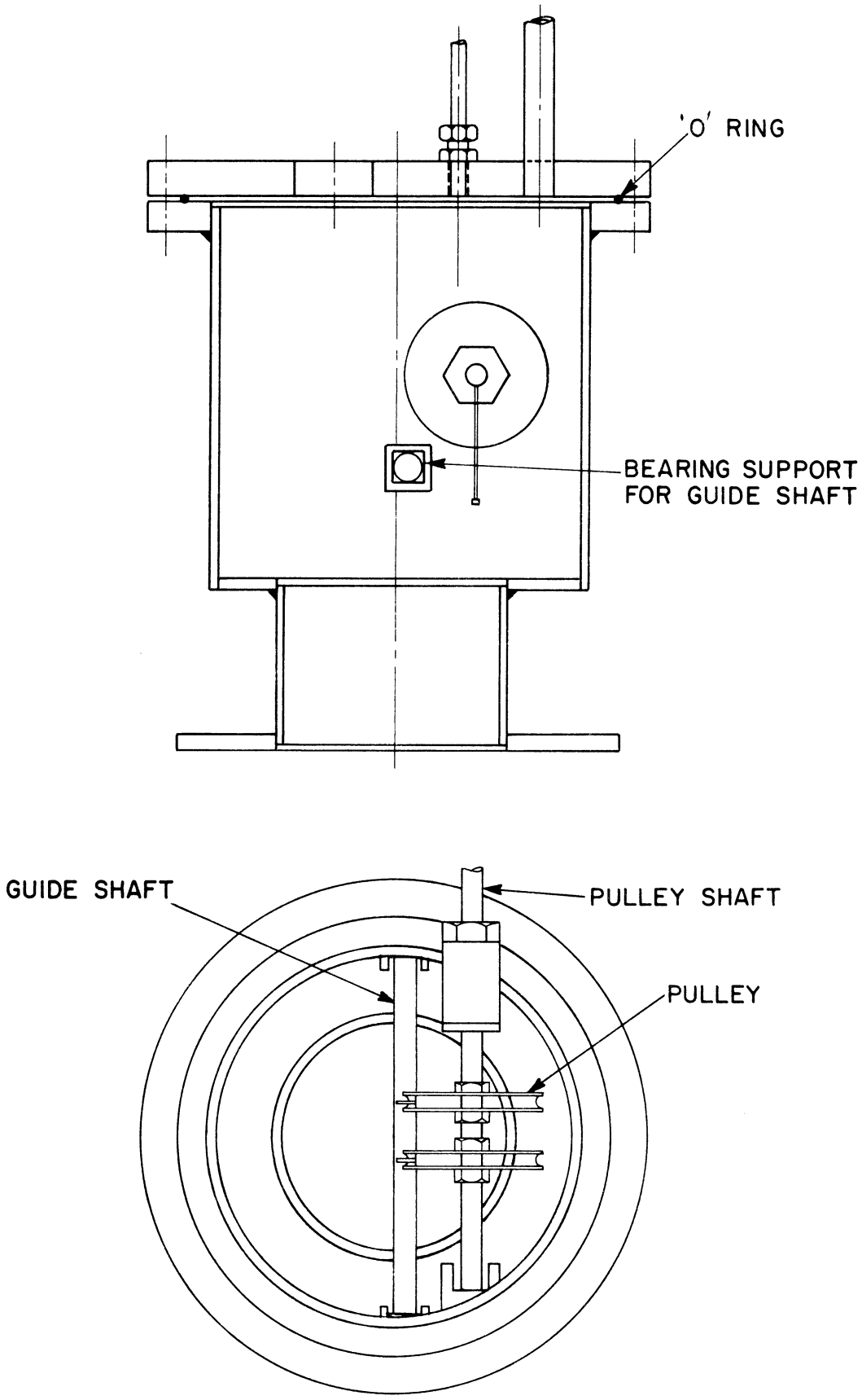

Figure 6. Device for raising and lowering test surface.

the intake of an exhaust fan. This arrangement permitted the safe evacuation of liquid hydrogen.

2. DROP PACKAGE DEWAR (Figure 7)

The stainless steel cylindrical dewar for the drop package is a double walled vessel with super insulation. The inner vessel is 8 in. diameter x 12 in. deep with a neck opening of 4 in. diameter. To the top of the dewar is attached a heating chamber into which the test piece can be drawn and heated by an electrical heating coil. A reservoir for liquid nitrogen is provided at the top of the dewar; the liquid nitrogen in this reservoir precools the dewar before filling it with liquid hydrogen.

A double walled fill line, a vent line, three thermocouples—two at different heights in the test liquid and one in the vapor space—a tube carrying two liquid level indicating sensors—one high level and one low level—pass through the lower flange of the heating chamber. Two more thermocouples and the electrical leads for the heater pass through the top flange of the heating chamber. A gland through which the tube carrying the test piece slides is mounted on this top flange. By raising or lowering this tube the test piece is removed or immersed from the test liquid. Two liquid level indicating sensors are mounted in the reservoir on the top of the dewar.

The dewar itself is suspended from the cover plate of the drop package by stainless steel rods. Appropriate fittings for the fill lines, vent line, pressure release, etc., are mounted on the cover plate. After filling the dewar with the test liquid, two pressure relief valves were attached to the

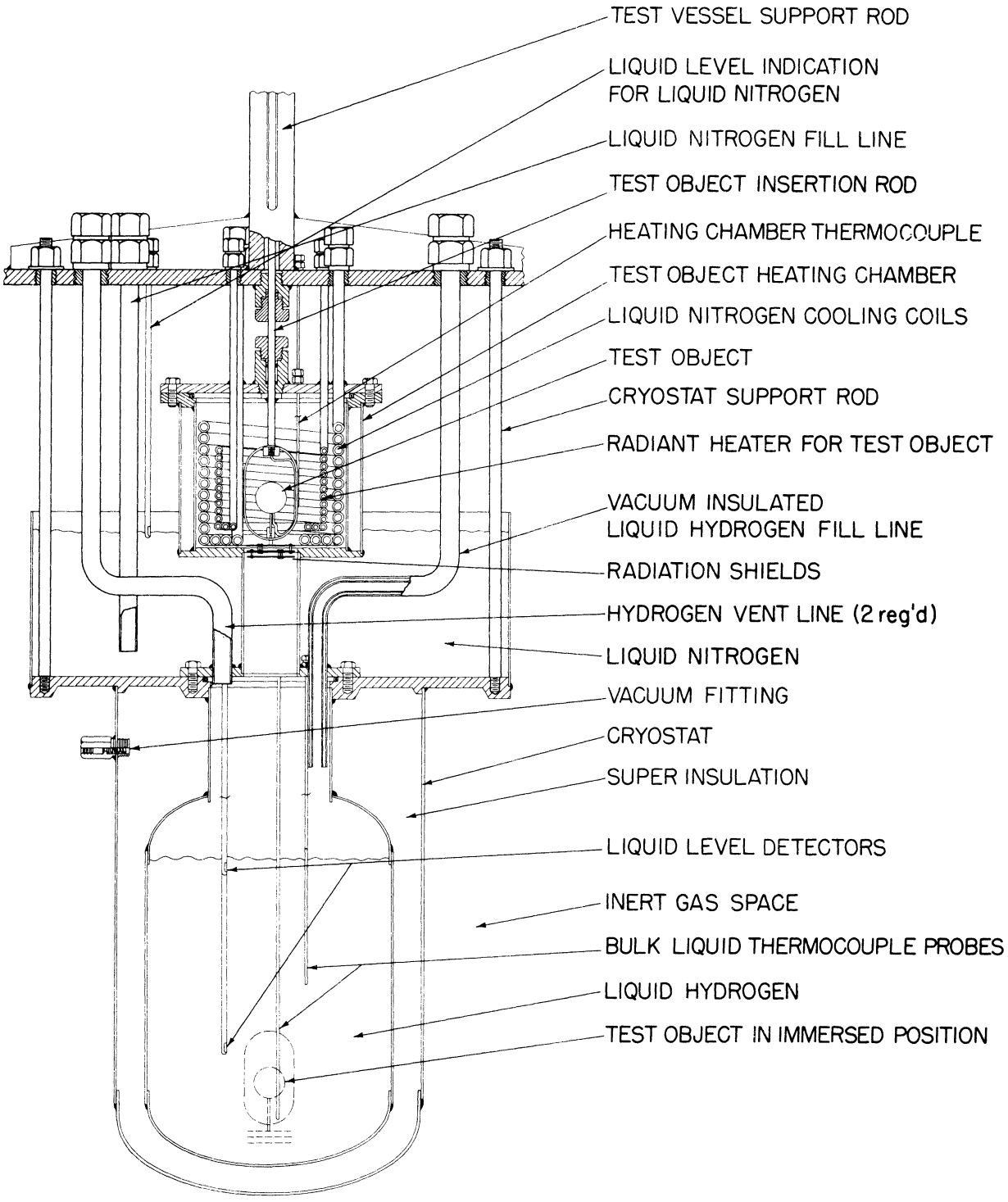

Figure 7. Drop tower test package.

fill line, to regulate the pressure in the dewar. A small lecture bottle mounted on the drop package provides helium for pressurizing the system for studies in subcooled liquids.

The thermocouple wires from the test pieces pass through the 1/4 in. diameter supporting tube. The thermocouple outputs are connected to a recorder via a drop cable, consisting of eight 24-gauge copper wires and 24-gauge constantan wires. Double shielding of this cable was necessary to minimize noise pick up, particularly when operating at high sensitivities. The constantan wires served to make the reference junctions in ice.

Details of drop tower, package construction, deceleration device, etc., are given in Appendix A.

3. DEWAR FOR PHOTOGRAPHIC STUDIES (Figure 8)

A stainless steel rectangular dewar of inside dimensions 5 in. x 8 in. x 14 in. was fabricated for the purpose of obtaining motion pictures of film boiling. The dewar was double walled permitting the evacuation of the space between them. For obtaining photographic films, four window glasses of 3 in. diameter Pyrex were installed, two on each side. To provide a seal between the window glasses and the frame, "O" rings generally available were not effective as they hardened at the low temperatures of liquid nitrogen. "O" rings of Rulon (made by Dixon Corporation) and of Compound 6317 (made by Precision Rubber Co.) were found to be satisfactory.

Frequent chipping of the edges of the window glasses initially observed was eliminated by grinding the edges of the glasses. Contraction of the "O"

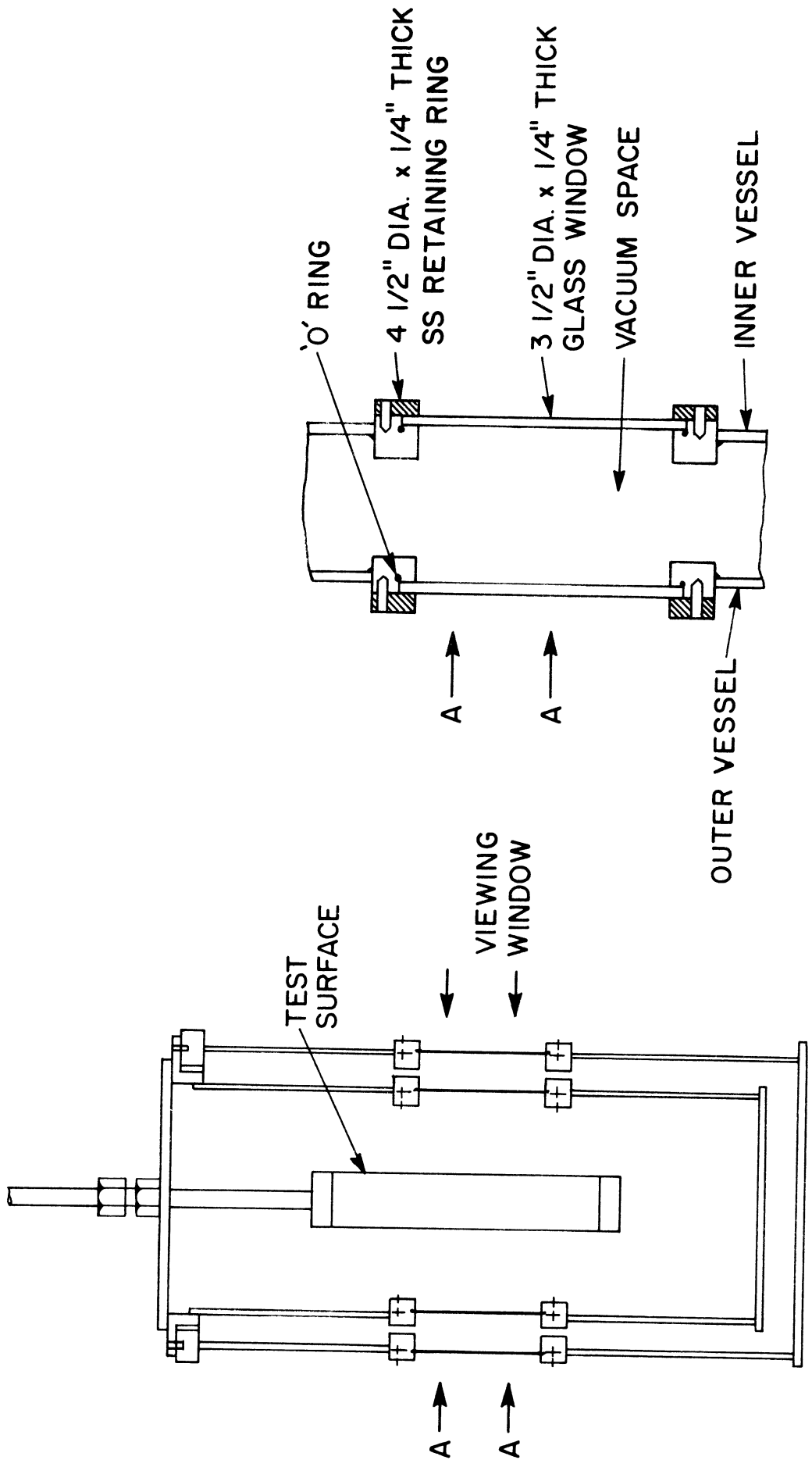

Figure 8. Stainless steel dewar for photographic studies

rings at low temperatures resulted in slackening of the bolts holding the windows with a loss of vacuum. This was corrected by the use of spring washers. With a vacuum pump running continuously, a vacuum of approximately 1/4 in. less than the barometric pressure was possible, with liquid nitrogen in the dewar.

C. Assembly of Test Surfaces

Before final assembly of the test surfaces, the copper pieces were temporarily assembled and polished so that a smooth alignment was obtained. This was then disassembled. Three thermocouples of copper constantan of the required length were made by welding one junction. The thermocouple wire was then passed through the hole in the test section, and soldered to an OFHC copper plug which was then driven into the test section. Excess length of the plug was filed off and peened in place. This was then lightly filed, smoothed with emery cloth and finally polished with jeweler's polish till a smooth surface was obtained. After polishing it was not possible to locate the plug by normal visual inspection. The test piece dimensions were measured with a vernier calipers and recorded. The weight of the test section with the thermocouple was determined in a chemical balance. Subtracting the weight of the thermocouple gave the net weight of the test section. The thermocouple wires were insulated by slipping a 24-gauge Teflon or polyethelene tubing up to the bare wire thermocouple gland at the top. The test piece was then assembled with end pieces of stainless steel shim stock and 0.005 in. Teflon insulators

between the test sections and spacer pieces. The stainless steel bolts holding the sections together were insulated from the test piece with Teflon tape.

After assembling the test piece the bolts were slightly tightened, the excess Teflon trimmed, and the pieces properly aligned by pressing between two V-blocks. The bolts were then tightened and the edges smoothed with crocus cloth, and finally polished. The stainless steel end pieces were sealed with a 0.005 in. stainless steel disc using RTV to seal the edges. The thermocouple wires from the gland on the test surface to the gland on the hoisting device were also insulated with Teflon tubing. The thermocouple wires leading from the gland on the test piece to the gland on the hoisting device required greater flexibility. Since Teflon has greater felxibility than polyethelene, particularly at low temperatures, it was used in this section. The thermocouple wires were then passed through the gland on the hoisting device. The test piece was attached to the stainless steel hoisting cable, and adjusted, so that the test piece remained vertical. The hoisting device with the test piece was then installed on the glass dewar.

D. Photographic Apparatus

To measure the vapor film thickness and the extent of interfacial oscillations, motion pictures were taken with a high-speed drum camera, Dynafax Model 326 (manufactured by Beckman and Whitley). A 35 mm film strip of 33-7/8 in. length is used and the maximum number of frames exposed was 224. The filming rate could be varied from 180 frames/second to a maximum of 26,000

frames/second. Backlighting was provided by a 500-watt projector with a 3-1/2 in. diameter condensing lens. The speed at which the camera drum rotated (and hence the filming rate) was monitored by a magnetic tachometer mounted on the camera and read on an electronic counter. Kodak Pan-X film (ASA 125) was used. The arrangement of the equipment used to obtain motion pictures is shown in Figure 9.

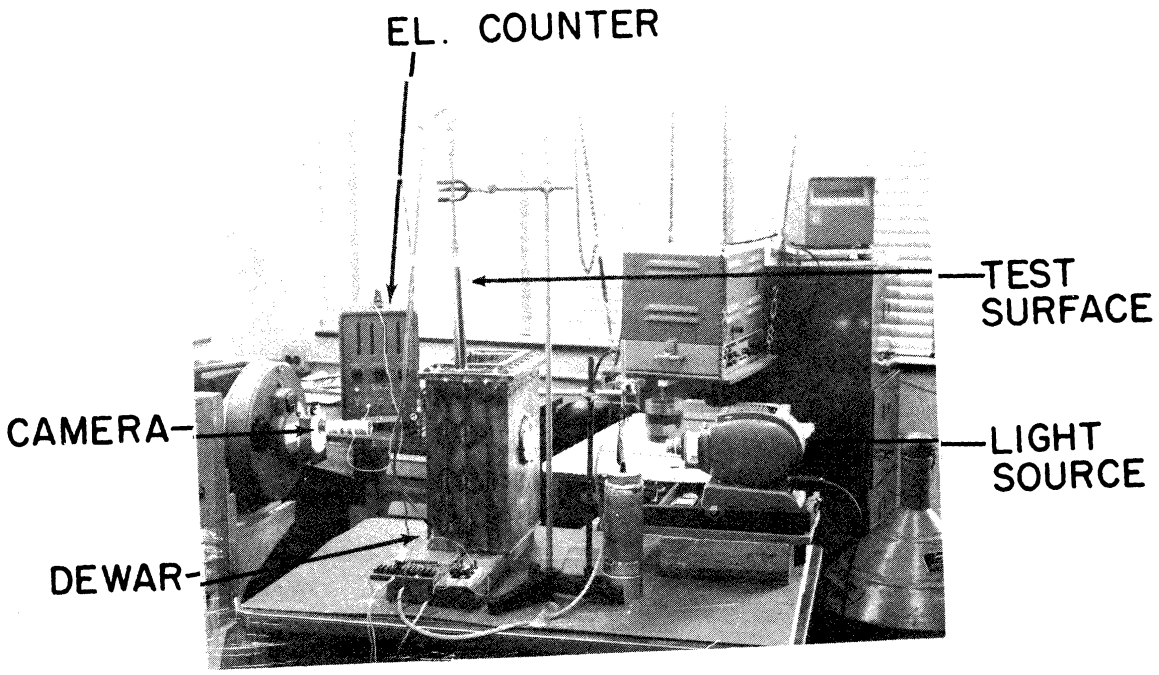

Figure 9. Arrangement for photographic studies.

CHAPTER III

INSTRUMENTATION

To calculate the local heat flux values at different temperature levels, the thermocouple outputs from the test sections in the heating surfaces were recorded on a Sanborn Recorder. The Sanborn Recorder itself was calibrated by comparison with a potentiometer. The potentiometer was also used for measuring the thermocuple output in liquid nitrogen and liquid hydrogen for purposes of calibrating the thermocouples.

A. Thermocouples

All thermocouple outputs were measured relative to the ice point. The thermocouples were made of 30-gauge copper-constantan wires. The precise location of the thermocouples in the test section was unimportant as a lumped analysis was employed in the calculation of heat flux (Chapter IV) which gave acceptable accuracy (Appendix D). Copper-constantan thermocouples have relatively low thermal power at the low temperatures at which data were obtained in the present experiments and it was necessary to operate the recorder at high sensitivities of up to 2 μv/div. To minimize noise pickup when operating at this high sensitivity all thermocouple lead wires were covered by a double electrostatic shield. The lead wires were led to a switch box which permitted:

(1) the thermocouple outputs to be fed into the recorder;

(2) the thermocouple outputs to be measured by the potentiometer for purposes of calibrating the thermocouples; and

(3) the potentiometer output to be fed into the recorder for calibrating the recorder.

B. Potentiometer

To calibrate the thermocouples installed in the test surface, the outputs from the thermocouples in the test liquid (liquid nitrogen or liquid hydrogen) were read on a Leeds and Northrup Model K3 potentiometer; the unbalance in the potentiometer was amplified and detected with a Rubicon Model 3550 photoelectric galvanometer and amplifier system. The potentiometer has an accuracy of $\pm$ (0.015% + 0.5 μv). The maximum output measured in liquid hydrogen was -6190 μv and the maximum error was $\pm$ 1.43 μv corresponding to $\pm$ 0.5°R. To reduce the effect of building vibration, the amplifier for the null detection system was located on a platform suspended from the ceiling with soft springs in the supports. A Honeywell series 3100 spotlight galvanometer indicated the unbalance in the circuit.

C. Sanborn Recorder

Model 7708 A Sanborn Recorder was used to record the thermocouple output from the test section, as a function of time.

The recorder had eight channels, and appropriate preamplifiers could be used for each channel depending on the input signal. For recording the

thermocouple outputs, Model 8803 high gain DC amplifier was used. The maximum usable deflection of the recorder stylus was 4 cm divided into 50 divisions on the recording chart paper. The recording chart could be run at speeds varying from 0.25 mm/sec to 100 mm/sec in nine steps. Generally, a chart speed of 25 mm/sec was used. A time marker recorded 1 sec (or 1 min) timing pulses. The preamplifier could be operated at sensitivities from 1000 μv/div to 1 μv/div, with the usual operation at 2 μv/div or 5 μv/div. The nonlinearity of the recorder is specified by the manufacturer to be ± 0.25 div, which corresponds to ± 0.5 μv and ± 1.25 μv at sensitivities of 2 μv/div and 5 μv/div, respectively. The minimum temperature at which the recorder was operated at 2 μv/div was 136°R, and at this temperature, the recorder nonlinearity contributes an uncertainty corresponding to ± 0.05°R. The corresponding values at 5 μv/div are 400°R and ± 0.067°R.

D. Pressure

The pressure in the glass dewar and in the drop package dewar was observed on a calibrated 12 in. Heise pressure gauge with a range of 0-25 psig with a calibrated accuracy of ± 0.025 psi. The gauge was divided into 0.1 psi steps.

CHAPTER IV

EXPERIMENTAL PROCEDURES AND DATA REDUCTION

A. Filling Dewars

To obtain local heat flux values in liquid nitrogen, the upper chamber with the test piece was assembled on the glass dewar. The dewar was evacuated of air with the vacuum pump and then filled with nitrogen gas to atmospheric pressure. The dewar was then filled with liquid nitrogen by pressurizing the liquid nitrogen container with nitrogen gas. When the proper quantity of liquid nitrogen was filled in the dewar, venting took place through two relief valves mounted on the hoisting device which were set to open at 1/2 psig. These relief valves maintained a constant pressure in the dewar during the experiments. Before obtaining the data, the atmospheric pressure was measured with a mercury barometer.

For operation in liquid hydrogen a more elaborate purging sequence was followed to reduce the possibilities of contamination. The system was evacuated of all air, the vacuum broken with nitrogen gas, and pressurized to a positive pressure of 6-8 psig. This sequence was repeated three times with nitrogen gas and then three times with hydrogen gas before filling the dewar with liquid hydrogen. In all cases the outer dewar was filled with liquid nitrogen before filling the inner dewar with the test liquid.

B. Calibration of Recorder and Thermocouples

Before proceeding to obtain the cooling curves at different temperatures, the thermocouples in the test surfaces and the recorder were calibrated and the recorder accuracy checked by the following procedure. The test surface was lowered into the test liquid and allowed to come to thermal equilibrium. The output of the thermocouples in the test sections was measured with the potentiometer. This was used to find the deviation of the thermocouple output from the standard tables. The output of the thermocouple corresponding to the temperature at which heat flux data were to be obtained was determined by using the standard tables (55) and assuming the deviation of the thermocouple outputs to vary linearly from the liquid temperature to the reference temperature (ice bath). The appropriate zero suppression was applied to the recorder using the potentiometer as the signal source. The recorder gain was also calibrated by changing the input from the potentiometer by a known value and observing the corresponding deflection on the recorder. The same procedure was adopted for all the channels on which the output from the test sections were to be recorded.

The test surface was then raised from the test liquid and allowed to warm up to the desired temperature level. During this warming up a 650-watt movie lamp was used with appropriate masking on the glass dewar to locally heat the test surface to obtain an isothermal surface while recording the data. When the test surface temperature was just a few degrees higher than the temperature at which the data were to be obtained, the recorder chart speed was set at

25 mm/sec and the test surface lowered into the test liquid. In general, cooling to the desired temperature took place within a few seconds—10-15 sec. Figure 10 shows a typical recorder output. As soon as the test surface cooled down a few degrees past the desired temperature the test surface was raised, warmed, and the sequence repeated. The test conditions under which data were thus obtained are given in Table III.

TABLE III

TEST CONDITIONS FOR DATA UNDER NORMAL GRAVITY: a/g = 1

Test Surface Identification Number (and dia in.)	Test Section Location Above Leading Edge, in.	Test Liquid	$T_w - T_s$ (°R) (Nominal)
2 (1)	3/8, 3, 4-1/2	LN_2 LH_2	315, 251, 204, 99.7 400, 300, 200, 100
4 (1)	5/8, 3, 5-5/8	LN_2 LH_2	315, 251, 204, 99.7 400, 300, 200, 100
5 (1)	1/4, 1-1/2, 3	LN_2 LH_2	315, 251, 204, 99.7 400, 300, 200, 100
6 (2-1/4)	7/8, 3, 3-1/2	LN_2	315, 251, 204, 99.7
7 (2-1/4)	2, 3, 4	LN_2	315, 251, 204, 99.7

In liquid nitrogen, five sets of data were obtained under each one of these conditions, and in liquid hydrogen, three sets of data were usually obtained.

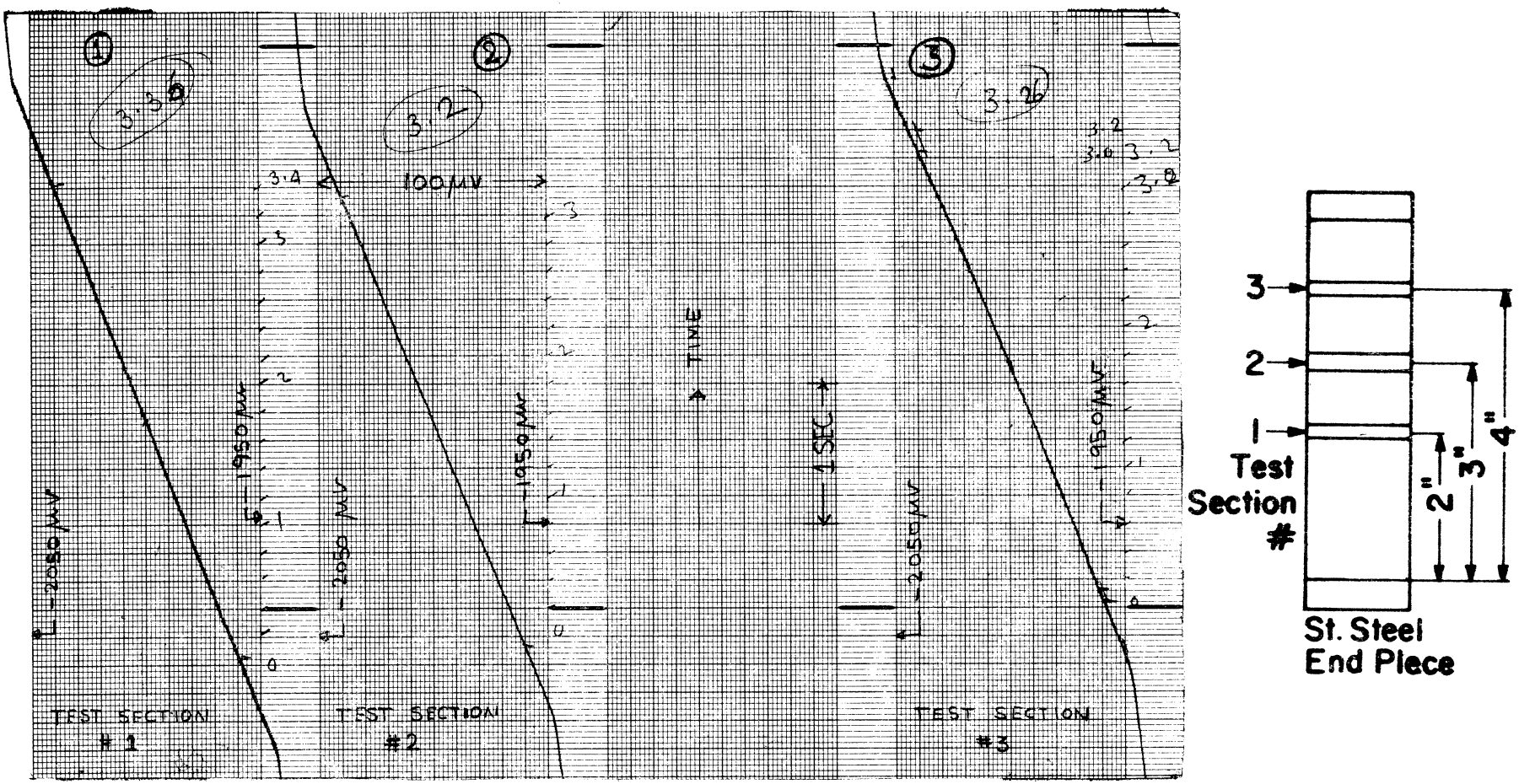

DATE: 12/25/69 LIQUID NITROGEN 0.5psig. sat. TEST SURFACE # 7
RUN # 7004 Zero Suppression = -2050μv; SENS. = 2μv/Div; Chart Speed = 25mm/sec

Figure 10. Typical cooling curve--recorder output a/g = 1. Liquid nitrogen.

C. Drop Package Operation

The filling sequence for the metallic dewar in the drop package, used for obtaining local heat flux data under reduced gravity and subcooled conditions was similar to that with the glass dewar. The dewar was filled with the package resting on a platform. When the dewar was filled with the test liquid, the test surface was immersed and allowed to cool down to the saturation temperature. The thermocouple outputs were measured with the potentiometer. The test surface was raised into the heating chamber where it was heated with an electrical heater lining the chamber. The heater was operated intermittently for short durations of approximately 15 sec at about 30 watts to avoid over heating. The package was then raised and held suspended in the release mechanism. The recorder was adjusted as described previously and the chart speed brought up to 25 mm/sec. The test surface was then immersed in the test liquid, and the package released at the appropriate time. The instant of release was marked on the recorder chart by a signal provided by a dry cell in the package release circuit. The package was then hoisted back into position. Figure 11 shows the recorder output during one such drop.

The method of inserting the test surface limited the data to only one value of ΔT, corresponding to room temperature. In some of the earlier experiments with spheres it was observed that when the sphere at a temperature much lower than the room temperature, was immersed in the test liquid, very high heat flux values were obtained. The cause of these high heat fluxes was found to be the ingress of moisture into the dewar; the moisture adhering to

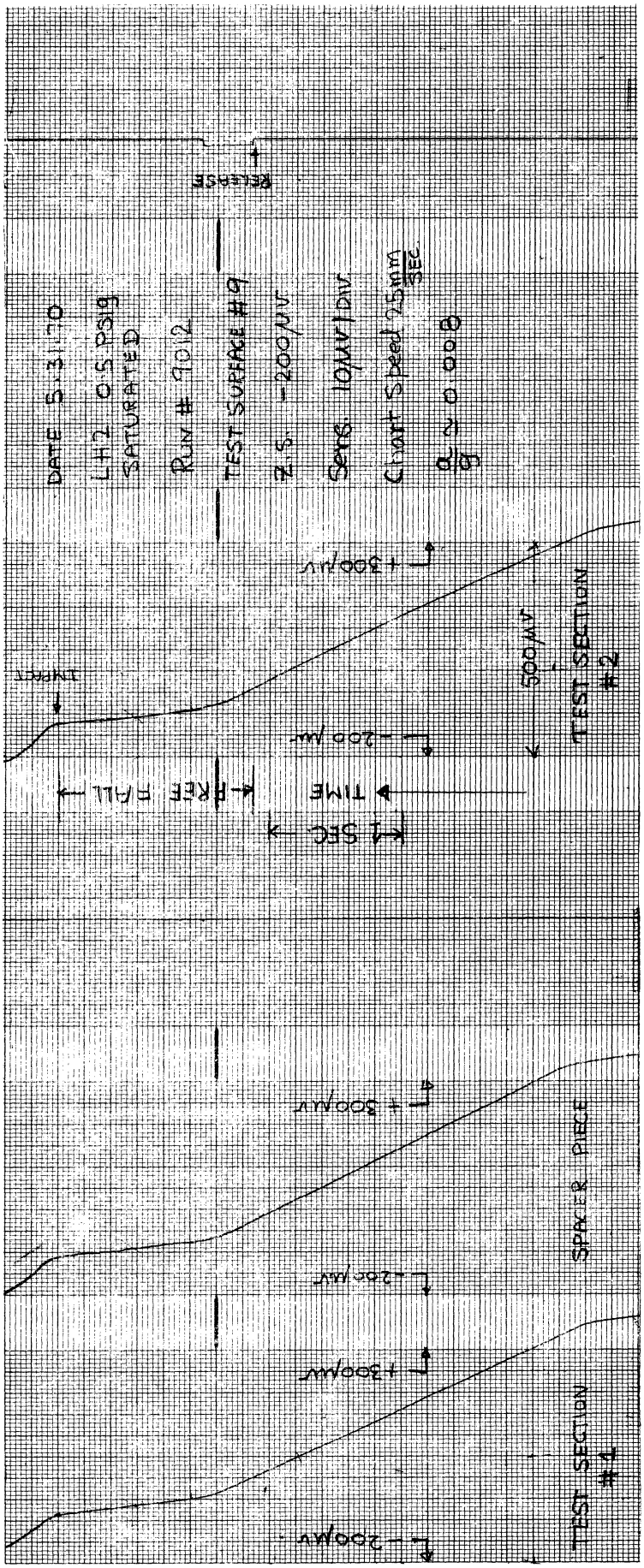

Figure 11. Typical cooling curve—recorder output a/g ≅ 0.008. Liquid hydrogen.

the supporting tube in its raised position found its way into the dewar when the sphere was lowered. This moisture on the warm tube vaporized and remained in the dewar. When the cold sphere was raised, part of this moisture condensed on the sphere and remained until its temperature was above approximately 32°F. Thus, in order to avoid this condensation, it was necessary to raise the temperature of the test surface to at least 32°F. Starting with the test surface at this high temperature, it was impossible to obtain an isothermal surface at low temperatures.

For obtaining subcooled data, two relief valves, one set at 1/2 psig and the other to a higher pressure were used. Just before introducing the test surface, the 1/2 psig relief valve was isolated and the dewar pressurized to a high pressure with corresponding gas; the test surface was then introduced into the subcooled liquid and the data obtained. The conditions under which the data were obtained are given in Table IV.

TABLE IV

TEST CONDITIONS FOR DATA UNDER
REDUCED GRAVITY AND SUBCOOLED CONDITIONS

Test Surface Identification	Test Section Location Above Base, in.	Test Conditions				
		Test Liquid	P, psig	Subcooling (Nominal) °R	a/g	ΔT, °R
8	3/8, 2	LN_2	1/2	0	1.0, 0.008	354
		LN_2	34	21	1.0	333
9	5/8, 3	LH_2	1/2	0	1.0, 0.008	451
10	1-1/8, 3-1/2	LH_2	32.5	8	1.0	443

D. Photographic Studies

For photographic studies a test surface (Figure 4) which could be maintained in steady condition was used. The rectangular dewar was filled with LN_2. The camera was loaded with Kodak Pan X film. The test surface was introduced into the dewar, initiating film boiling, which was maintained by the electrical cartridge heater. The temperature of the test surface was determined by measuring the output of the two thermocouples in the test surface with the potentiometer. The camera was then brought up to the desired speed, the light source was switched on and the exposure made. When the first film was made, it was discovered that the test surface was indistinguishable from the vapor film. To determine the location of the test surface, the power supply to the heater was shut off, allowing the test piece to cool down to the liquid temperature. When all boiling ceased, a second exposure was made at the same filming speed as before but for a much shorter duration to give double exposures on 4-5 frames, which provided the reference surface. Conditions under which motion pictures were obtained are given in Table V.

TABLE V

CONDITIONS FOR MOTION PICTURES

Nominal Height	0 in., 2 in., 4 in., 6 in.
Height Covered	3/4 in.
Speed/Writing Time	200 frames/sec/1 sec 500 frames/sec/0.5 sec
Nominal Height	1 in., 4-1/2 in.
Height Covered	1-1/2 in.
Speed/Writing Time	200 frames/sec/1 sec 500 frames/sec/5 sec
$(T_w - T_s)$ °R	300, 200, 100

E. Data Reduction

With liquid nitrogen as the test fluid, the range of thermocouple output recorded on the recorder chart was determined from the zero-suppression applied to the recorder and the sensitivity at which it was operated. The value of the zero-suppression applied was determined from the output of the thermocouple at approximately the desired temperature at which the data were to be obtained; the sensitivity at which the recorder was operated was such as to give a reasonable slope on the recorder. It was found that when the recorder was run at a chart speed at 25 mm/sec, a writing time of approximately 2-6

sec provided a reasonable slope by operating at a sensitivity of 5 μv/division at higher ΔT and 2 μv/division at lower ΔT.

The heat flux was determined from the relation: rate of change of enthalpy = heat transfer to test section. In calculating the rate of change of enthalpy, a lumped analysis was employed, i.e., it was assumed that the error due to assuming the temperature profile in the section to be independent of time was negligibly small. The justification for this is given in Appendix D, where it is shown that the error in assuming lumped analysis for computing rate of enthalpy change is less than 0.05%. The assumption of lumped analysis is equivalent to saying that the time rate of change of temperature determined at any one location in the test section can be assumed to be valid at all points in the section. In Appendix D one of the assumptions made in justifying this assumption is that the value of the heat transfer coefficient is constant at a given section. Experimental values show that this is approximately the case for film boiling in the range of temperature employed in the present study.

We therefore have

$$m\, C_p(T)\, \frac{d\Delta T}{dt} = q \tag{4.1}$$

or

$$q' = \frac{q}{A} = \frac{m\, C_p(T)}{A}\, \frac{d\Delta T}{dt} \tag{4.2}$$

and

$$h = \frac{q'}{\Delta T} \tag{4.3}$$

To compute the value of q' and h, m, C_p, A, ΔT, and $d\Delta T/dt$ must be determined.

The mass of the test section was determined by weighing the thermocouple after it was made and then weighing the test section-thermocouple combination after attaching the thermocouple to the test section. The area of heat transfer from the test section was determined by measuring the diameter of the test section along two perpendicular diameters and taking the arithmetic average of the two. The thickness of the test sections was measured at four locations. These measurements were made with a vernier calipers reading to 0.001 in. The value of C_p at the appropriate temperature was taken from Reference 58, tabulated values of which are given in Appendix E. The time rate of change of thermocouple output was measured directly from the recorder chart by measuring the local slope and then converted to time rate of change of temperature.

The following sample calculation illustrates the method adopted for reducing heat flux data:

Test Surface 7

Nominal diameter of test piece, 2.25 in.

Test Section, 2

Location of test section, 3 in. above leading edge

Weight of thermocouple, 2.067 gm

Weight of section + thermocouple = 80.619 gm

Weight of test section = 78.552 gm = 0.17317 lb

Thickness of section at four locations = 0.247 in, 0.250 in., 0.254 in., 0.249 in.

Average thickness = 0.250 in.

Diameter at two locations, 2.249 in., 2.250 in

Average diameter = 2.2495 in.

Area of heat transfer = 3.14159 x 2.2495 x 0.250

$= 1.7668 \text{ in.}^2$

$= 0.012269 \text{ ft}^2$

$(\frac{m}{A}) = \frac{0.17317}{0.012269} = 14.114 \text{ lb/ft}^2$

Date: 12/25/69

Run #7004: liquid nitrogen 1/2 psig, saturated

Zero suppression measured with potentiometer = -2050 μv

Sensitivity, 2 μv/div

Speed of chart drive: 25 mm/sec

Reading obtained = 25 div from zero suppression base

Thermocouple output at which data obtained (reference to ice point)

$= -2050 \text{ μv} + \frac{2\text{μv}}{\text{Div}} \times 25 \text{ div} = -2000 \text{ μv}$

Calibration of Thermocouple and Recorder

Thermocouple output in liquid nitrogen from potentiometer, -5521 μv

Barometric pressure, 29.24 in. Hg = 14.4 psi

Liquid nitrogen pressure = 1/2 psig = 14.9 psia

Saturation temperature of LN_2 corresponding to 14.9 psia = 139.4°R

Thermocouple output from standard tables at 139.4°R = -5526 μv

Deviation at - 5526 μv = -5 μv

Standard table thermocouple output at -2000 μv = $-2000 + \frac{-2000}{5521} \times 5$

$= -2001.8$ μv

Temperature corresponding to -2001.8 μv (from standard table) =

390.2°R μv

$\Delta T = T_w - T_s = 390.2 - 139.4 = 250.8°R$

Thermopower at this temperature = $\frac{33.25 \mu v}{°K} = 18.47 \frac{\mu v}{°R}$

Time Rate of Change of Temperature

Thermocouple output change corresponding to 40 divisions on chart

paper at 2 μv/div = 80 μv

Temperature change corresponding to 80 μv = $\frac{80 \ \mu v}{18.47} = 4.33°R$

Time for this change = 3.2 sec

Time rate of change of temperature = $\frac{4.33}{3.2} \times 3600$

$= 4871.2 \frac{°R}{Hr.}$

C_p (390.2°R) = 0.0865/lb °R

$(q/A) = \frac{m}{A} C_p \frac{d\Delta T}{dt}$

$= 14.114 \times 0.0865 \times 4871.2$

$= 5466.1$ Btu/hr ft^2

Data for subcooled and reduced gravity conditions were similary reduced.

F. Measurement of Vapor Film Thickness from Photographic Films

The films were projected on a ground glass with an enlargement of approximately ten times. The film gave a field on the test surface corresponding to a height of approximately 3/4 in.

The diameter of the reference wire was 0.040 in. —and established the scale of the projected image. The film was positioned to project the double exposed image defining the boundary of the test piece heating surface. The pinch marks on the reference wire established the location of the test section in terms of its height from the leading edge. The distance between the reference wire and the edge of the vapor film on the other images was similarly measured and from these measurements the film thickness was computed. In some of the images, it was difficult to define the vapor film boundary precisely, and in such cases the boundary was averaged over the entire image and the thickness measured.

The film thickness was computed at a filming rate of approximately 200 frames/sec after studying the film thickness at 500 frames/sec and 200 frames/sec under identical conditions and establishing that study of films at 200 frames/sec gave all the desired information. The filming rate was established by counting the number of images in the strip and from the fact that these were exposed in a writing time of 1 sec giving approximately 200 frames/sec or 1/2 sec giving approximately 500 frames/sec.

CHAPTER V

MODEL AND ANALYSIS

Several analyses are available for the solution of laminar film boiling with a steady interface and have been described earlier in Chapter I, "Literature Survey"(6, 8-16). Little experimental data are available to support the analyses. The region of validity of such analyses has not been defined and from existing experimental evidence, laminar film boiling with a steady interface is unlikely to be encountered except under unusual circumstances such as very near the leading edge, stagnation points, reduced gravity conditions, etc.

The modelling of film boiling on a vertical surface to predict heat transfer rates is complicated by two main factors:

(a) The probable onset of turbulence and insufficient knowledge to define transition from laminar to turbulent flow regime.

(b) Onset of interfacial oscillations of considerable amplitude. At present there is no way of predicting the amplitudes of interfacial oscillations. It will be shown, later, that these interfacial waves play an important role in enhancing heat transfer rates.

Recognizing these difficulties, an attempt will be made to predict heat transfer rates in film boiling on vertical surfaces using some of the well known and experimentally proven concepts in single phase turbulent flows, taking into consideration the effect of interfacial waves.

A vertical surface, immersed in a liquid at its saturation temperature T_s is maintained at a uniform temperature $T_w > T_s$, inducing film boiling, Figure 12. To find the heat transfer rates, the following assumptions will be made:

(i) The liquid is incompressible; within the range of pressure used the density of the vapor is evaluated at the film temperature, and is assumed constant over the entire vapor film.

(ii) The vapor has constant properties evaluated at the mean vapor film temperature.

(iii) The liquid is uniformly at its saturation temperature and the variation of saturation temperature with height is negligible.

(iv) The increase in enthalpy of the vapor as it flows is negligible compared with the heat transfer to the liquid resulting in vaporization. In other words, the heat transfer rate is constant across the vapor film. It is recognized that this is not strictly true. The effect of increase of enthalpy of vapor, is to reduce heat transfer to the liquid leading to a decrease in the rate of vaporization at the interface. This is usually accounted for by applying a correction factor to the enthalpy of vaporization. Bromley (7) used the correction factor $[1 + 0.4\ C_p \Delta T/h_{fg}]^2$. Frederking and Clark (57) and Dougal and Rohsenow (56) have used the factor $[1 + 0.5\ C_p \Delta T/h_{fg}]$. In turbulent flows, the major part of the vapor can be expected to be at the mean film temperature and hence, for this application the factor $(1 + 0.5\ C_p \Delta T/h_{fg})$ seems to be more appropriate and will be used.

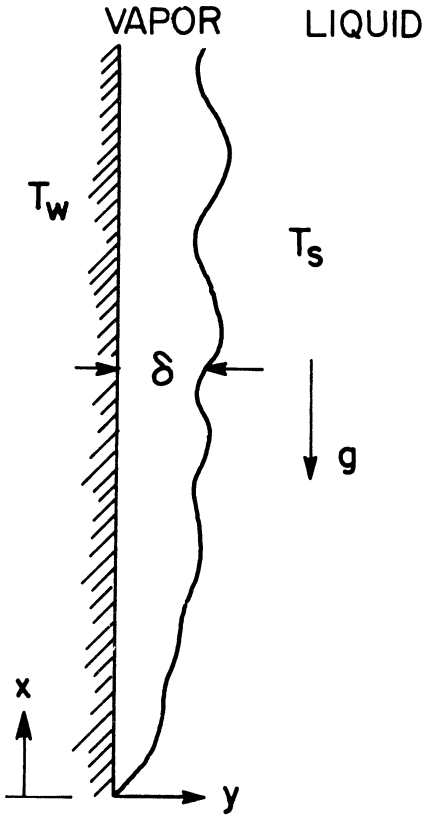

Figure 12. Film boiling model.

(v) Velocity profile and shear stress distribution are not affected by vaporization at the liquid-vapor interface.

(vi) The eddy diffusivities for heat and momentum are equal.

(vii) Steady state prevails and time averaged values can be used for all parameters.

(viii) Heat transfer from the test surface by radiation is negligible and the vapor and liquid are transparent to radiation.

(ix) The interfacial velocity is zero. For laminar vapor flow with a smooth interface, Koh (9) has shown that this is a reasonable assumption if the ratio $[(\rho\mu)_v/(\rho\mu)_\ell]^{1/2}$ is less than 1.0. For most common fluids this condition is satisfied, e.g., for liquid nitrogen and hydrogen these ratios are 0.014 and 0.067, respectively, and hence the interfacial velocity can be neglected in the laminar region. On a qualitative basis, it can be expected that a similar behavior would persist in the turbulent regime also.

(x) Other researchers (39,50) have attempted to seek a parameter to define transition from laminar to turbulent flow. It will be assumed that transition takes place gradually. The universal velocity profile (44) proposed by Spalding is an accepted approximation for single-phase turbulent flows. This will be assumed to be valid for half the vapor film thickness from the heating surface. Coury and Dukler (50) consider the liquid-vapor interface to be rough and have used different velocity profiles for the two halves of the vapor film. However, in the present analysis, from assumption (v), its mirror image will be assumed to be applicable to the other half of the vapor film adjacent to the interface. The velocity profile is expressed as

$$y^+ = u^+ + \frac{1}{E}\left[e^{ku^+} - 1 - ku^+ - \frac{(ku^+)^2}{2!} - \frac{(ku^+)^3}{3!} - \frac{(ku^+)^4}{4!}\right]$$

$$= F_1(u^+) \qquad (5.1)$$

with k = 0.407, and 1/E = 0.0991. For small values of u^+, this may be approximated to $y^+ = u^+$ implying a linear velocity profile. For large values of u^+, Eq. (5.1) can be approximated to

$$y^+ \simeq \frac{1}{E} e^{ku^+} \quad \text{or}$$

$$u^+ \simeq 5.7 + 2.5 \ln y^+$$

which is the well known logarithmic velocity profile. Figure 13 shows the close correspondence between this velocity profile and Von Karman's three-layer model (48). The main difference lies in the fact that very close to the wall, Von Karman's profile assumes a total absence of turbulent effects. Diessler (53) proposed that this assumption of turbulence effects disappearing at an arbitrary distance from the wall is unrealistic and proposed his velocity profile valid for $y^+ \leq 26$ which rendered $\epsilon_M \to 0$ as $y^+ \to 0$; beyond $y^+ = 26$, Diessler used the logarithmic velocity profile. Spalding combined these concepts of Diessler and proposed his velocity profile given by Eq. (5.1).

The assumption that this expression is valid for all values of film thickness thus yields an approximately linear velocity profile for thin films—near the leading edge or close to the heating surface, where viscous effects may be expected to be dominant and hence the flow more nearly laminar, and a logarithmic velocity profile for large values of film thickness away from the leading edge and heating surface.

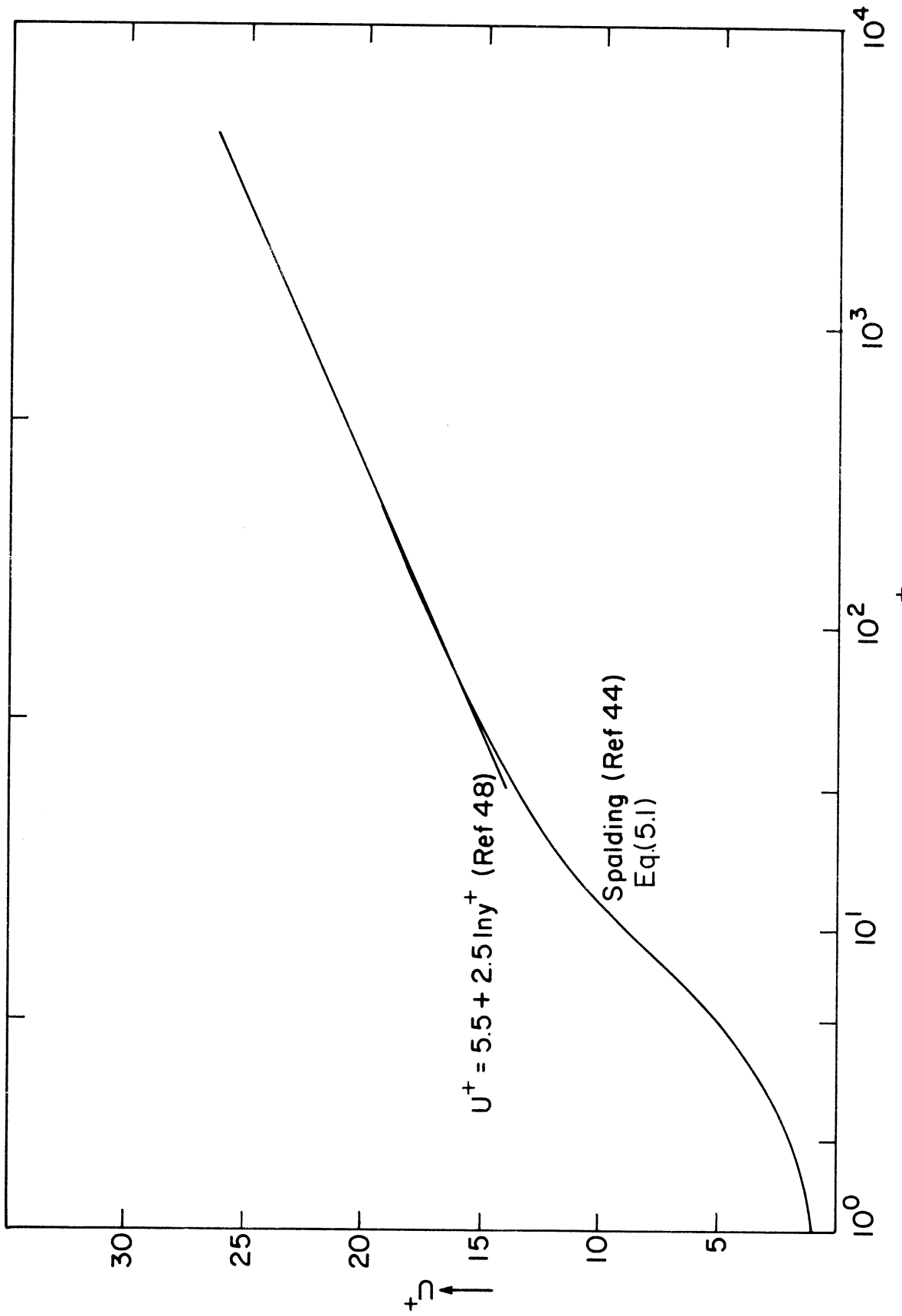

Figure 13. Comparison of Spalding's universal velocity profile and Karman's three-layer model.

(xi) It has been observed that, in general, the interface is not steady but that it oscillates with considerable amplitude—of the order of vapor film thickness. It may be anticipated that the influence of these oscillations on the heat transfer rates is considerable and must be taken into account. As little is known about the effect of such oscillations on the temperature and velocity profiles, the following simple approach will be adopted in an attempt to take into consideration the interfacial oscillations. It will be assumed that the dimensionless temperature profile is unaffected by the oscillations. This can be expressed as

$$\Phi = \frac{T_w - T}{T_w - T_s} = f(\eta); \quad \eta = \frac{y}{\delta}$$

with

$$\eta = 0 \qquad \Phi = 0 \qquad f(0) = 0$$

$$\eta = 1 \qquad \Phi = 1 \qquad f(1) = 1$$

and

$$q' = \frac{q}{A} = -k \frac{dT}{dy}\bigg|_{y=0} = k \Delta T f'(0) \frac{d\eta}{dy}\bigg|_{y=0} \tag{5.2}$$

Consider the case with a steady interface where δ is not a function of time, denoted by $\delta(s)$ and the corresponding heat flux by $q'(s)$. Then

$$q'(s) = k \Delta T f'(0) \frac{1}{\delta(s)}$$

It may be noted that $f(\eta)$ is independent of time and hence $f'(0)$ is a constant.

Let δ now be a function of time denoted by $\delta(t)$. Since the nature of the oscillation is not known, it is assumed to oscillate sinusoidally about the above mean value $\delta(s)$ so that

$$\delta(t) = \delta(s) + a \sin \omega t$$

$$= \delta(s) [1 + b \sin \omega t]$$

Here

a = amplitude of oscillations

b = dimensionless amplitude $\frac{a}{\delta(s)}$

$\frac{\omega}{2\pi} = f$ = frequency of oscillations

Then, $q'(t)$, the instantaneous heat transfer is given by

$$q'(t) = k \Delta T f'(0) \frac{1}{\delta(t)}$$

$$= \frac{k \Delta T f'(0)}{\delta(s)} \frac{1}{1 + b \sin \omega t} \tag{5.3}$$

Replacing

$\frac{k \Delta T f'(0)}{\delta(s)}$ by $q'(s)$,

$$q'(t) = \frac{q'(s)}{1 + b \sin \omega t} \tag{5.4}$$

The time averaged value of the heat flux is then obtained by

$$\overline{q'(t)} = \frac{\omega}{2\pi} \int_0^{2\pi/\omega} \frac{q'(s)}{1 + b \sin \omega t} dt$$

$$= \frac{q'(s)}{\sqrt{1 - b^2}} = C\, q'(s) \tag{5.5}$$

with

$$C = \frac{1}{\sqrt{1 - b^2}} \qquad (5.5a)$$

The coefficient C is an indication of the extent of increase in heat transfer due to interfacial oscillations and may be termed the heat transfer enhancement coefficient. The maximum limiting value of "b" is unity, when the liquid comes in contact with the heating surface(at which point the "film boiling" model breaks down). Its minimum value is zero, giving a steady interface. In general, $0 \leq b \leq 1$ and the value of the coefficient $C \geq 1$.

Thus the effect of interfacial oscillations is to increase the heat flux as compared with a steady interface. This is also confirmed by Coury and Dukler (50) who measured the instantaneous heat transfer rates. There is, as yet, no way to predict the amplitude of oscillations from first principles and the value of "C" must be found by some other means. One possibility is to compute it from measurements of vapor film thickness, and another is to determine it empirically from measurements of heat flux. This is discussed in detail under Chapter VI, "Results and Discussions."

(xii) For the vapor film, boundary layer equations are applicable and $p = p(x)$. In particular, $p \neq p(y)$.

With these assumptions we have, from the velocity profile

$$y^+ = u^+ + \frac{1}{E}\left[e^{ku^+} - 1 - ku^+ - \frac{(ku^+)^2}{2!} - \frac{(ku^+)^3}{3!} - \frac{(ku^+)^4}{4!}\right] \qquad (5.1)$$

From the expression for shear stress we have

$$\frac{\tau}{\rho} = \nu\left[\frac{\epsilon_M}{\nu} + 1\right]\frac{du}{dy}$$

or

$$\frac{\epsilon_M}{\nu} = \frac{dy^+}{du^+} - 1$$

$$= \frac{k}{E}\left[e^{ku^+} - 1 - ku^+ - \frac{(ku^+)^2}{2!} - \frac{(ku^+)^3}{3!}\right] = F_2(u^+) \qquad (5.6)$$

From assumption (vi) we have

$$\frac{\epsilon_H}{\nu} = \frac{\epsilon_M}{\nu} = F_2(u^+) \qquad (5.7)$$

From assumption (iv) the differential form of energy equation takes the form

$$\frac{q'}{\rho C_p} = \frac{q'_w}{\rho C_p} = -(\epsilon_H + \alpha)\frac{dT}{dy}$$

$$= -\nu\left[\frac{\epsilon_H}{\nu} + \frac{1}{Pr}\right]\frac{dT}{dy} \qquad (5.8)$$

Letting

$$\theta^+ = \frac{\rho C_p u^*(T_w - T)}{q'(s)} \qquad (5.9)$$

and, for $T = T_s$

$$\theta_w^+ = \frac{\rho C_p u^*(T_w - T_s)}{q'(s)} \qquad (5.9a)$$

and substituting Eq. (5.9) in Eq. (5.8) we get

$$\frac{d\theta^+}{dy^+} = \frac{1}{\epsilon_H/\nu + \frac{1}{Pr}} \qquad (5.10)$$

Noting, from Eq. (5.1)

$$dy^+ = 1 + \frac{k}{E}\left[e^{ku^+} - 1 - (ku^+) - \frac{(ku^+)^2}{2!} - \frac{(ku^+)^3}{3!}\right] = F_3(u^+) \quad (5.11)$$

we get

$$\frac{d\theta^+}{du^+} = \frac{F_3(u^+)}{F_2(u^+) + \frac{1}{Pr}} \quad (5.12)$$

It has been assumed that the velocity profile and shear stress distribution are not influenced by conditions at the interface and this leads to a symmetric velocity distribution, with the velocity distribution in $\delta/2 \leq y \leq \delta$ being the mirror image of that in $0 \leq y \leq \delta/2$. Similarly, for the temperature we expect the temperature profile for θ^+ in $\delta/2 \leq y \leq \delta$ to be the inverted mirror image of that in $0 \leq y \leq \delta/2$. These profiles are indicated in Figure 14. From a consideration of these profiles we expect the temperature at $y = \delta/2$ to be $(T_w + T_s)/2$. Denoting the corresponding dimensionless temperature by $\theta_w^+/2$, Eq. (5.12) can be integrated to yield

$$\theta_w^+ = 2\int_0^{u_M^+} \frac{F_3(u^+)}{F_2(u^+) + \frac{1}{Pr}}\, du^+ \quad (5.13)$$

where u_M^+ is the value of u^+ at $y^+ = \delta^+/2$. It may be noted that since $F_3(u^+) = F_2(u^+) + 1$, for $Pr = 1$, the temperature profile is identical with the velocity profile in $0 \leq y \leq \delta/2$ and is the inverted image of it in $\delta/2 \leq y \leq \delta$. From conservation of mass, for the control volume with its boundaries in the vapor, Figure 15A we have

$$\frac{d}{dx}\int_0^{\delta} \rho u dy = \dot{m} \quad (5.14)$$

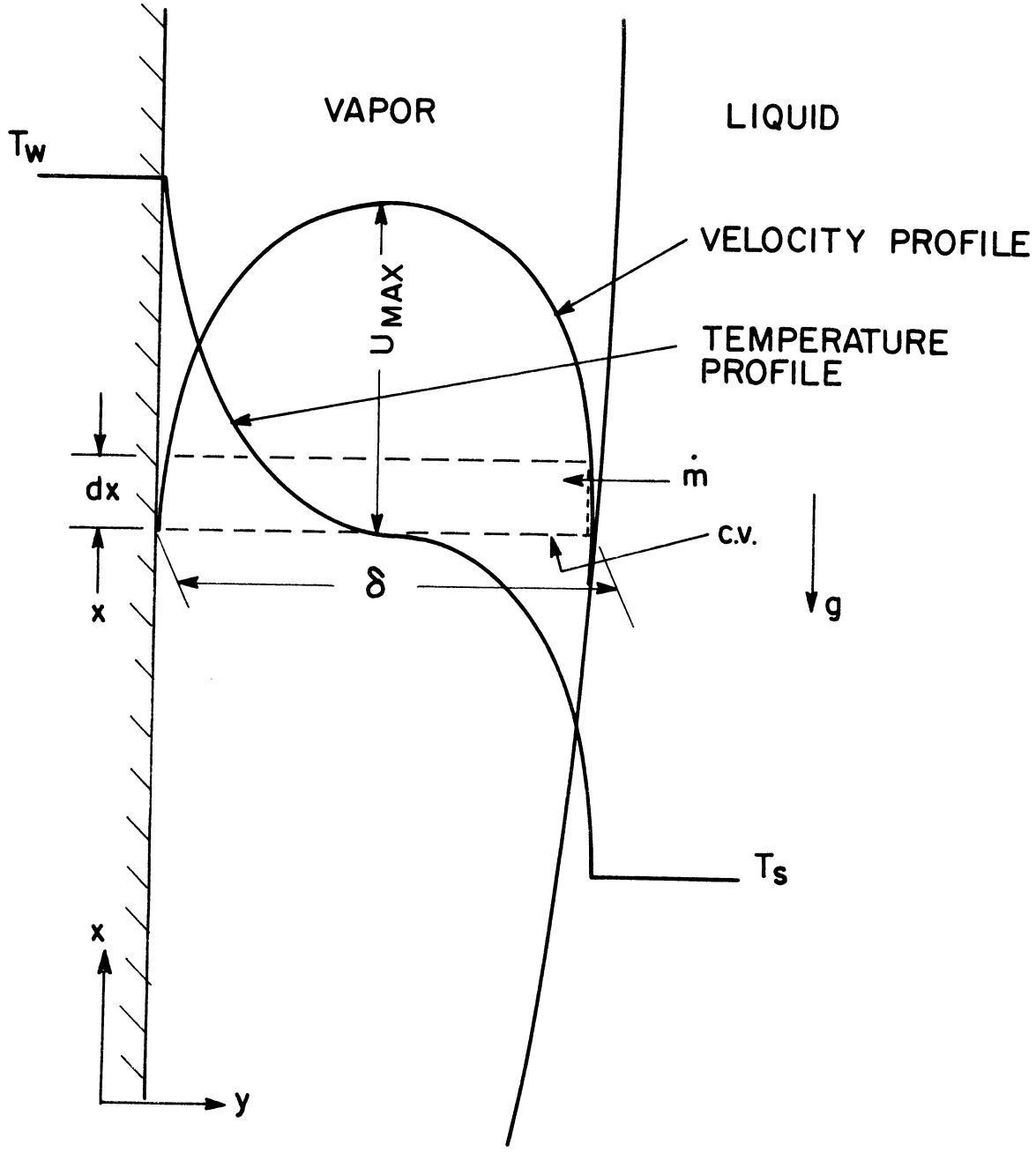

Figure 14. Velocity and temperature profiles in vapor film.

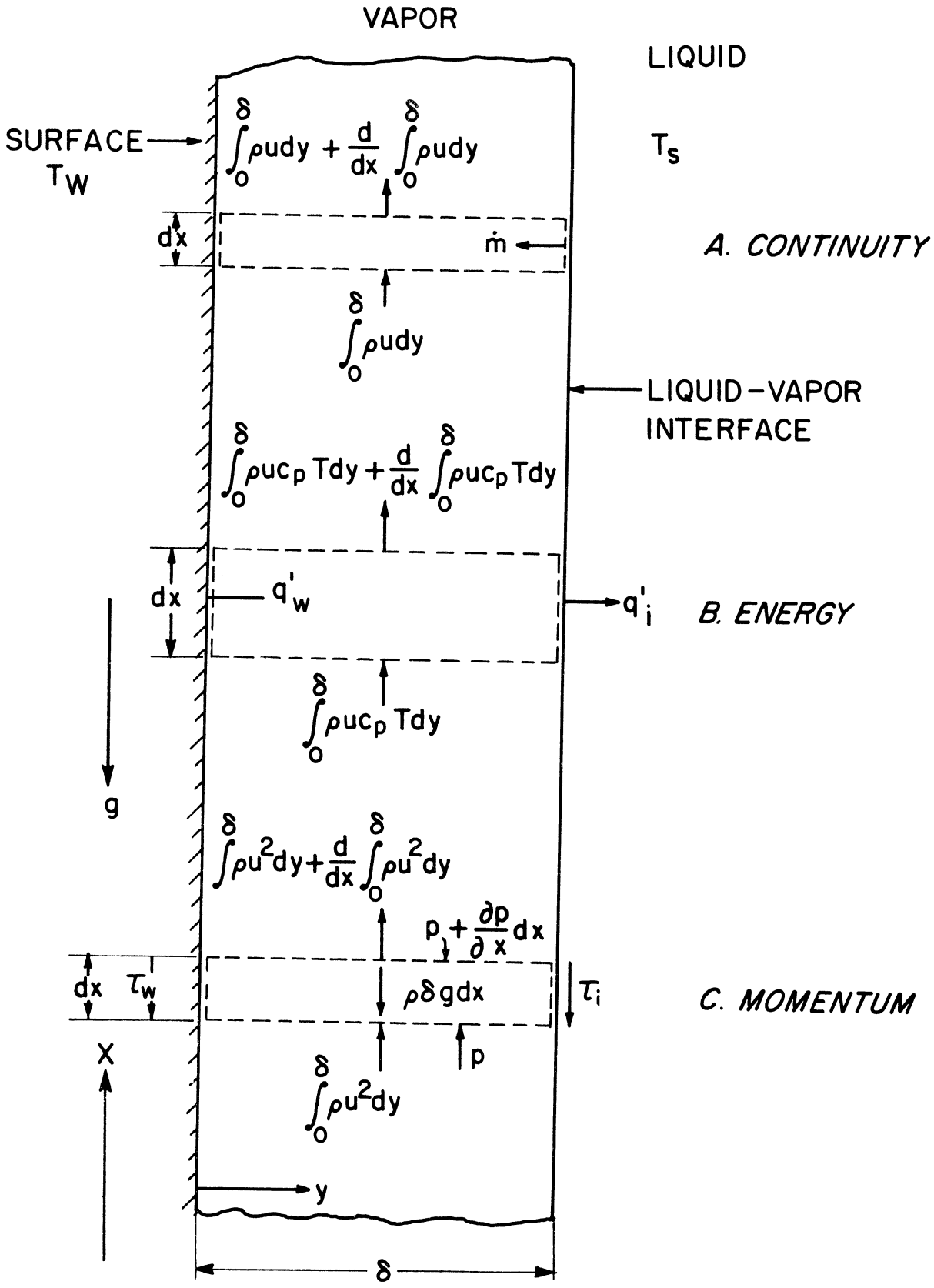

Figure 15. Control volume—film boiling.

where $\dot{m}$ = rate of mass crossing from the liquid-vapor interface into the control volume in the vapor space. To evaluate $\dot{m}$ we have from conservation of energy for a steady flow process, control volume—Figure 15B,

$$\Sigma H_{in} + \Sigma q_{in} = \Sigma H_{out} - W_s$$

where

H_{in} = enthalpy flow into the control volume

H_{out} = enthalpy flow out from the C.V.

q_{in} = heat transfer into the C.V.

all enthalpy terms are referenced above the saturation temperature of vapor.

W_s = shaft work

Applying this to the control volume (and noting that $W_s = 0$) we get per unit width in the z-direction

$$\int_0^\delta \rho u C_p T \, dy + q'_w \, dx - q'_i \, dx$$

$$= \int_0^\delta \rho u C_p T \, dy + \frac{d}{dx} \int_0^\delta \rho u C_p T \, dy \, dx \qquad (5.15)$$

Here q'_w = heat flux from the heating surface and

q'_i = heat flux from the vapor to the liquid at the interface

causing mass flux $\dot{m}$ to cross into the vapor space by evaporation of the liquid. Replacing q'_i by $\dot{m} h_{fg}$ we obtain

$$q'_w = \dot{m} h_{fg} + \frac{d}{dx} \int_0^\delta \rho u C_p T \, dy \qquad (5.16)$$

The last term in Eq. (5.16) represents the increase in enthalpy of the vapor that enters the C.V. at x which for fully developed temperature profile is zero, and the increase in enthalpy of the mass m in crossing the C.V. at the liquid-vapor interface. A correction to take the latter into account has been made by using the modified value h'_{fg} in place of h_{fg}, so that Eq. (5.16) takes the form

$$\dot{m} = \frac{q'_w}{h'_{fg}} = \frac{\overline{q'(t)}}{h'_{fg}} \tag{5.17}$$

The L.H.S. of (5.14), after changing the variables, yields

$$\begin{aligned}
\frac{d}{dx}\int_0^{\delta} \rho u dy &= 2\frac{d}{dx}\rho\nu \int_0^{\delta^+/2} u^+ dy^+ \\
&= 2\frac{d}{dx}\rho\nu \int_0^{u_M^+} u^+ F_3(u^+)\, du^+ \\
&= 2\rho\nu \left[u_M^+ + \frac{1}{E}\left(ku_M^+ e^{ku_M^+} - ku_M^+ - (ku_M^+)^2 \right.\right. \\
&\quad \left.\left. - \frac{(ku_M^+)^3}{2!} - \frac{(ku_M^+)^4}{3!} \right) \right] \frac{du_M^+}{dx} \\
&= 2\rho\nu\, F_4(u_M^+) \frac{du_M^+}{dx}
\end{aligned} \tag{5.18}$$

with

$$F_4(u_M^+) = u_M^+ + \frac{1}{E}\left(ku_M^+ e^{ku_M^+} - (ku_M^+) - (ku_M^+)^2 - \frac{(ku_M^+)^3}{2!} - \frac{(ku_M^+)^4}{3!} \right) \tag{5.18a}$$

Substituting Eqs. (5.17) and (5.18) into (5.14), we get

$$\frac{du_M^+}{dx} = \frac{1}{F_4(u_M^+)} \frac{\overline{q'(t)}}{2h'_{fg}\rho\nu} \tag{5.19}$$

Momentum equation applied to the control volume, Figure 15C consistant with assumption (xii) gives

$$2\frac{d}{dx}\int_0^{\delta/2}\rho u^2 dy = -\frac{dp}{dx}\delta - \tau_i - \tau_w - \rho g\delta \tag{5.20}$$

L.H.S. of Eq. (5.20) $= 2\frac{d}{dx}\int_0^{\delta/2}\rho u^2 dy$

$$= 2\frac{d}{dx}\int_0^{u_M^+}\rho u^* \nu\, u^{+2} F_3(u^+)\, du^+$$

$$= 2\rho\nu F_5(u_M^+)\frac{du^*}{dx} + 2\rho\nu\, u^* F_6(u_M^+)\frac{du_M^+}{dx} \tag{5.21}$$

where

$$F_5(u_M^+) = \int_0^{u_M^+} u^{+2} F_3(u^+)\, du^+$$

$$= \frac{(u_M^+)^3}{3} + \frac{1}{k^2 E}\left[(ku_M^+)^2 e^{ku_M^+} - 2\,ku_M^+ e^{ku_M^+} + 2e^{ku_M^+}\right.$$

$$\left. - 2 - \frac{(ku_M^+)^3}{3} - \frac{(ku_M^+)^4}{4} - \frac{(ku_M^+)^5}{10} - \frac{(ku_M^+)^6}{36}\right] \tag{5.22}$$

and

$$F_6(u_M^+) = u_M^{+2} F_3(u_M^+) \tag{5.23}$$

From assumption (xii) we have

$$\left(\frac{dp}{dx}\right)_{\text{vapor}} = \left(\frac{dp}{dx}\right)_{\text{liquid}} = -\rho_\ell g \tag{5.24}$$

From assumption (v) we have

$$\frac{\tau_i}{\rho} = \frac{\tau_w}{\rho} = u^{*2} \tag{5.25}$$

From Eq. (5.1) and definition of δ^+, we obtain

$$\frac{\delta}{2} = \frac{\nu}{u^*}\frac{\delta^+}{2} = \frac{\nu}{u^*} F_1(u_M^+) \tag{5.26}$$

Combining Eqs. (5.20), (5.21), (5.24), (5.25), and (5.26), we obtain

$$F_5(u_M^+)\frac{du^*}{dx} + u^* F_6(u_M^+)\frac{du_M^+}{dx} = \left(\frac{\rho_\ell - \rho}{\rho}\right) g \frac{F_1(u_M^+)}{u^*} - \frac{u^{*2}}{\nu} \tag{5.27}$$

We thus end up with a system of equations to be solved, given by Eqs. (5.5), (5.9a), (5.13), (5.19), and (5.27) repeated below in sequence for convenience, and redesignated as Eqs. (5.28).

$$\left.\begin{aligned}
\overline{q'(t)} &= C\, q'(s) \\
q'(s) &= \frac{\rho C_p u^*(T_w - T_s)}{\theta_w^+} \\
\theta_w^+ &= 2\int_0^{u_M^+} \frac{F_3(u^+)}{F_2(u^+) + \frac{1}{Pr}}\, du^+ \\
\frac{du_M^+}{dx} &= \frac{1}{F_4(u_M^+)} \frac{\overline{q'(t)}}{2h'_{fg}\,\rho\nu} \\
F_5(u_M^+)\frac{du^*}{dx} + u^* F_6(u_M^+)\frac{du_M^+}{dx} &= \frac{(\rho_\ell - \rho)}{\rho} g \frac{F_1(u_M^+)}{u^*} - \frac{u^{*2}}{\nu}
\end{aligned}\right\} \tag{5.28}$$

Here the forms of the functions F_1, F_2, F_3, F_4, F_5, and F_6 are given by Eqs. (5.1), (5.6), (5.11), (5.18a), (5.22), and (5.13). For the solution of the above system of equations, it is necessary to have the value of the heat transfer enhancement coefficient C and the values of u_M^+ and u^* at some location $x = x_o$ (say).

The value of the coefficient can be expected to be a function of both ΔT and the height x for a given liquid. It may be expected that the dimensionless amplitude of oscillations is relatively small near the leading edge where interfacial instabilities begin to appear, increasing with height thereafter. There are no known ways of determining its value and recourse will have to be taken to find its value by some semi-empirical relationship between C and another known parameter based on experimental results. A more detailed discussion on the value of C and its variation with height is contained in Chapter VI. For the present it is assumed that the function $C = C(x)$ is known.

To initialize the values of u^* and u_M^+, Bromley's correlations (6) were used. From his solution we have

$$u = \frac{A\delta^2}{2}(\eta - \eta^2) \tag{5.29}$$

with $A = \frac{\rho_\ell - \rho}{\rho}\frac{g}{\nu}$; $\eta = \frac{y}{\delta}$

$$u_{max} = \frac{A\delta^2}{8} \tag{5.30}$$

$$\delta = \left[\frac{16\, k\, \Delta T\, x}{\rho\, h'_{fg}\, A}\right]^{\frac{1}{4}} \tag{5.31}$$

$$\tau_w = \mu \left.\frac{du}{dy}\right|_{y=0} = \frac{\rho_\ell - \rho}{\rho}\frac{g}{\nu}\frac{\mu\delta}{2} \tag{5.32}$$

Recasting these we obtain

$$u^* = \sqrt{\frac{\tau_w}{\rho}} = \left[\frac{\rho_\ell - \rho}{\rho}\, g\, \frac{\delta}{2}\right]^{1/2} \tag{5.33}$$

$$u_M^+ = \frac{u_{max}}{u^*} = \frac{A\delta^2}{8}\left[\frac{\rho}{\rho_\ell - \rho}\frac{2}{g\delta}\right]^{\frac{1}{2}}$$

$$= 0.177\left[\frac{\rho_\ell - \rho}{\rho}\, g\right]^{\frac{1}{8}} \nu^{-\frac{5}{8}}\left[\frac{16\, k\, \Delta T\, x}{\rho\, h'_{fg}}\right]^{\frac{3}{8}} \qquad (5.34)$$

From Eqs. (5.31), (5.33), and (5.34), the values of u_M^+ can be calculated for any given value of x and the numerical integration of the system of Eqs. (5.28) can proceed. These nonlinear equations were numerically solved on an IBM 360 computer using Runga Kutta procedure. In the actual solution the numerical procedure was started with $u_M^+ = 2$ and the corresponding values of x and u* computed.

CHAPTER VI

RESULTS AND DISCUSSIONS

A. Validity of Experimental Technique

The objective of the present work was to obtain local heat transfer rates in film boiling on a plane vertical surface. To eliminate the edge effects in finite plane surfaces, cylindrical surfaces were used; to obtain local heat flux values, the time rate of change of enthalpy of the test surface was computed. Neglecting heat transfer by radiation, it was assumed that this change in enthalpy was due solely to heat transfer to the surrounding saturated liquid. The validity of the use of a cylindrical surface under transient conditions to give data for plane surface under steady state conditions and the assumption of negligible radiation from the surface will now be examined.

1. SIMULATION OF A PLANE SURFACE BY A CYLINDRICAL SURFACE

The principal differences between a cylindrical surface and a plane surface arise from two sources: effect of surface tension and the change in area with radius.

Within the vapor film, surface tension is of no consideration. At the interface, however, its effects on the pressure within the vapor film should be considered as cylindrical test surfaces were used. One of the assumptions in the analysis is that the pressure in the vapor film is a function of the height x only and does not vary in a horizontal plane. But at the interface, because

of the curvature of the test surface, surface tension introduces a pressure difference between the liquid and the vapor, whose magnitude is given by

$$\Delta P^{\sigma} = \sigma\left(\frac{1}{R_H} + \frac{1}{R_V}\right) \tag{6.1}$$

where R_H and R_V are the principal radii of curvature. One of the principal radii of curvature will be taken to be the minimum radius of the test surface equal to 0.5 in. in the present experiments. The curvature in the vertical plane is caused by the thickening of the vapor film and interfacial waves. There is some difficulty in estimating the value of R_V but for simplicity it will be arbitrarily set equal to R_H so that $\Delta P^{\sigma} = 2\sigma/R_H$. For nitrogen σ = 8.8 dynes/cm = 63.4 x 10^{-5} lbf/ft so that ΔP^{σ} = 3.04 x 10^{-2} lbf/ft^2. For hydrogen σ = 8.8 dynes/cm = 14.4 x 10^{-5} lbf/ft so that ΔP^{σ} = 0.692 x 10^{-2} lbf/ft^2. The lowest pressure at which the experiments were run was = 14.7 psia (2140 lbf/ft^2) so that in comparison with this pressure, the change in pressure at the interface due to surface tension is, indeed, negligible.

It is possible that at the leading edge R_H is small and ΔP^{σ} is of some significance. But such effects at the leading edge are ignored as, in any case, they are confined to a very small height from the leading edge.

The change in area with radius can be ignored if the ratio of the vapor film thickness to the radius of the heating surface δ/r is much less than unity. From the solution to the system of Eqs. (5.28) resulting from the present analysis, the value of this ratio δ/r lies between 0.1 and 0.05. From the results of the photographic studies it has a value between 0.1 and 0.2.

To show that the geometrical effects of using a cylindrical test surface as compared with a plane surface are negligible, reference is made to Figure 16 where heat flux values obtained from 1 in. dia. cylindrical test surfaces and those obtained from 2-1/4 in. dia test surfaces at the common location of 3 in. above the leading edge are represented. Each data point in Figure 16 represents the mean of a number of runs made with a test surface, the number of such runs being indicated next to each data point. The range of values obtained with each surface is indicated by a vertical line, passing through the point, the extremities of which represent the maximum and minimum values obtained with the test surface. If the geometry of the test surface had any appreciable effect on heat transfer rates, heat flux values obtained with 2-1/4 in. dia test surfaces would have been considerably different from those obtained with 1 in. dia test surfaces. Within the scatter of experimental data, heat flux values obtained with 2-1/4 in. dia test surface agree with those obtained with 1 in. dia test surfaces and it is concluded that for the present applications, the use of cylindrical surfaces of 1 in. dia and above do not introduce any significant errors due to effects of geometry and surface tension as compared with a plane surface.

2. USE OF TRANSIENT TECHNIQUE TO OBTAIN STEADY STATE DATA

To estimate the effect of employing a transient technique to obtain data under steady state conditions, consider the energy equation in its simplified form consistent with the assumptions made in Chapter V, "Model and Analysis." The differential form of the energy equation for the transient case (as

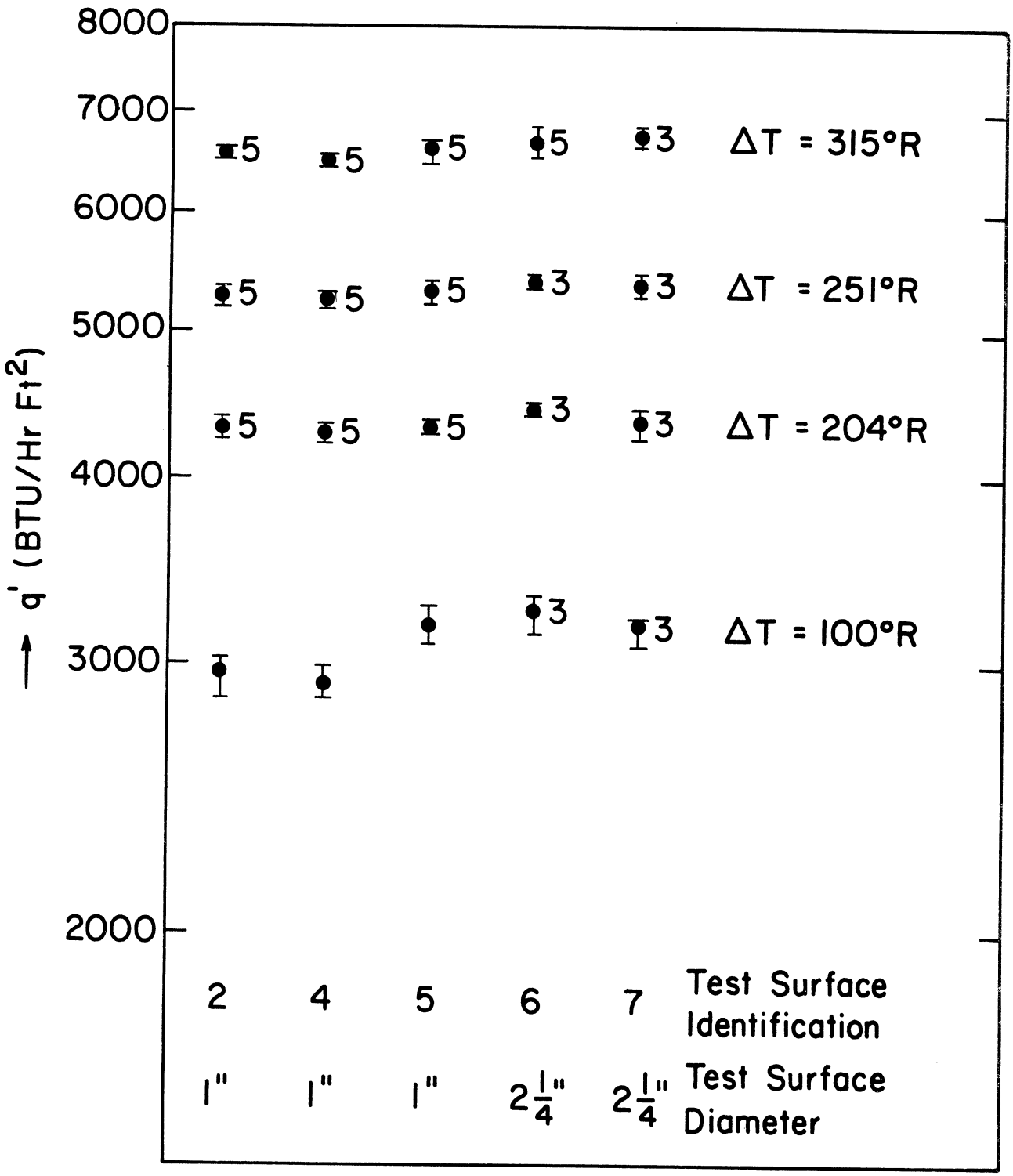

Figure 16. Comparison of heat flux—1 in. dia and 2-1/4 in. dia heating surfaces.

opposed to the steady case resulting in Eq. (5.8) takes the form

$$\frac{\partial T}{\partial t} = \frac{1}{\rho C_p} \frac{\partial q'_y}{\partial y} \tag{6.2}$$

If, in the nondimensional form of Eq. (6.2), the time rate of change of temperature is shown to be small compared to unity, the transient technique can be expected to give results close to that under steady state conditions. For nondimensionalizing the different variables, the characteristic temperature will be taken to be ΔT, the difference between the heater surface temperature and the saturation temperature of the boiling liquid. The characteristic time will be based on a representative length and a representative velocity. The choice of a representative length will be the height of the test piece L. In the turbulent regime, the average velocity is close to the max-velocity and hence an arbitrary value of $0.75\ U_{max}$ will be taken to be the characteristic velocity. With these nondimensional parameters, we have

$$\theta = \frac{T}{\Delta T} \qquad \tau = \frac{t}{L/u}$$

$$Q = \frac{q'_y}{\rho C_p u \Delta T} \qquad Y = y/L \tag{6.3}$$

and

$$\frac{\partial \theta}{\partial \tau} = \frac{\partial Q}{\partial Y} \tag{6.4}$$

If $\partial\theta/\partial\tau \ll 1$, $\partial Q/\partial Y$ can be assumed to be zero, which is the steady state condition. To find the value of $\partial\theta/\partial\tau$, we note that at Y = 0, the vapor undergoes the greatest time rate of change of temperature (equal to that of the test surface) since the temperature of the other boundary—the liquid-remains constant at its saturation value. Computed values of $\partial\theta/\partial\tau$ are given in Table VI.

TABLE VI

TRANSIENT TECHNIQUE—RATE OF CHANGE OF DIMENSIONLESS TEMPERATURE

Liquid	$\Delta T(^\circ R)$	u (ft/hr)	L(ft)	$\frac{\partial T}{\partial t}\left(\frac{^\circ R}{hr}\right)$	$\frac{\partial\theta}{\partial\tau}$
LN_2	315	66,000	0.5	9,000	0.00022
LN_2	100	45,000	0.5	5,700	0.00055
LH_2	400	90,000	0.5	24,000	0.00033
LH_2	100	45,000	0.5	10,000	0.0011

In Table VI, u is taken as 0.75 u_{max}, with u_{max} obtained from the solutions of Eqs. (5.28). $\partial T/\partial t$ values are experimental values. From these computations it is seen that the nondimensional time rate of change of temperature is indeed small and hence the transient technique employed in the present experiments can be expected to give acceptable equivalent steady state results.

To further test the validity of the transient technique employed in the present work to give data under steady conditions, comparison will be made between heat flux values obtained under these two conditions.

Column "A" in Table VII gives average heat flux values obtained with the steady state test surface used for photographic studies described in Section A-2, Chapter II. This test surface was one continuous piece and hence it is possible to measure only the overall mean heat transfer rate. Column "B" gives the integrated heat flux values computed by using the local heat transfer rates obtained with the transient technique. These two are seen to agree quite well, thus indicating that employing the transient technique to obtain steady state values is acceptable.

TABLE VII

COMPARISON OF HEAT FLUX VALUES OBTAINED UNDER STEADY STATE CONDITIONS AND TRANSIENT CONDITIONS LIQUID NITROGEN

ΔT, °R	A (Steady State Btu/hr ft^2)	B (Transient Btu/hr ft^2)
315	7050-7350	7011
200	4690	4692
100	3400	3543

3. HEAT TRANSFER BY RADIATION

It is assumed that the vapor is transparent to radiant heat flux from the ambient or the heater surface. In order to assess the heat transfer by radiation from the test surface, several conservative assumptions will be made. In the present series of experiments relatively low heater surface temperatures

of the order of 500°R were used. The heater surface was immersed in liquid nitrogen or liquid hydrogen, and to obtain the upper limit of heat transfer by radiation an ambient temperature of 0°R will be assumed. For copper, values of 0.01-0.07 Btu/hr ft^2 $°R^4$ are given for the emissivity (37), the lower value being for polished surface and the higher value for "commercial, scraped shiny but not mirror-like" surface. The test surfaces used were given "mirror-like" finish but again, to find the upper limit, the higher value for emissivity will be used. With these values, for a test surface temperature of 500°R, we have

$$q'_{\text{Radiation}} = 0.072 \times 0.1713 \times 10^{-8} \times 500^4$$

$$= 7.7 \text{ Btu/hr ft}^2$$

For lower temperatures, these are much lower and for all surface temperatures used, this forms less than 0.1% of the computed heat flux and therefore ignored.

B. Results

Figures 17-26 are plots of experimental values of heat flux q' vs. height of the test surface. Each of Figures 17-24 includes:

(i) Experimental data for one value of ΔT. The data point is the mean of several runs under identical conditions, the vertical line through each point showing the maximum and minimum of experimental values obtained.

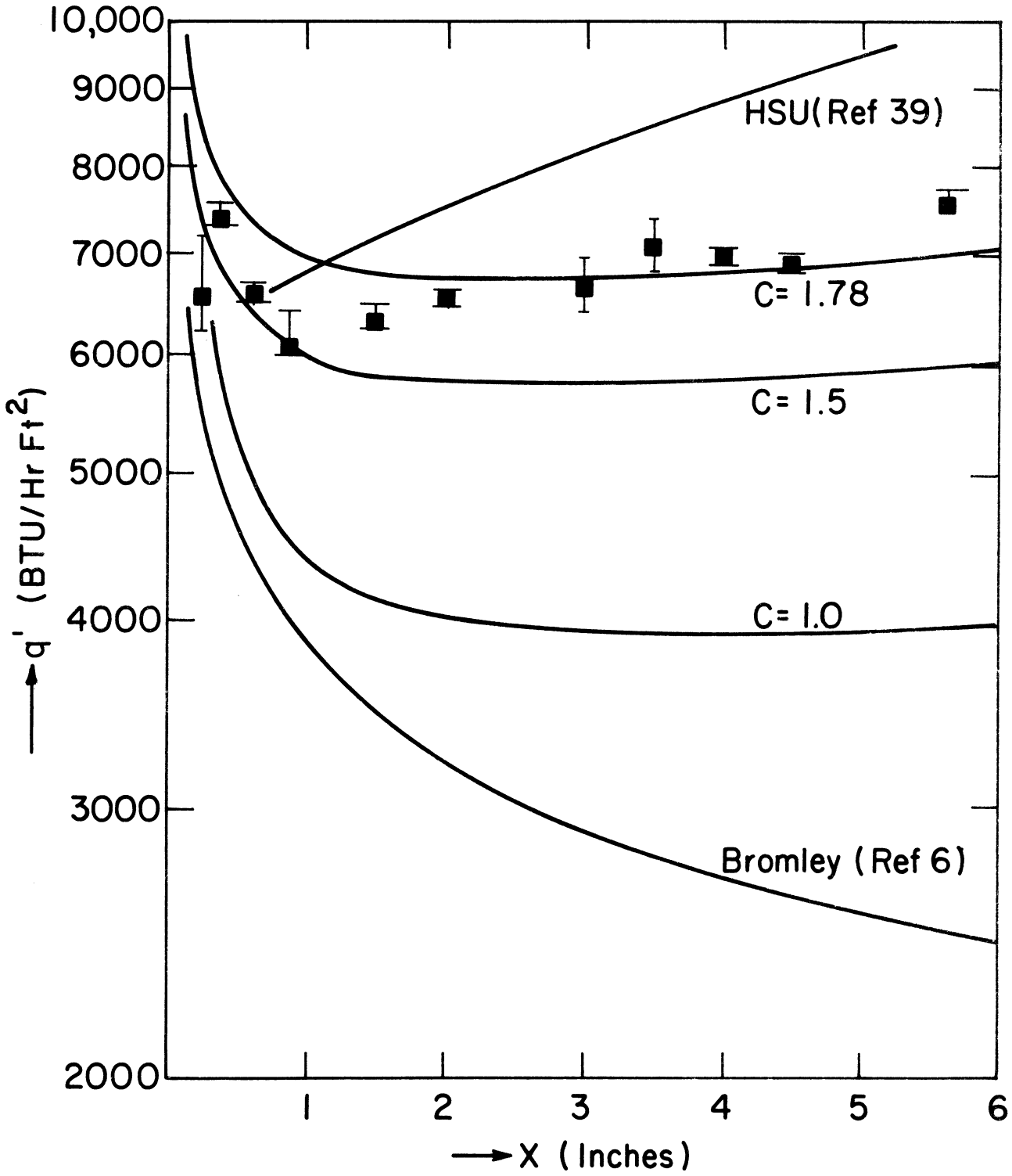

Figure 17. Effect of height on heat flux—film boiling. LN_2. ΔT = 315°R.

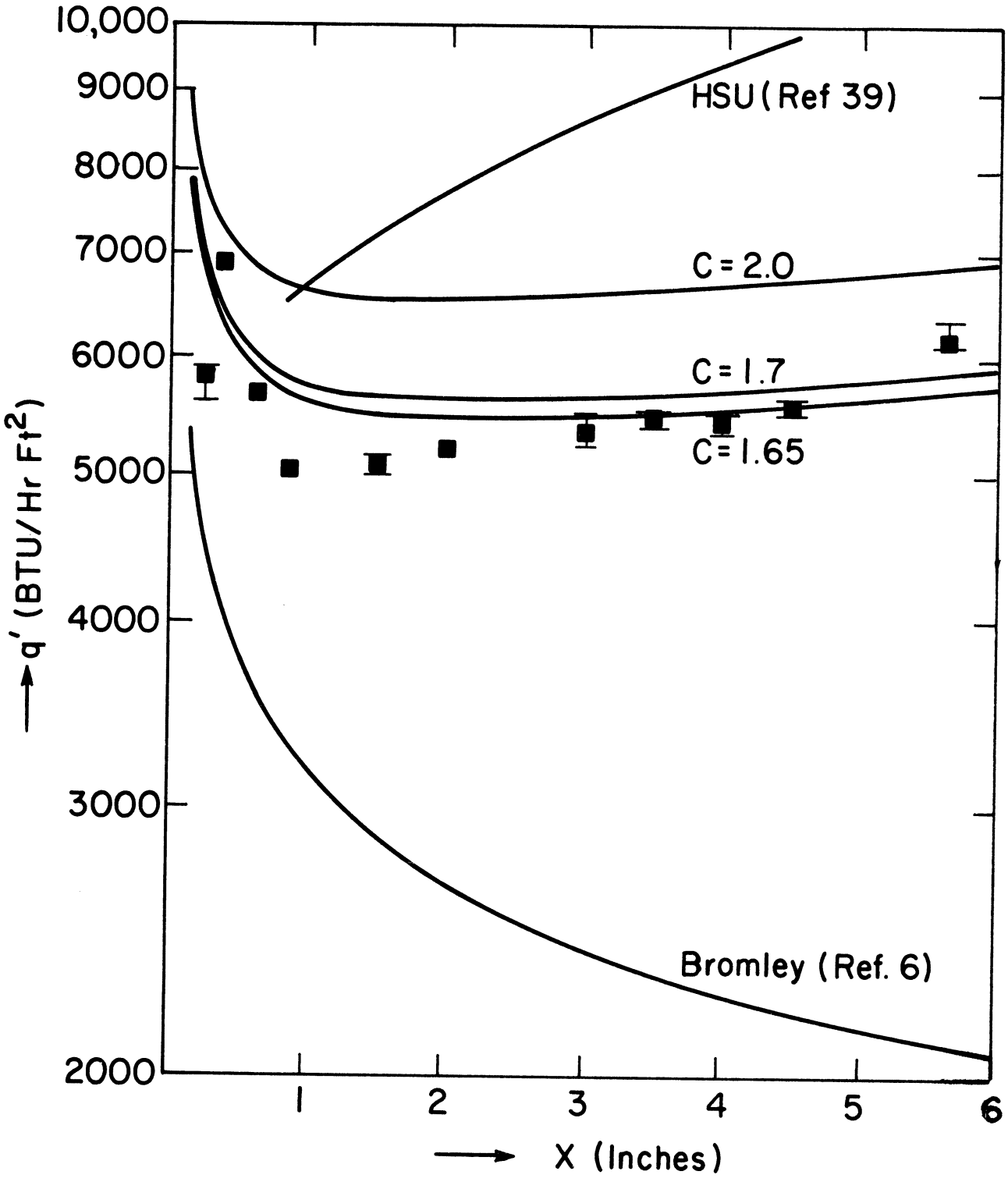

Figure 18. Effect of height on heat flux—film boiling. LN_2. ΔT = 251°R.

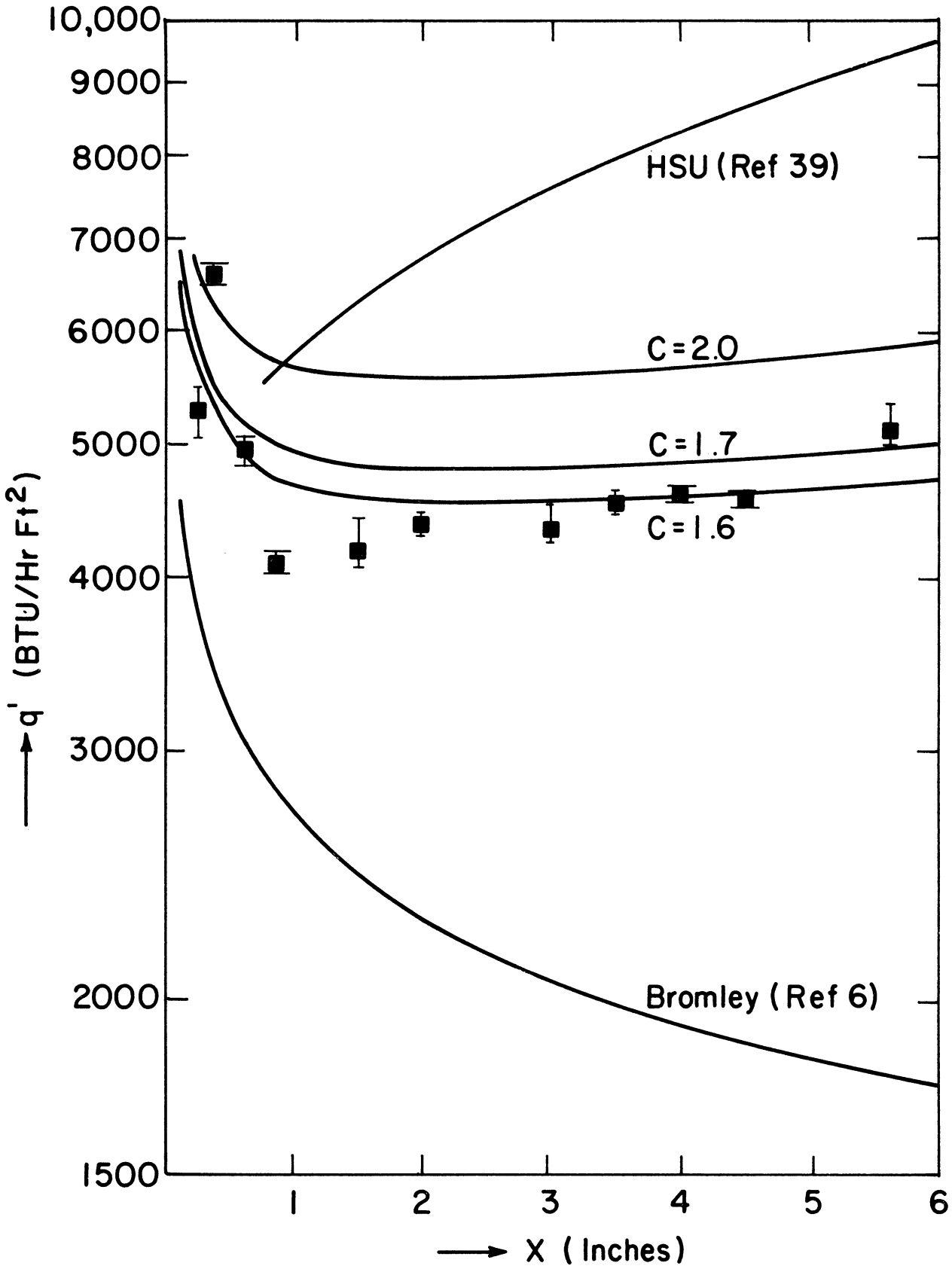

Figure 19. Effect of height on heat flux—film boiling. LN_2. ΔT = 204°R.

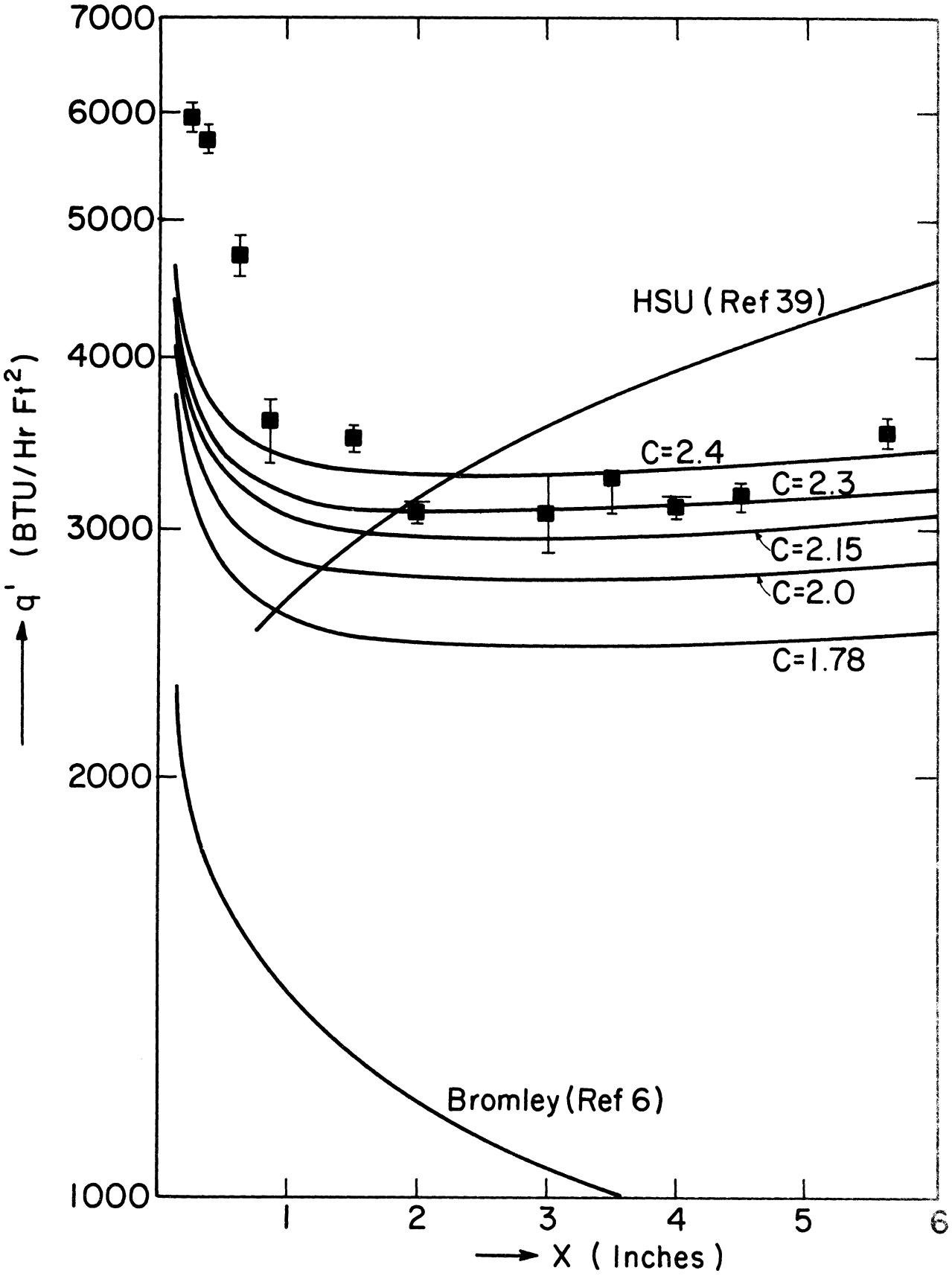

Figure 20. Effect of height on heat flux—film boiling. LN_2. ΔT = 100°R

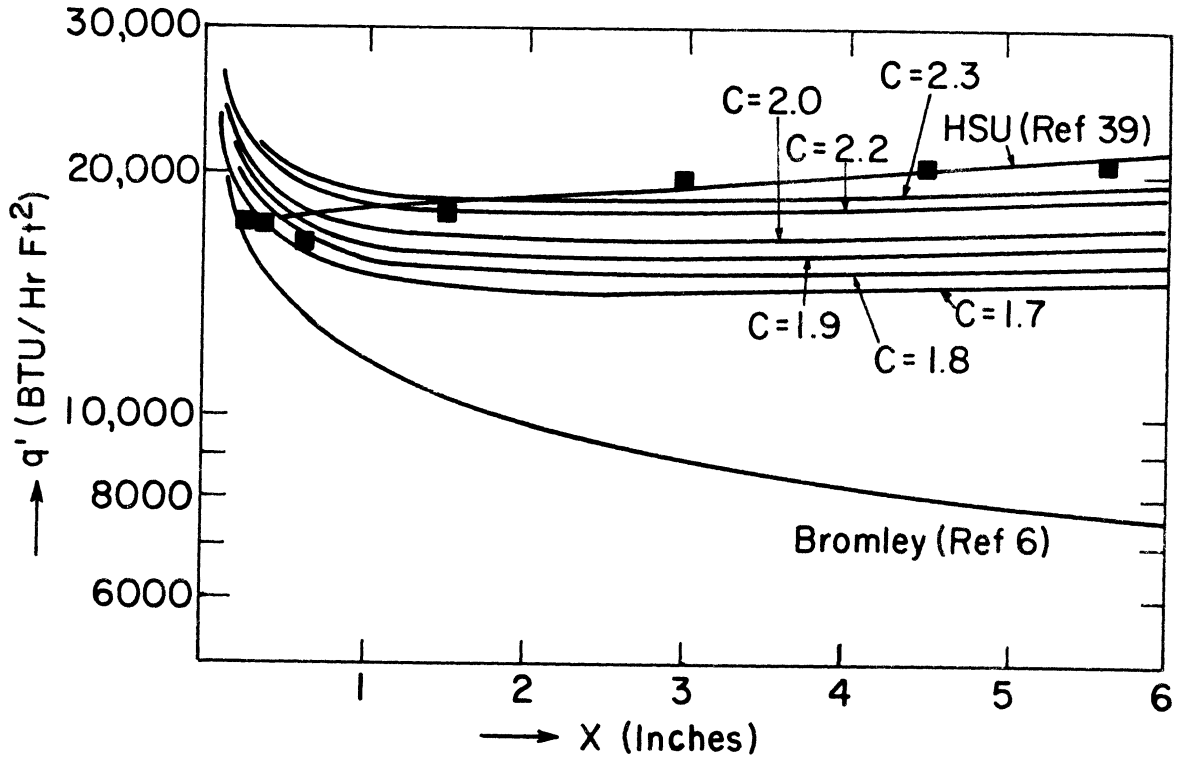

Figure 21. Effect of height on heat flux--film boiling. LH_2. ΔT = 400°R.

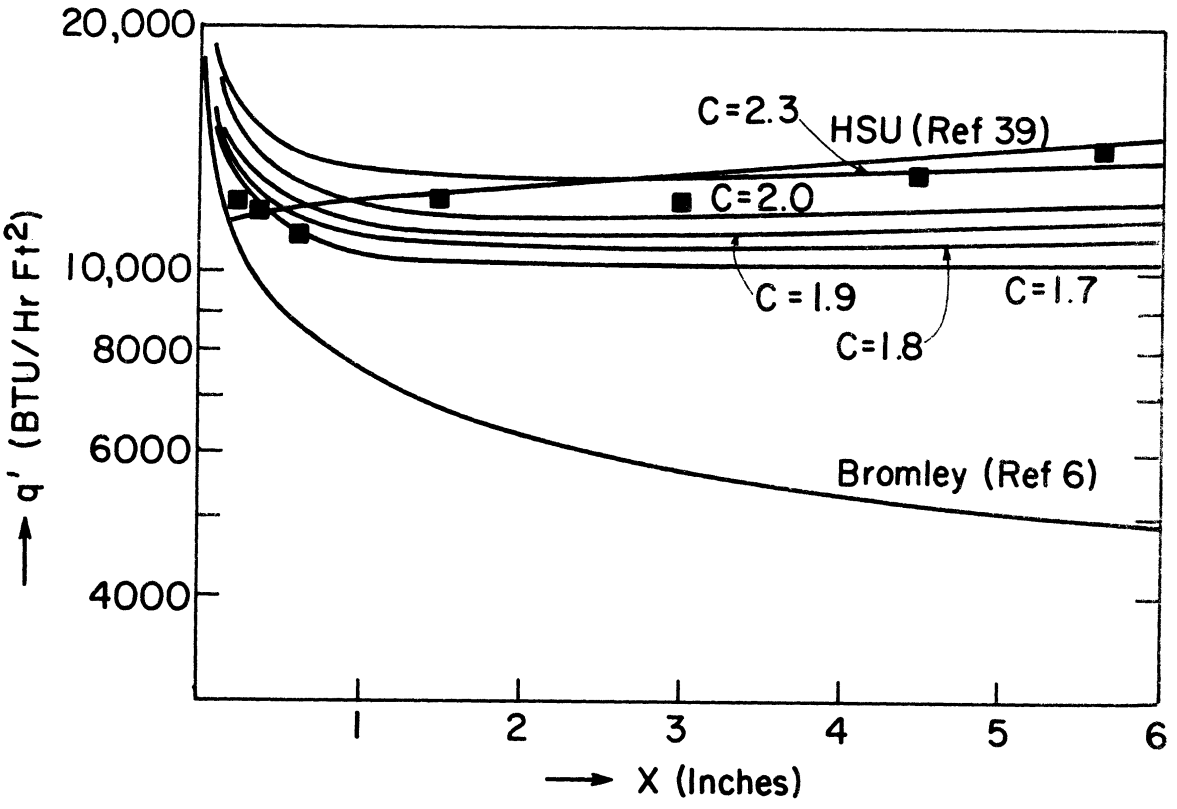

Figure 22. Effect of height on heat flux—film boiling. LH_2. ΔT = 300°R.

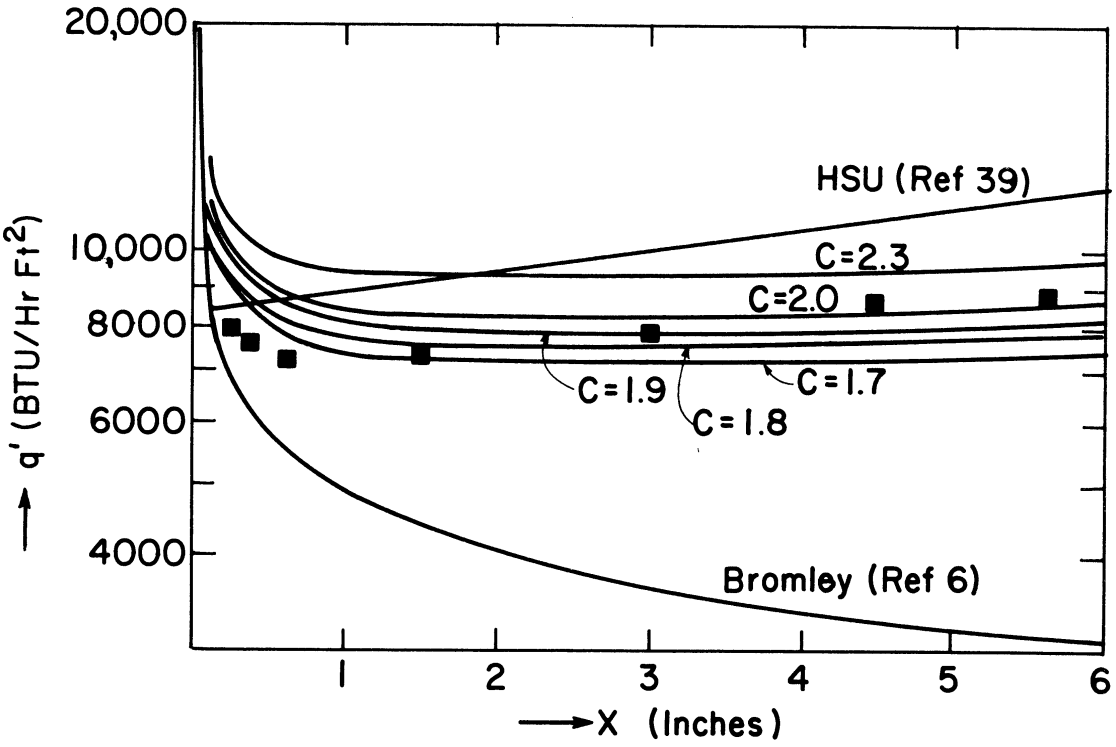

Figure 23. Effect of height on heat flux—film boiling. LH_2. ΔT = 200°R.

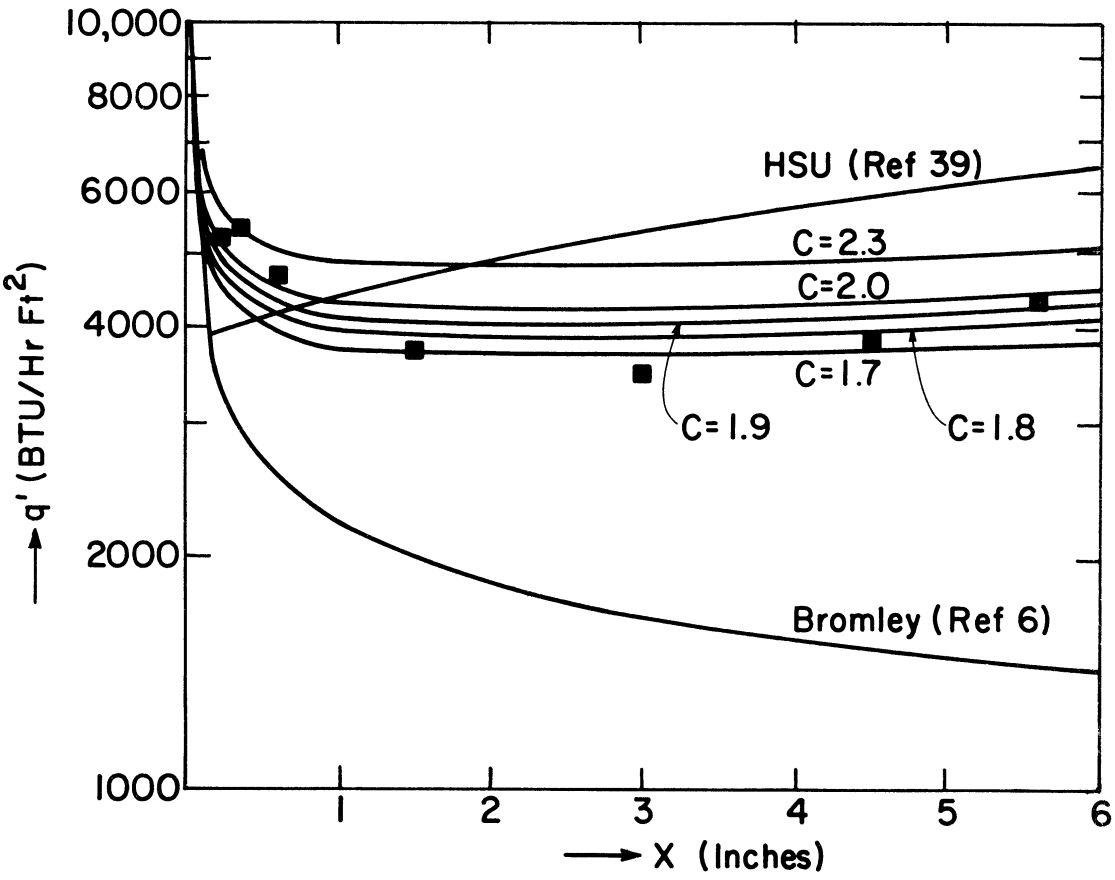

Figure 24. Effect of height on heat flux—film boiling. LH_2. ΔT = 100°R.

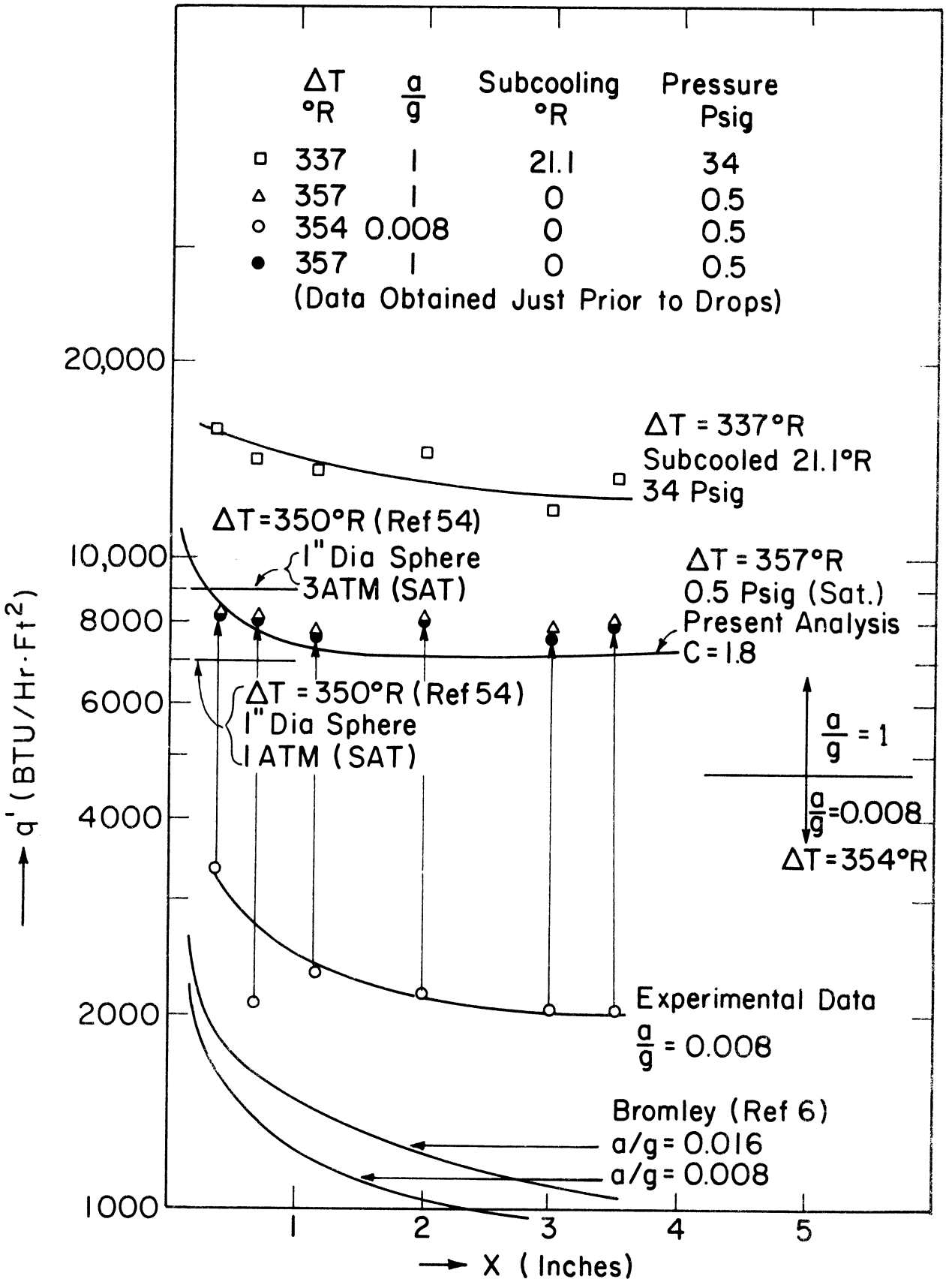

Figure 25. Effect of height, gravity, and subcooling on heat flux. LN_2.

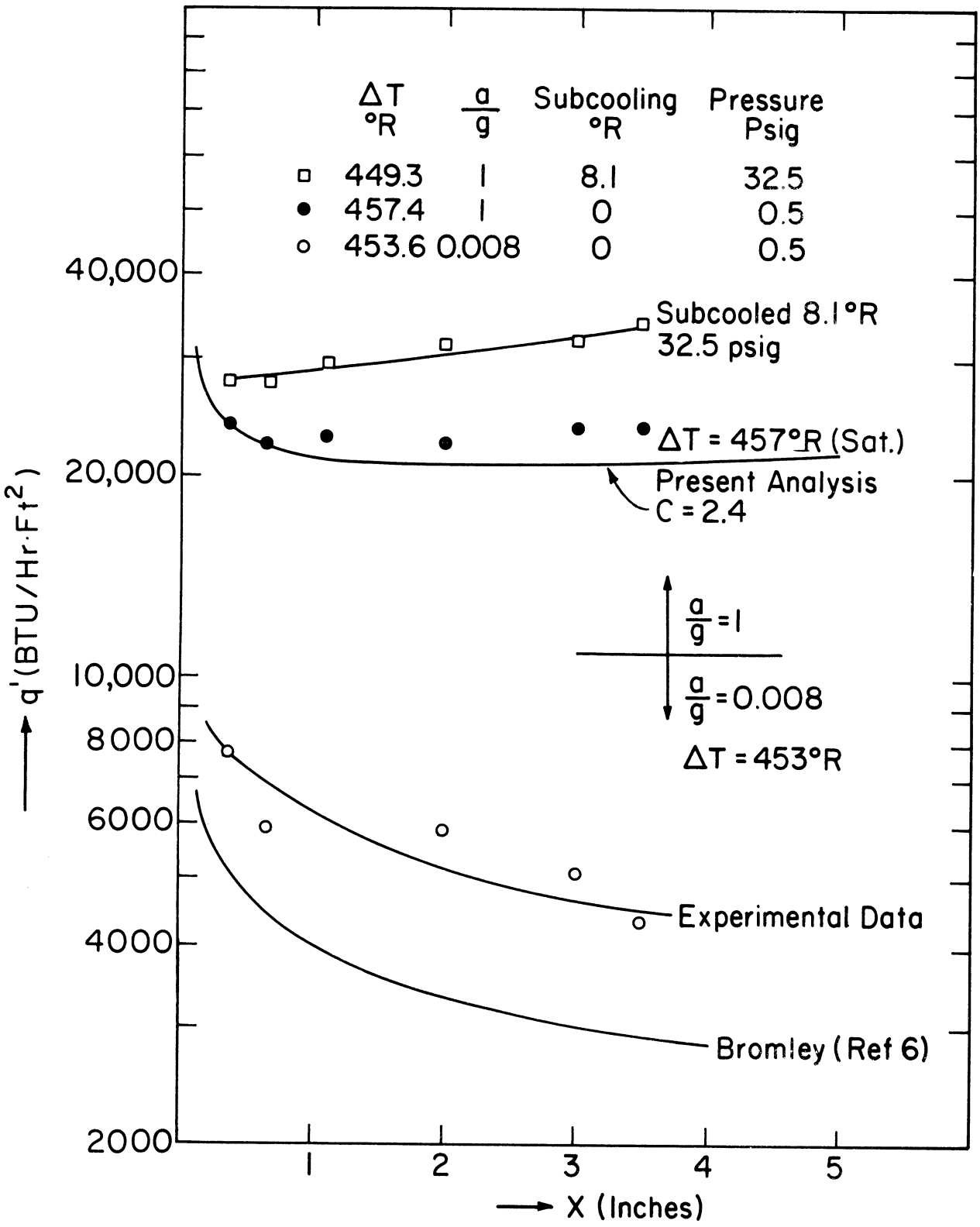

Figure 26. Effect of height, gravity, and subcooling on heat flux. LH_2.

(ii) Several curves showing variation of heat flux with height as predicted from the present analysis—Eqs. (5.28) for different values of the heat transfer enhancement coefficient, C, which indicates the influence of interfacial oscillations. The corresponding value of C for each curve, assumed constant over the entire height, is indicated in the plots.

(iii) Predictions from the laminar analysis of Bromley (6) and from the turbulent model of Hsu (39).

Figures 17-20 are for liquid nitrogen at nominal ΔT values of 315°R, 251°R, 204°R, and 100°R at 0.5 psig and a/g = 1 and Figures 21-24 are for liquid hydrogen at nominal ΔT values of 400°R, 300°R, 200°R, and 100°R at 0.5 psig and a/g = 1. Five sets of data were taken in liquid nitrogen at each test condition. The plots in Figures 17-20 include data obtained from both 1 in. dia and 2-1/4 in. dia test surfaces. Figures 21-24 for liquid hydrogen represent the mean of experimental values from three runs with 1 in. dia test surfaces.

Figures 25 and 26 show:

(i) Experimental values of heat flux vs. height for a/g = 1, a/g $\tilde{=}$ 0.008 for one value of ΔT at 0.5 psig.

(ii) Experimental values of heat flux vs. height for subcooled liquid for one value of ΔT at a/g = 1, at a pressure higher than 0.5 psig.

(iii) Bromley's (6) predictions of q' - x for a/g = 0.008 and a/g = 0.016 for liquid nitrogen and a/g = 0.008 for liquid hydrogen.

(iv) Predictions of q' vs. x from present analysis with a constant heat transfer enhancement coefficient C = 1.8 for liquid nitrogen and 2.4 for liquid hydrogen.

Figure 25 shows the above q' vs. x values for liquid nitrogen; a subcooling of 21.1°R at 34 psig was obtained. Figure 26 is a similar plot for liquid hydrogen; a subcooling of 8.1°R at a pressure of 32.5 psig was obtained.

In computing the predictions from the present analysis, properties of nitrogen and hydrogen were evaluated at the film temperature—the arithmetic mean of the surface and liquid temperatures. Appendix E gives the values used in the analysis for nitrogen and hydrogen and their sources.

C. Discussion

1. VALIDITY OF LAMINAR ANALYSIS

In Figures 17-24, it is clearly seen that the laminar analysis of Bromley (6) with a steady interface predicts much lower values than obtained, the departure of predictions from experimental values being greater for higher values of x. For liquid nitrogen, for example, at a $\Delta T = 315°R$ experimental values are 18.2% higher at a height of 1/4 in. and 212% higher at a height of 5-5/8 in. than predicted by laminar analysis. For liquid hydrogen, at a $\Delta T = 400°R$, the corresponding figures are 4.25% and 171%. This trend shows that the assumptions under which Bromley derived his correlations are probably valid only near the leading edge.

Of greater importance than the deviation from experimental values is the qualitative difference between the predictions and actual values. Laminar analysis (6) predicts a heat flux which is a continuously decreasing function of height. But experimental values clearly establish that there is a reduction in heat flux with height for small values of the height x, though the reduction is not as high as predicted in the laminar analysis, the heat flux reaches a minimum value and reversing the trend, begins to increase with height; the rate of increase is much smaller than the rate of reduction observed close to the leading edge.

2. EFFECT OF TURBULENCE

The first attempt to explain this departure of experimental values from those predicted by laminar analysis was made by Hsu (39). He used a two-layer model in the turbulent region, a laminar sublayer adjacent to the heating surface where both the velocity and temperature distributions are linear, and a turbulent core where both velocity and temperature are uniform; the interface was assumed to be steady and smooth. The predictions using his analysis are also shown in Figures 17-24. His assumption that the temperature in the turbulent core is the saturation temperature and all the temperature drop takes place in the laminar sublayer appears unrealistic and has been questioned by Dougall and Rohsenow (56). In liquid nitrogen, experimental values are lower than predictions from Hsu's theory—about 50% lower at $\Delta T = 315°R$ and height $x = 5\text{-}5/8$ in. The predictions are high for other values of ΔT in liquid nitrogen; the extent of deviation varies with height, being low for low values

of x and then progressively increasing with x. For liquid hydrogen, the predictions are high for low values of ΔT but this deviation decreases with an increase in ΔT, till at $\Delta T = 400°R$, Hsu's predictions are almost a perfect fit for the experimental data. Considering the simplifications made in his model, this fit is indeed remarkable.

So far, no definite study has been made to determine the onset of turbulence in film boiling. Generally, attempts have been made to apply the traditionally accepted views on transition to film boiling with some modifications. In condensation, values of transition Reynolds number based on equivalent hydraulic diameter, $4\Gamma/\mu = 1800$ to 400 (36) have been used. For film boiling Hsu (39) used a value of Re = 100 to signify transition to turbulence, the Reynolds number being evaluated at the maximum vapor velocity. In a recent work Coury and Dukler (50) have used a value of 35 for the transition Reynolds number in film boiling.

There are several complications that must be considered in specifying the transition of the laminar vapor flow to turbulent flow. In general, vaporization at an interface, which is physically equivalent to blowing, and heat transfer from a surface have destabilizing effects (48). It has also been remarked (48) that there is a possibility that the decrease in the viscosity of liquid at higher temperatures may have a stabilizing effect. Frederking (35) has given a linearized analysis of the onset of instability in film boiling but, as he has also remarked, the onset of instability does not necessarily indicate that transition to turbulence will take place. He has

reported values of transition Reynolds number ranging from 15 to 200 for falling liquid films.

In the present approximate analysis, no critical Reynolds number has been used to signify transition to turbulence. As indicated in Chapter V, "Model and Analysis," the universal velocity profile (Eq. (5.1)) used is assumed valid in the entire flow field. This gives a straight line velocity distribution and a very small value of ϵ_H/ν (compared with 1/Pr) for small values of dimensionless film thickness y+. The flow can be expected to be laminar for small values of y+ when molecular diffusion predominates over any turbulent effects. The values of ϵ_H/ν as a function of y+, Eqs. (5.6) and (5.7), for the profile employed are given in detail for values of y+ up to 10 in Table VIII. Figure 27 shows a plot of y+, Re (= $2\Gamma/\mu$) and ϵ_H/ν. From Table VIII and Figure 27 it is seen that ϵ_H/ν is quite small for small values of y+. The heat transfer across the vapor film is given by Eq. (5.13) reproduced below:

$$\theta_w^+ = 2\int_0^{u_m^+} \frac{F_3(u^+)}{F_2(u^+) + 1/Pr}\, du^+ \qquad (5.13)$$

where $F_2(u^+) = \epsilon_m/\nu = \epsilon_H/\nu$. For $1/Pr \simeq 1.0$, then ϵ_H/ν is less than 0.46×10^{-1} for $y^+ \leq 5$ and begins to increase until it is of the same order as 1/Pr at around $y^+ = 10$; thereafter it begins to increase rapidly and for $y^+ \simeq 40$, 1/Pr becomes insignificant in comparison with ϵ_H/ν, indicating that in this region molecular diffusion is of little importance compared with eddy diffusivity. This implies that so far as eddy diffusivity or the effects of turbulence on heat transfer is concerned, it begins to be of significance at

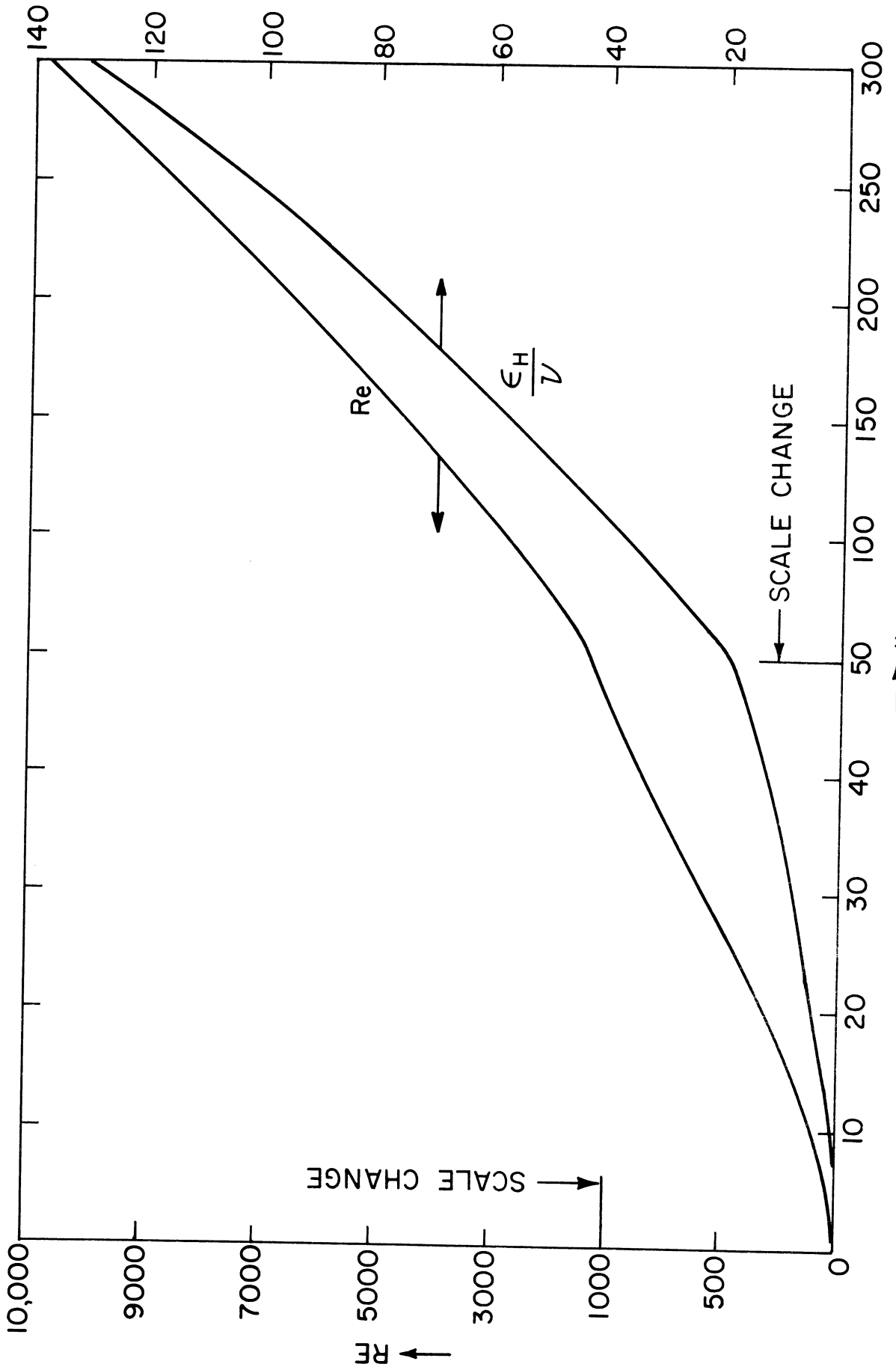

Figure 27. Relation between y^+, Re, and (ϵ_H/ν) for universal velocity profile Eq. (5.1).

TABLE VIII

VALUES OF EDDY DIFFUSIVITIES

y^+	ϵ_H/ν	y^+	$\epsilon H/\nu$
0.2	0.68×10^{-7}	7.3	0.22
0.4	0.12×10^{-5}	8.6	0.43
0.6	0.62×10^{-5}	10.1	0.78
1.0	0.5×10^{-4}	12.2	1.37
2.0	0.88×10^{-3}	19.1	3.83
3.0	0.49×10^{-2}	33.9	9.86
4.0	0.17×10^{-1}	67.9	24.13
5.0	0.46×10^{-1}	146.7	57.22
6.1	0.11	328.6	132.97

$y^+ \simeq 10$. If Re is defined on the basis of mass flow rate, $Re = 2\Gamma/\mu$, $y^+ = 10$ corresponds to a $Re \simeq 100$. It is interesting to note that Hsu (39) also used a Re = 100 to signify transition of laminar vapor film to turbulence in his analysis, though based on a somewhat different reasoning.

The profile used implies a Reynolds number based on mass rate of flow which depends on the value of y^+. If one used Von Karman's three-layer model instead, then $y^+_{min} = 30$ for the turbulent core, and implies a transition Re = 600. Considering the destabilizing effects of vaporization at the liquid-vapor interface and heat transfer from the surface in film boiling, it seems more appropriate to consider that turbulent effects begin to appear at values

of Re lower than that implicit in the three-layer model. Therefore, as an alternative, portions of the three-layer model may be used as appropriate, depending on the value of y^+_{max}. The universal velocity profile employed here has the advantage that it is a reasonably good approximation for all values of u^+_{max} (and y^+_{max}). As has been remarked earlier, ϵ_H/ν becomes significant around $y^+ = 10$ and Re $\simeq$ 100 for $1/Pr \simeq 1$. Also above $y^+ = 10$, the velocity distribution begins to show logarithmic behavior. Hence it may be considered that a critical transition Re $\simeq$ 100 is implied in the present analysis, above which turbulence effects begin to dominate over molecular diffusion.

Using the velocity profile Eq. (5.1) and the implied values of eddy diffusivities, and ignoring the effects of interfacial oscillations, predictions from the present analysis are shown in Figure 17, with C = 1.0. This predicts higher heat flux values than predicted by laminar analysis (6), the heat flux reaches a minimum and begins to increase gradually. Qualitatively the predictions show the same trend as experimental values but the departure from the experimental values is significant—the prediction being about 50% lower than the actual value at a height of 5-5/8 in. for liquid nitrogen at a $\Delta T = 315°R$. The height at which the minimum heat flux is predicted is also considerably greater than obtained in experiments. It is, therefore, clear that the onset of turbulence alone will not explain all the departures from laminar analyses.

3. EFFECT OF INTERFACIAL OSCILLATIONS

In the previous section, it was concluded that the onset of turbulence alone is not sufficient to explain the departure of predictions from

experimental values. In Chapter V, under assumption (ix) it was shown that interfacial oscillations will increase heat transfer rates as compared with a smooth steady interface.

Figures 28-34 show photographs of film boiling in liquid nitrogen for ΔT values of 315°R, 204°R, and 100°R at three different heights. The scale of the photographs, position and ΔT are indicated in each set of photographs. These were taken with a high-speed camera and the effective filming speed for each set is indicated in terms of frames per second. As can be seen from the photographs, the vapor is opaque to the light from the source and in order to determine the location of the heating surface a few frames were double exposed when there was no boiling. Such a double exposed frame is also shown in each set. To establish the location, x, of the heating surface and the scale for the photographs a .040 in. dia wire with pinch marks at regular intervals was stretched parallel to the heating surface and can be seen in the photographs.

Photographs in Figures 28, 31, and 33 show that even very close to the leading edge, the interface begins to oscillate and the assumption of a steady interface, except, possibly, very close to the leading edge is unrealistic, particularly with the large amplitudes of oscillations observed at some distance away from the leading edge which tends to enhance heat transfer rates considerably.

Frederking (35) has given an analytical solution to the problem of interfacial instability in film boiling assuming a parabolic velocity profile for the vapor film. He concludes that for all values of Re_δ, there is a finite range of unstable wave numbers such that the flow never is completely stable.

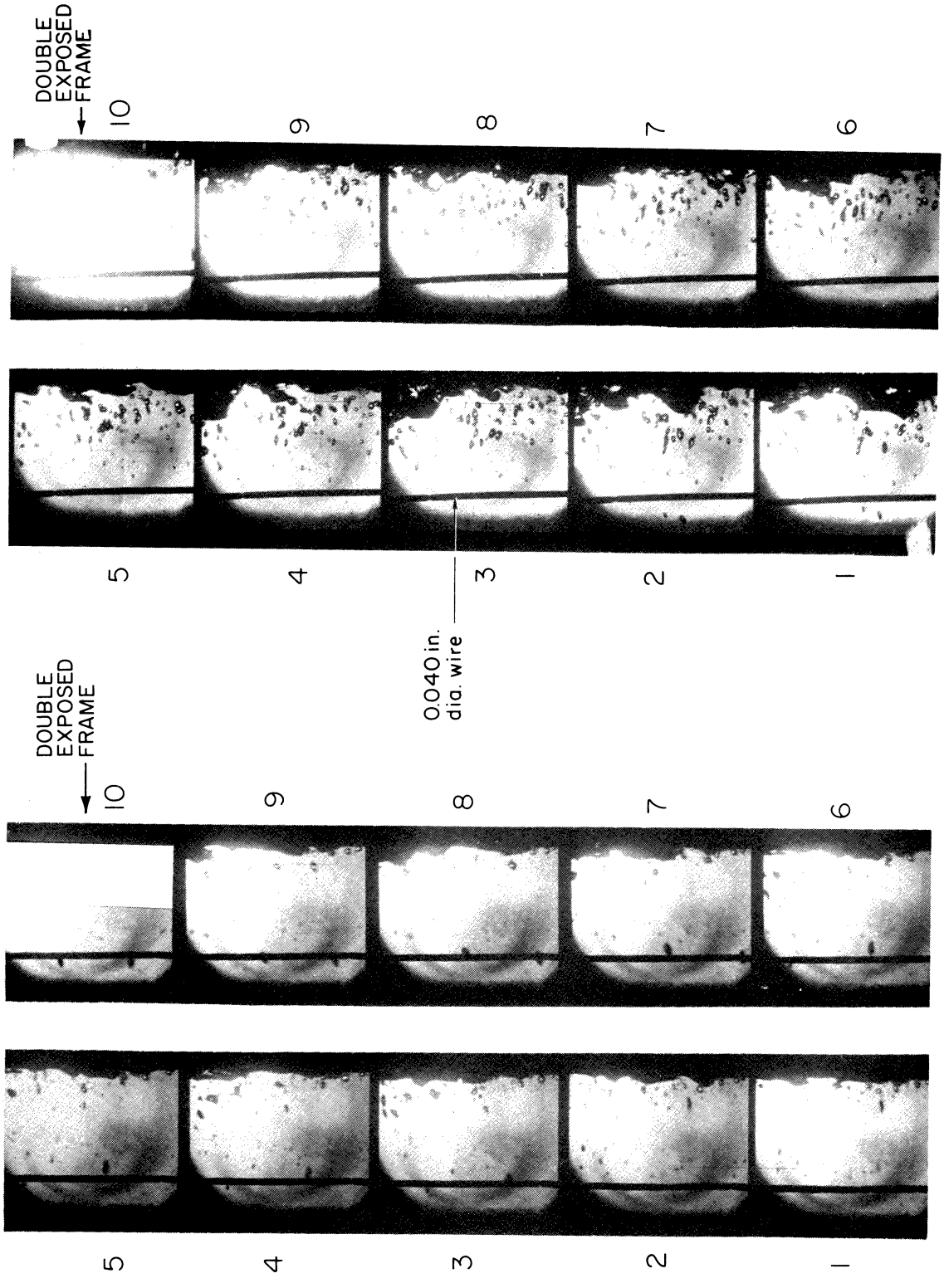

Figure 28. Film boiling: LN_2; ΔT = 315°R; x = 0-1 in.; 105 frames/sec.

Figure 29. Film boiling: LN_2; ΔT = 315°R; x = 1.5-2.25 in.; 103 frames/sec.

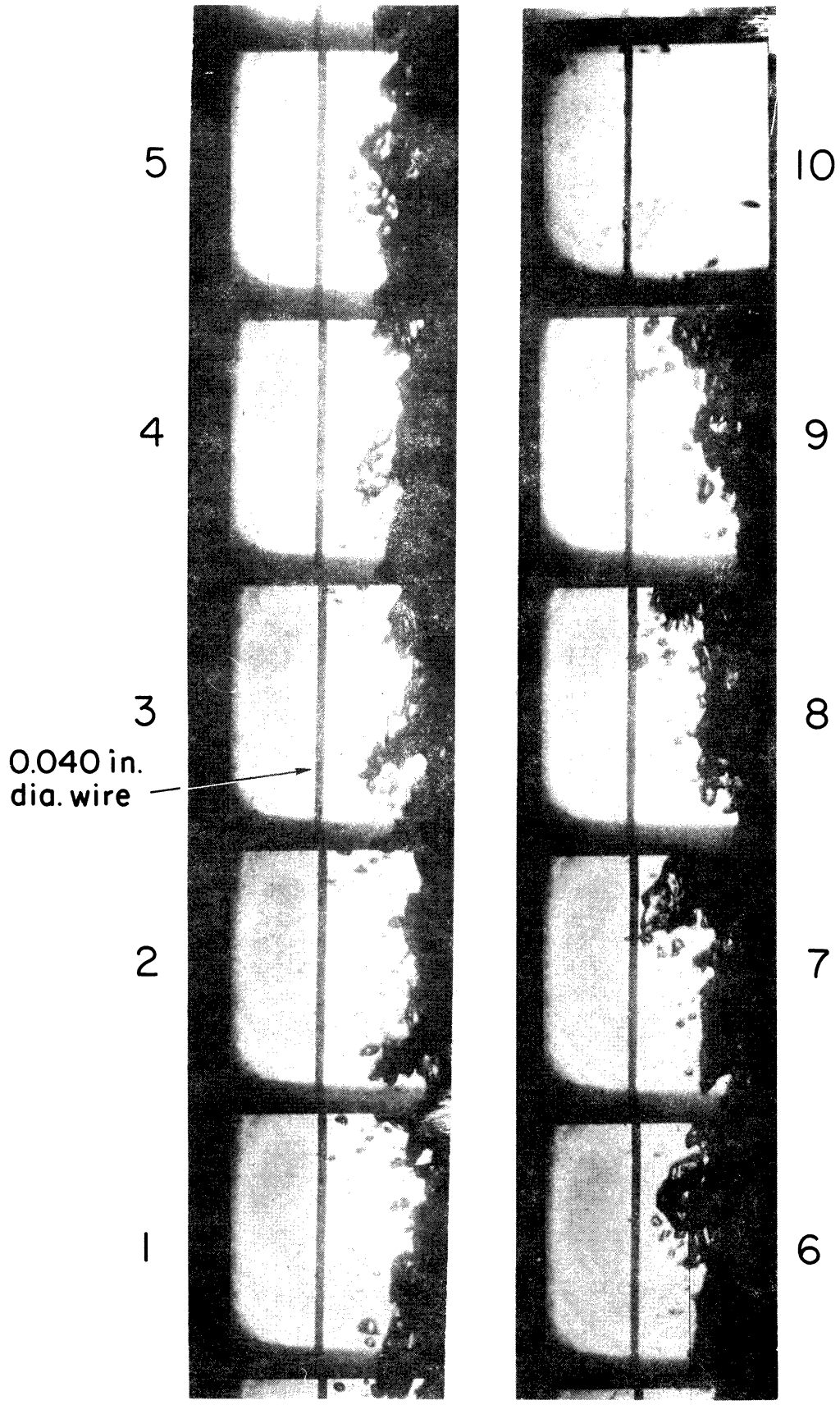

Figure 30. Film boiling: LN_2; ΔT = 315°R; x = 4-5 in.; 110 frames/sec.

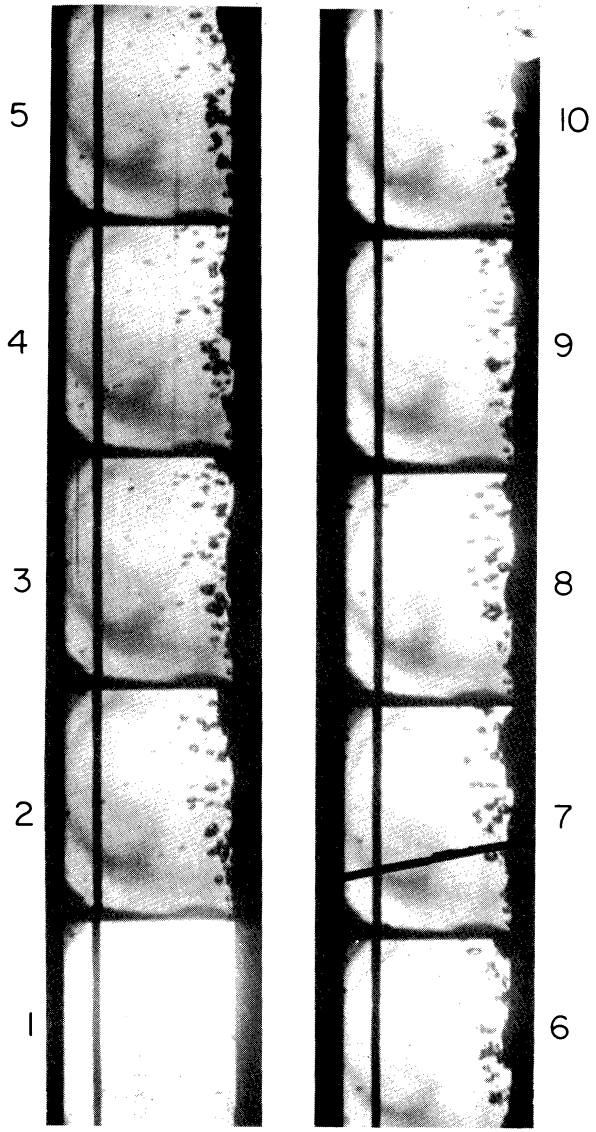

Figure 31. Film boiling: LN_2; ΔT = 204°R; x = 0-1 in.; 106 frames/sec.

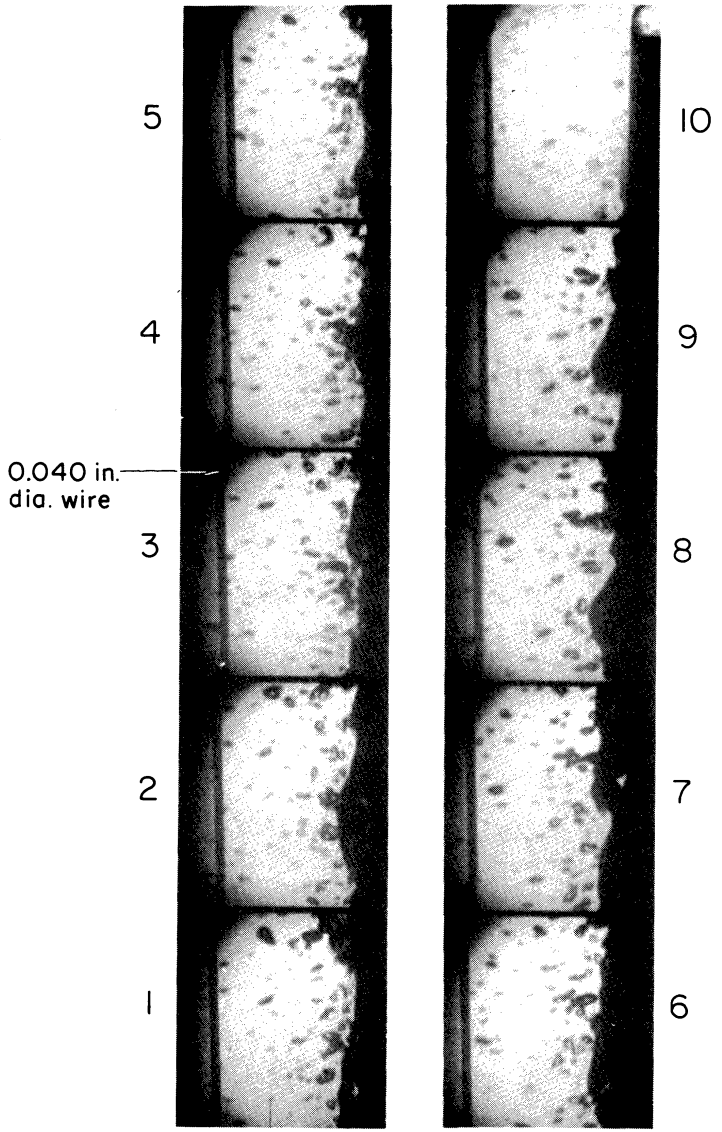

Figure 32. Film boiling: LN_2; ΔT = 204°R; x = 2-3 in.; 110 frames/sec.

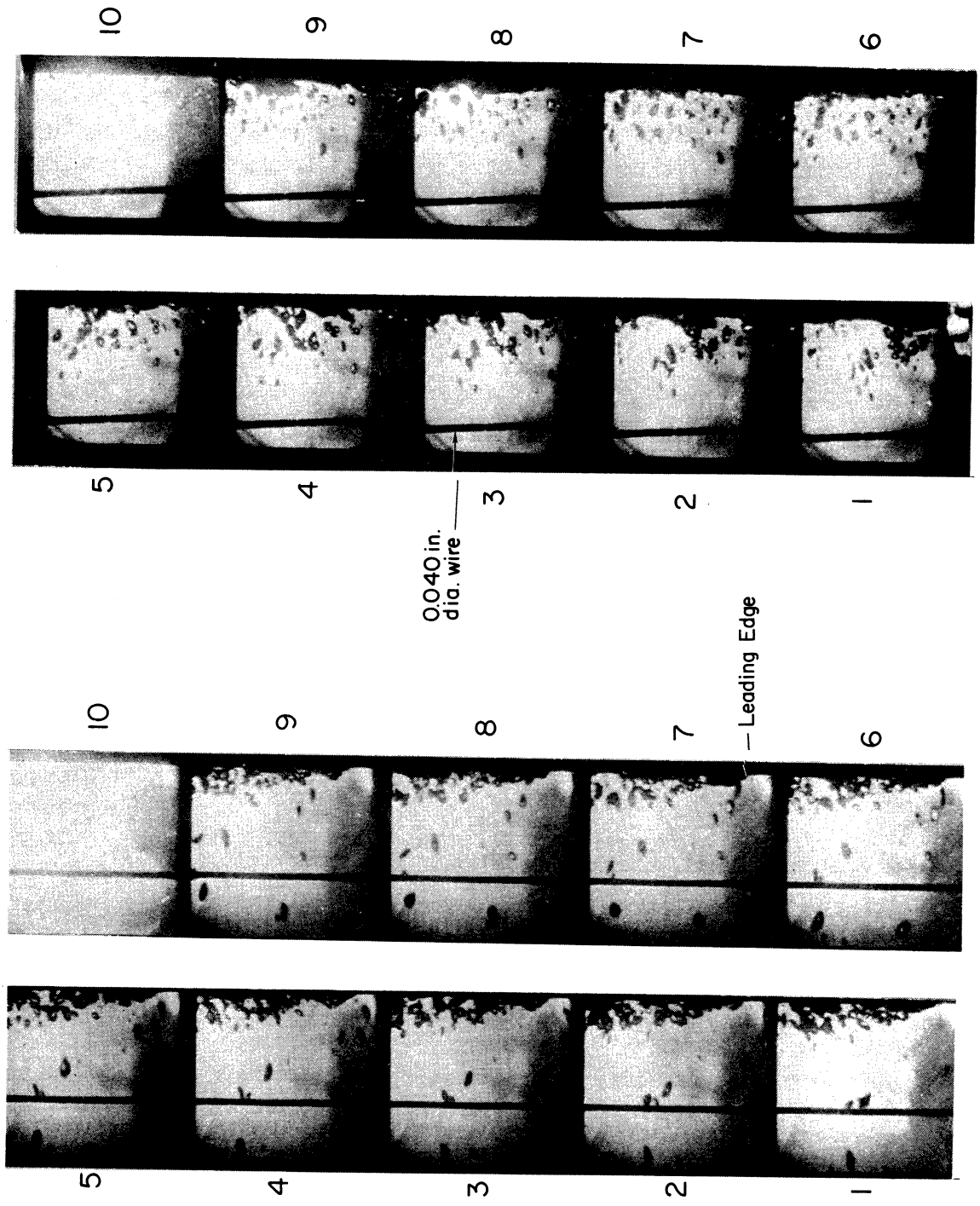

Figure 33. Film boiling: LN_2; ΔT = 100 °R; x = 0-1 in.; 104 frames/sec.

Figure 34. Film boiling: LN_2; ΔT = 100 °R; x = 1.5-2.5 in.; 109 frames/sec.

This analysis is based on a plane interface. In film boiling there is a thickening of the vapor film because of vaporization of the liquid, giving rise to a finite curvature of the interface. This is particularly significant near the leading edge as can be observed from Figures 28, 31 and 33, showing photographs of film boiling in liquid nitrogen near the leading edge and is also indicated in Figure 35 showing the model for predicting the instability of the interface. Analysis for two fluids of different densities flowing with some relative velocity u (52) shows that the critical wavelengths for small velocities are large. Hence the onset of instability is indicated by the appearance of waves of long wavelengths. Near the leading edge, velocities are small, being zero at the leading edge itself, and hence the critical wavelengths are large in this region. The question then is, does the finite curvature of the interface at the leading edge inhibit the appearance of waves of wavelength larger than a certain multiple of the height? As indicated in Figure 35 showing the model for instability, as an approximation one can visualize the curved interface near the leading edge to be a part of a wave, of wavelength nx, where n is an integer and x is the distance from the leading edge. At any height, the vapor film thickness δ is increasing with the height x because of the vaporization of the liquid and hence $d\delta/dx$ is positive at every x so that n cannot take a value less than 4. Thus the longest wavelength of any disturbance that can be superimposed on the interface is $\lambda \leq 4x$. At a given height $x = x_o$, the vapor velocity is u_o. We may now hypothesize that for instabilities to occur at x_o, the critical wavelength $\lambda_c \leq 4x_o$; if $\lambda_c > 4x_o$ it is a

stable configuration. From Reference 52, we have for parallel flows in a vertical plane with one fluid (liquid in the present case) stationary, the condition for the stability of the interface given by

$$\alpha_1 \alpha_2 u^2 < \frac{k\sigma}{\rho+\rho_\ell} \qquad (6.5)$$

where

$$\alpha_1 = \frac{\rho}{\rho+\rho_\ell} \; ; \; \alpha_2 = \frac{\rho_\ell}{\rho+\rho_\ell}$$

k = wave number = $\frac{2\pi}{\lambda}$

λ = wavelength

σ = surface tension

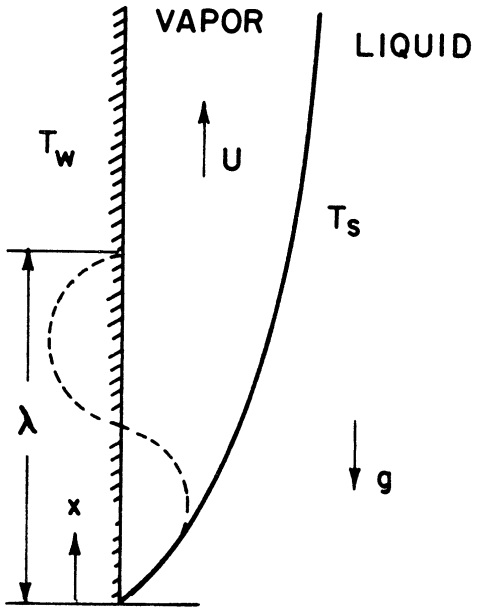

Figure 35. Model for predicting instability of interface.

From Eq. (6.5), the critical wave number is given by

$$k_c = \frac{\rho_\ell \rho}{\rho_\ell+\rho} \frac{u^2}{\sigma} \qquad (6.6)$$

Thus every height x is associated with a critical wavelength and wave number λ_c and k_c and a critical velocity u_c given by Eq. (6.6). Also, from the laminar solution (6), at a given x the vapor has a maximum velocity u_v. It is hypothesized that if at any given value of x, $u_v(x) > u_c(x)$ then instabilities are possible; if $u_v(x) < u_c(x)$ then it is a stable configuration.

Figure 36 is a plot of u_v and u_c vs. x for liquid nitrogen and liquid hydrogen at different values of ΔT. At some $x = x_c$, $u_v(x) = u_c(x)$ and

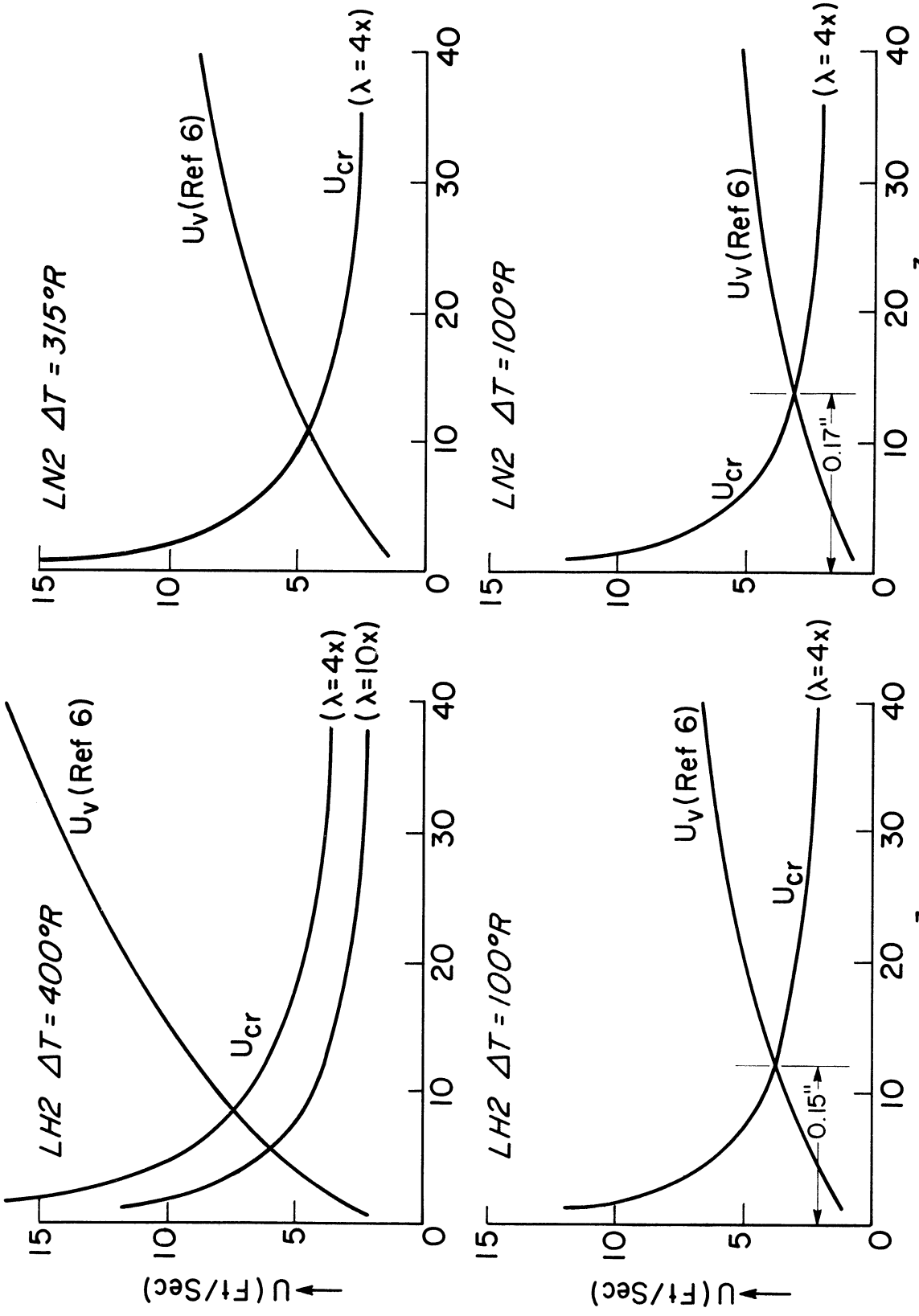

Figure 36. Critical velocity vs. height for interfacial instability: a/g = 1.

interfacial instabilities appear. To the left of x_c, it is hypothesized that the interface is stable. Figure 37 is a similar plot for liquid nitrogen for $a/g = 0.008$.

From these plots it can be seen that the greatest height over which the interface can be expected to be stable is 14×10^{-3} ft (0.17 in.) for liquid nitrogen at $\Delta T = 100°R$, a very small region. Thus from these approximate calculations, supported by linearized analyses and photographic studies, it can be concluded that a steady interface, if it exists, will be limited to an extremely small region under normal gravity conditions. For liquid nitrogen at $a/g = 0.008$, however, instabilities appear at a height of approximately 0.23 ft (2.8 in.). This will be discussed in greater detail under Section 5, "Effect of Reducing Gravity."

From the above discussion it is clear that interfacial oscillations appear quite close to the leading edge, and under assumption (ix) Chapter V it has been shown that the effect of such oscillations is to increase the heat transfer rates. This is also confirmed in a recent paper by Coury and Dukler (50). Analyses of photographs such as reproduced in Figures 28-34 discussed in greater detail in Section 7, "Effect of Height on Heat Transfer Coefficient," clearly establish that the amplitude of interfacial oscillations are of the same order as the vapor film thickness. Recalling from Eq. (5.5a) that the increase in heat transfer due to interfacial oscillations is given by

$$C = \frac{1}{\sqrt{1-b^2}} \qquad (5.5a)$$

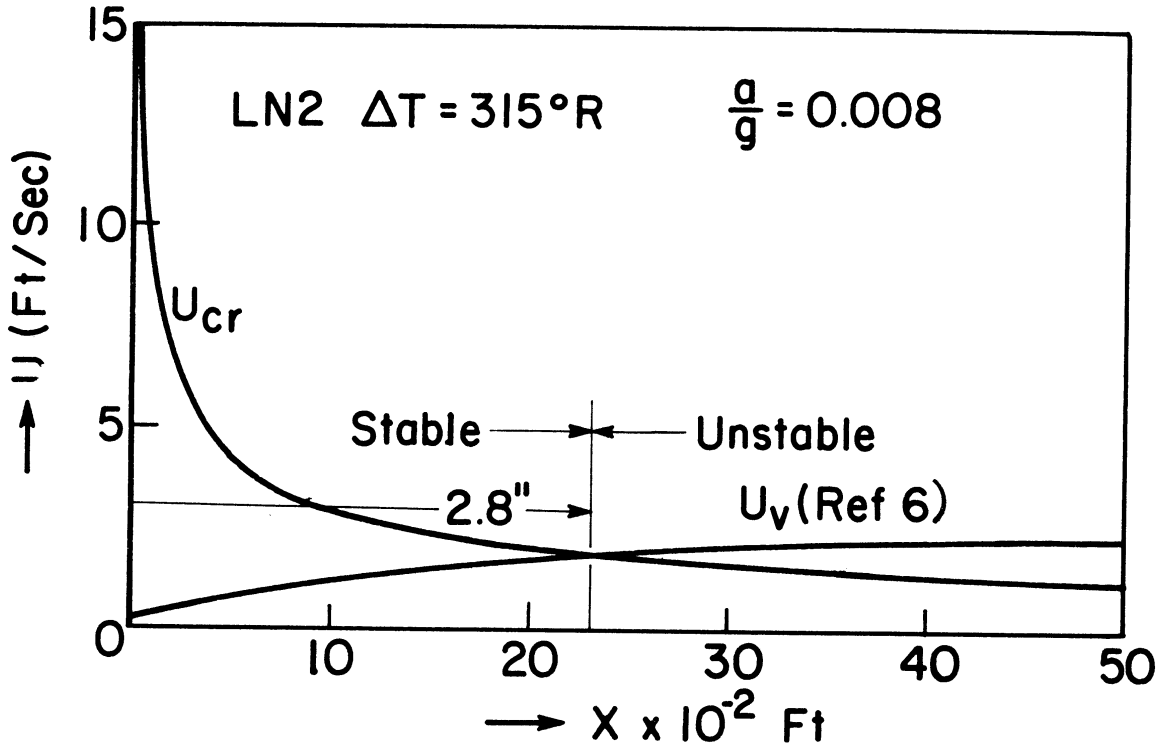

Figure 37. Critical velocity vs. height for interfacial velocity: a/g = 0.008.

with such oscillations b takes a value not very different from 1 and hence the value of C can be quite high.

Equations (5.28) were solved numerically for several values of the heat transfer enhancement coefficient for both liquid nitrogen and liquid hydrogen for the values of ΔT for which experimental data were obtained. Curves showing these predictions are plotted in Figures 17-24. It may be observed that the present analysis, even with a C-value independent of the height x, comes closer to the experimental values both quantitatively and qualitatively for both liquid nitrogen and hydrogen than either of the two predictions considered so far (6,39) if an appropriate value of C is used. This analysis shows the greatest deviation near the leading edge, particularly in liquid nitrogen. In liquid nitrogen the extent of deviation is given in Table IX.

In general the greatest departure from the predictions is observed within 1 in. from the leading edge, and if this is omitted, the limits on deviation are considerably reduced, as can be seen from the last column of Table IX.

TABLE IX

DEVIATIONS OF EXPERIMENTAL VALUES
FROM PREDICTIONS—LIQUID NITROGEN

ΔT (°R)	C	% Deviation	% Deviation Excluding 1 in. from Leading Edge
315	1.78	+21.7 - 1.8	+7.07 - -7.9
251	1.65	-9.5 - +14.1	-0.25 - +7.8
204	1.7	-19.5 - +18.4	+3.03 - +13.5
100	2.4	-50 - +7	-3.82 - +7.0

The deviations of experimental values from predictions for liquid hydrogen are shown in Table X.

TABLE X

DEVIATIONS OF EXPERIMENTAL VALUES FROM PREDICTIONS—LIQUID HYDROGEN

ΔT (°R)	C	% Deviation	% Deviation Excluding 5/8 in. from Leading Edge
400	2.3	-6.6 - +21.6	-6.6 - +3.22
300	2.3	-3.68 - +22.6	-3.68 - +5.7
200	1.9	-8.7 - +18.9	-8.7 - +8.7
100	1.9	-8.8 - +10.4	-1.67 - +10.4

Here also it can be observed that the deviations are greatest near the leading edge and predictions are much better away from it. The analyses is essentially for the turbulent region, and on this basis it can be said that the experimental values are within -8.7% - +13.5% of the prediction.

In these predictions, the values of the heat transfer enhancement coefficient C range from 1.7 to 2.4, and for the set of conditions for which results are obtained, these can be said to be the extreme limits for the value of C. For liquid hydrogen, using any value within these limits, the experimental values would be within -38.7% to +27% of the predictions over the entire height of the heating surface covered in the present series of experiments.

4. EFFECT OF INTERFACIAL VAPORIZATION ON VELOCITY PROFILE AND FRICTION VELOCITY

In the model employed to predict the heat transfer rates, Chapter V, one of the significant assumptions (v) is that the vaporization at the interface has no appreciable effect on the velocity profile and shear velocity. Marxman and Gilbert (45), Marxman (46), and Woolridge and Muzzy (47) have reported the results of their experimental studies regarding the effect of vaporization on flat plates, on the velocity and shear stress distribution in turbulent boundary layers. Defining the blowing parameter "B" as

$$B = \frac{2(\rho v)_{wall}}{\rho_e u_e C_f} \tag{6.7}$$

where ρ = density of the vapor at the wall

v = blowing velocity at the plate

ρ_e = density in the free stream

u_e = velocity in the free stream

C_f = friction factor = $2\tau_w/\rho_e u_e^2$

τ_w = wall shear stress

they show that the dimensionless velocity $\Phi = u/u_e$ is given by

$$\Phi = \eta^{\frac{1}{7}} \left(1 + \frac{1}{2} B\eta^{\frac{1}{7}}\right) / \left(1 + \frac{1}{2} B\right) \tag{6.8}$$

where η = dimensionless distance y/δ

δ = boundary layer thickness.

For the case of B = 0, indicating no blowing, this reduces to the well known 1/7 power law distribution. It was also shown (46) that the friction factor can be expressed in the form

$$C_f = g(Re_\delta) \frac{\ln(1 + B)}{B} \tag{6.9}$$

where $g(Re_\delta)$ is a function of Reynolds number which gives the friction factor for B = 0. To evaluate this use is made of the expression given by Schlichting (48)

$$C_f = 0.0225\ Re_\delta^{-0.25} \tag{6.10}$$

Denoting the friction factor for no blowing by C_{fo}, for the same free stream velocity, the friction factor with blowing is then given by

$$\begin{aligned} \frac{C_f}{2} &= 0.0225\ Re_\delta^{-0.25} \frac{\ln(1 + B)}{B} \\ &= 0.0225 \left(\frac{\delta_o}{\delta}\right)^{0.25} (Re_{\delta o})^{-0.25} \frac{\ln(1 + B)}{B} \\ &= \frac{1}{2} C_{fo} \left(\frac{\delta_o}{\delta}\right)^{0.25} \frac{\ln(1 + B)}{B} \end{aligned} \tag{6.11}$$

The ratio $(\delta_o/\delta)^{0.25}$ indicates the effect of boundary layer thickening due to blowing. Ignoring this effect, we obtain

$$\frac{C_f}{C_{fo}} = \frac{\ln(1 + B)}{B} \tag{6.12}$$

which is identical to the expression obtained earlier by Lees (49).

We now assume, for the purpose of estimating the effect of vaporization at the interface on the velocity distribution and shear stress at the interface, that the above expressions for flow on a flat plate are valid for flow between parallel plates, with free stream velocity u_e being replaced by the maximum velocity u_{max}. To obtain a numerical value for B we proceed as follows:

For a flat plate,

$$B = \frac{(\rho v)_w}{\frac{1}{2}\rho u_e^2 C_f} \tag{6.13}$$

where

$$C_f = \frac{2\tau_w}{\rho_e u_e^2}$$

For flow between parallel plates, u_e in Eq. (6.13) is replaced by u_{max}

$$B = \frac{(\rho v)_{interface}}{\frac{1}{2}\rho u_{max} \frac{2\tau_w}{\rho u_{max}^2}} \tag{6.14}$$

But $\frac{\tau_w}{\rho} = u^{*2}$ and $\frac{u_{max}}{u^*} = u^+_{max}$

Hence

$$B = \frac{(\rho v)_i \, u^{+2}_{max}}{\rho \, u_{max}} \tag{6.15}$$

It is now possible to estimate a numerical value for B. $(\rho v)_i$ is the rate at which vaporization is taking place at the interface and is given by q'_i/h_{fg}. With the assumption (iv-Chapter V) that $q'_i = q'_w$,

$$(\rho v)_i = \frac{q'_w}{h'_{fg}}$$

Experimental values of q'_w/h'_{fg} for liquid nitrogen at $\Delta T = 315°R$ are, $q'_w = 7000$ Btu/hr $ft^2°F$ and $h'_{fg} = 126.4$ Btu/lbm so that $q'_w/h'_{fg} = 55.5$ lb/ft^2hr. u^+_{max} and u_{max} are found from the solution to Eqs. (5.28) and are of the order of 10 and 80,000 ft/hr, respectively, for the above conditions. Using these values, B = 0.52 For this value of B the velocity profile ϕ is compared with that for B = 0 in Figure 38. It is seen that the velocity profile is not significantly affected by the vaporization at the liquid-vapor interface, in the present experiments. The friction velocity u* is reduced in the ratio $\sqrt{C_f/C_{fo}} = \sqrt{\ln 1.5/0.5} = 0.9$ due to the effect of vaporization. Although one may argue that a reduction of 10% in the friction velocity is not insignificant, this decrease in friction velocity due to vaporization is neglected in the present analysis.

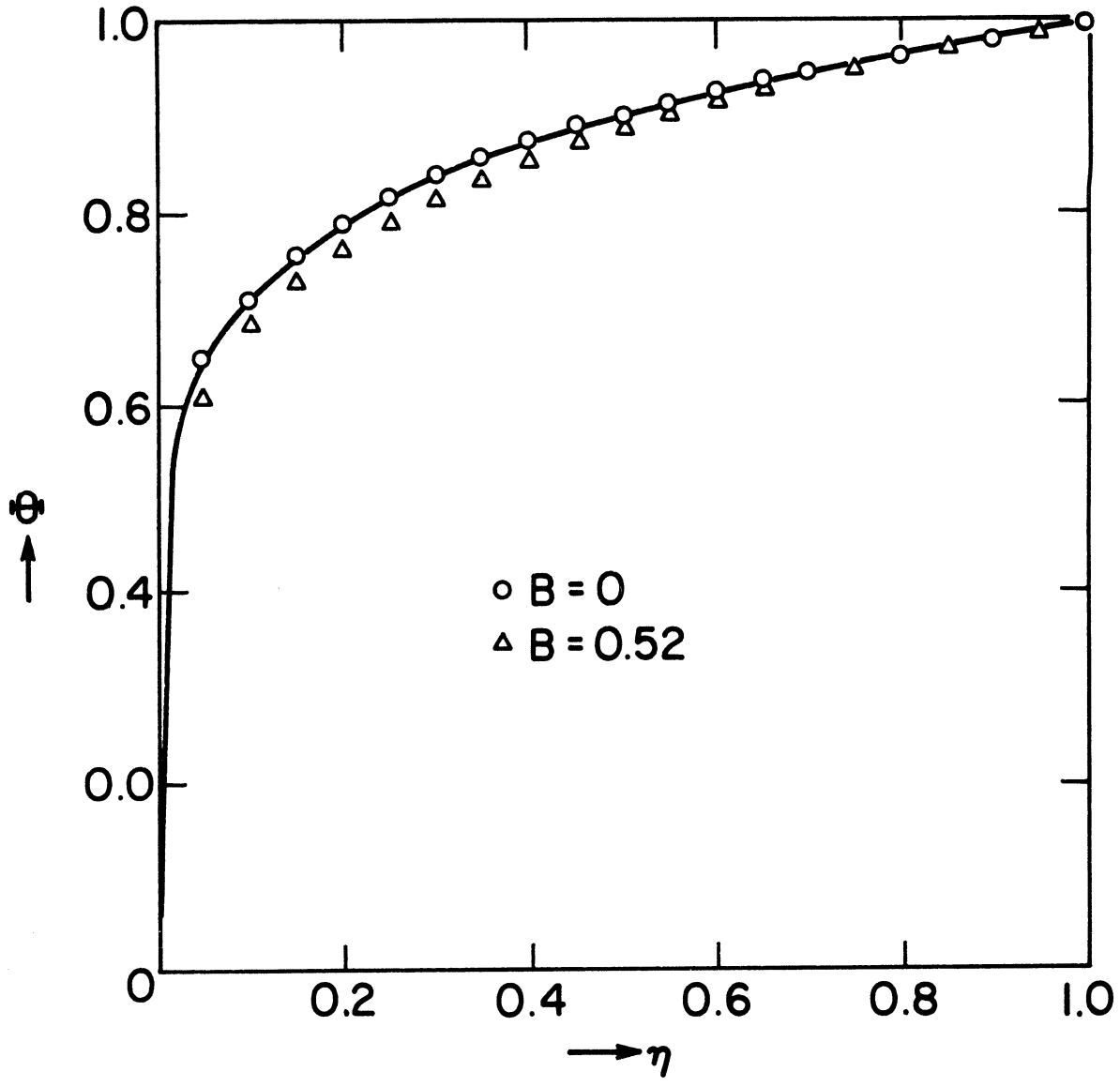

Figure 38. Effect of interfacial vaporization on velocity profile.

5. EFFECT OF REDUCING GRAVITY

Figures 25 and 26 show plots of heat flux vs. height for film boiling in liquid nitrogen and liquid hydrogen for $a/g = 1$, $a/g \tilde{=} 0.008$ and subcooled liquids. Also plotted on these figures are predictions from the present analyses for $a/g = 1$ with a heat flux enhancement coefficient $C = 1.8$ for liquid nitrogen and $C = 2.4$ for liquid hydrogen assumed constant for all heights x, Bromley's predictions (6) for $a/g = 0.008$ and $a/g = 0.016$ for liquid nitrogen and $a/g = 0.008$ for liquid hydrogen.

The $a/g = 1$ curves are for $\Delta T = 357°R$ for liquid nitrogen and $\Delta T = 457°R$ for liquid hydrogen; values of $C = 1.78$ for liquid nitrogen at a $\Delta T = 315°R$ and $C = 2.4$ for liquid hydrogen at $\Delta T = 400°R$ were used for predicting the heat transfer rates Figures 17 and 21 and on the basis that the ΔT values of $357°R$ and $453°R$ are not very different from $315°R$ and $400°R$ the same values for C were tried. It is seen that experimental values are within -2.4% - +12.7% of the predicted value.

As can be expected, heat transfer rates are reduced at lower gravity levels. Even up to a height of 3-1/2 in., the heat flux is decreasing with height, indicating the probability that the onset of interfacial oscillations or turbulence, or both, have been delayed. Predictions from laminar analysis of Bromley (6) for two values of $a/g = 0.008$ and 0.016 have also been plotted in Figure 25. From Appendix A, it can be seen that the maximum value of a/g attained in the drop tower was 0.008. However for comparison purposes, q' - x plot obtained from laminar analysis (6) for $a/g = 0.016$ has also been

included in Figure 25. Even these predictions with a/g = 0.016 are observed to be significantly lower than experimental values. The experimental values for liquid nitrogen are uniformly 100% higher, but qualitatively show the same behavior as predicted. The heat flux decreases with height, a characteristic of laminar flow with a steady liquid-vapor interface. In Figure 37, showing the plot of critical velocity vs. height for a/g = 0.008, it is noted that the onset of interfacial waves is delayed by the reduction of gravity to a height of 0.23 ft (2.8 in.) as opposed to 0.014 ft (0.17 in.) at a/g = 1. This is consistent with experimental values of heat flux which decreases with height up to a height of 3.5 in. for both liquid nitrogen and liquid hydrogen as can be seen from Figures 25 and 26. This supports the hypothesis that heat transfer enhancement is caused by interfacial waves. The results in liquid hydrogen are similar to those in liquid nitrogen in all respects.

Insofar as can be inferred from the experimental values of heat flux under reduced gravity, it may be said that the qualitative variation of the heat flux with height is consistent with those predicted by laminar analysis up to a height of 3-1/2 in. Hence the region of validity of laminar analysis was physically extended by the use of the drop tower.

6. EFFECT OF SUBCOOLING

Figures 25 and 26 give experimental values of heat flux vs. height for liquid nitrogen with a $\Delta T = T_w - T_s = 337°R$ at 34 psig giving a subcooling of 21.1°R; for liquid hydrogen the corresponding values are $\Delta T = 449.3°R$ at 32.5 psig giving a subcooling of 8.1°R In order to determine the effect of

subcooling it is necessary to know the effects of pressure as the subcooled data is available only at higher pressures than those without subcooling. From Lewis' experimental results on 1 in. dia sphere in liquid nitrogen (54), at $\Delta T = 357°R$, $p = 1$ atm, $q' = 7000$ Btu/hr ft^2 and at $p = 3$ atmospheres (corresponding to 29 psig), $q' = 9000$ Btu/hr ft^2. These are indicated in Figure 25 with horizontal lines labelled 1 in. dia sphere. On the assumption that the effect of increasing the pressure is constant all along the height of a vertical surface, and is of the same order as that for a sphere, it can be seen that, for the same heating surface temperature and liquid temperature, subcooling reduced the value of ΔT, defined as the surface superheat above the saturation temperature; but even with a decrease in the value of ΔT so defined, there is a substantial increase in the heat transfer rates through subcooling the liquid via pressurization.

7. EFFECT OF HEIGHT ON HEAT TRANSFER COEFFICIENT

Figures 39 and 40 show heat transfer coefficient h plotted against height x for liquid nitrogen and liquid hydrogen, respectively, for 4 values of ΔT each. It is interesting to observe from Figure 39 that for $x > 1$ in., h is substantially constant within approximately $\pm$ 6% for the range of ΔT between 204°R and 315°R. For heights less than 1 in. there is considerably greater variation in the value of h. From Figure 39 for $\Delta T = 315°R$, 251°R, and 204°R the following conclusions can be drawn:

(i) Initially up to a height of about 1 in., the heat transfer coefficient rapidly decreases with height.

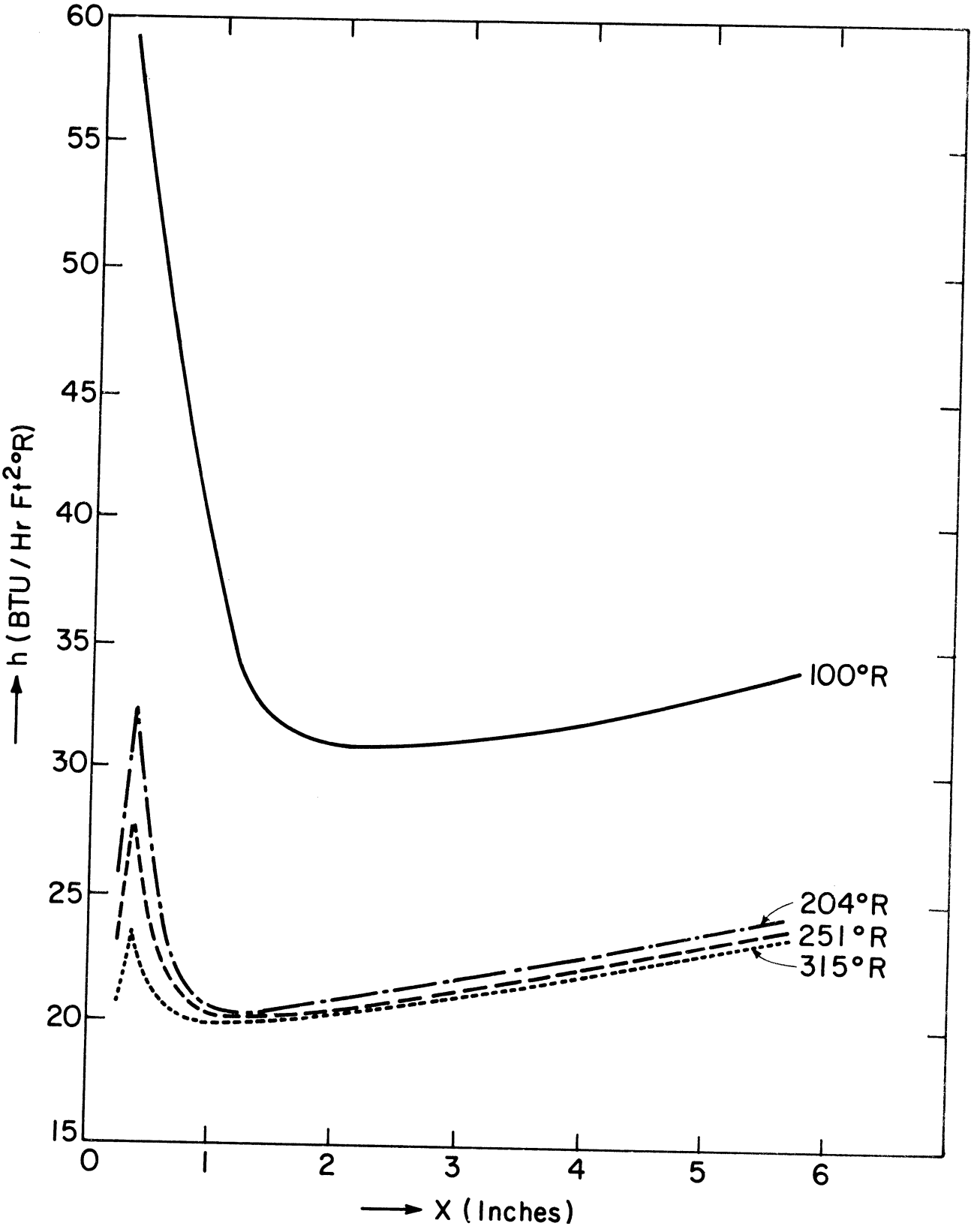

Figure 39. Effect of height on heat transfer coefficient. LN_2.

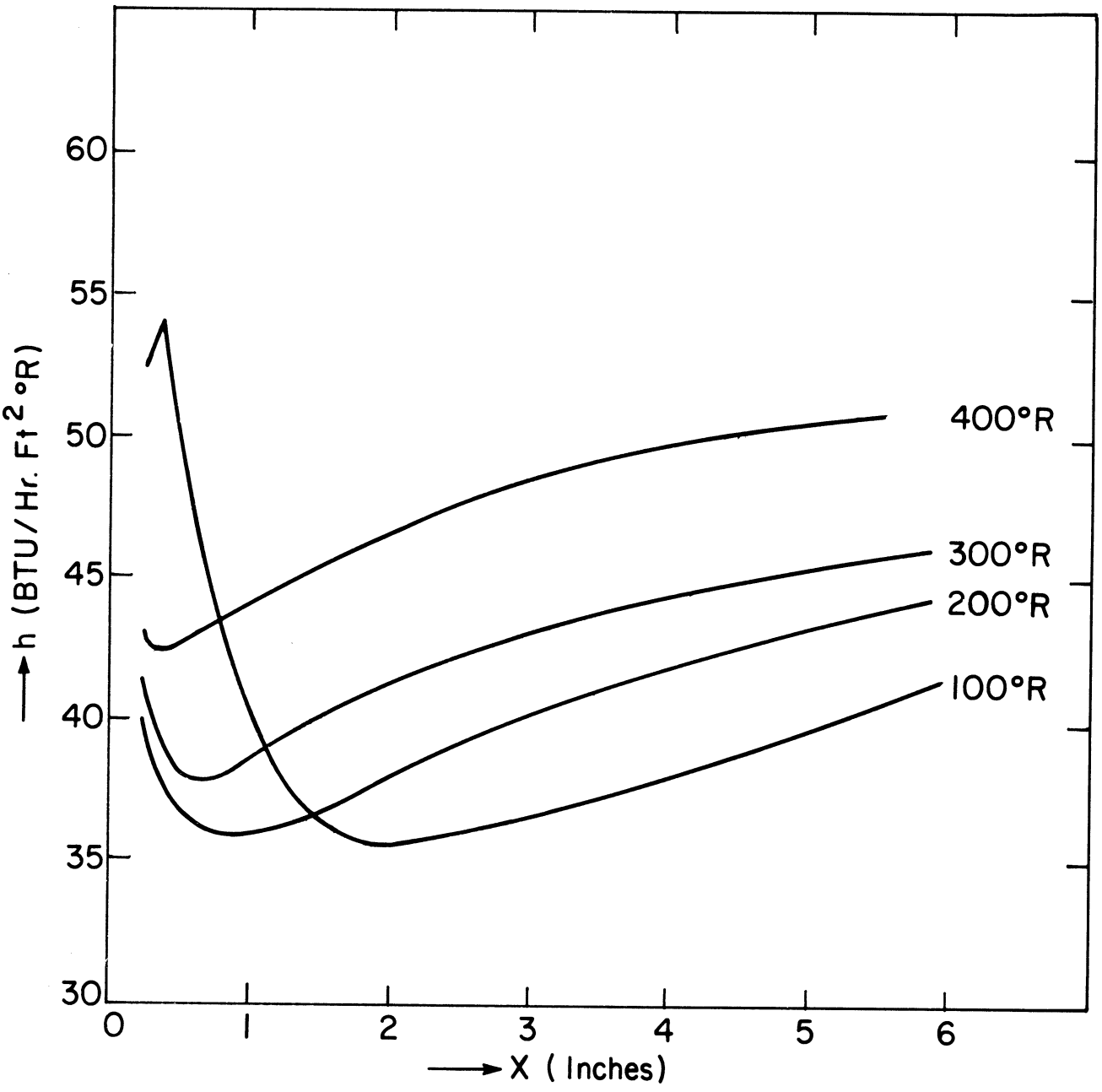

Figure 40. Effect of height on heat transfer coefficient. LH_2.

(ii) For all three levels of ΔT, approximately the same minimum value of h is reached.

(iii) For all three levels of ΔT, the minimum value of h is reached approximately at the same height of about 1 in. It is significant that the minimum is reached at about 1 in., for $\Delta T = 315°R$. It was already pointed out in Section 2 that it may be said, from values of ϵ_H/ν, that turbulence effects begin to be significant at Re = 100. From the results of the present analysis, Re(x = 1 in.) = 104 for $\Delta T = 315°R$.

(iv) Above this height at which h reaches its minimum value, h begins to increase gradually.

(v) At a given height x, the value of h is higher for lower ΔT.

Trends similar to each of the above were also observed by Breen and Westwater (24) in experiments with horizontal tubes in isopropanol, where the tube diameter was varied. On the basis of observations similar to (iii) above, they concluded that the "critical diameter" is independent of ΔT. It may also be noted that for $\Delta T = 100°R$, while the general behavior of the h-x plot is similar to those of h at other ΔT values, h is consistently higher. The minimum value of h seems to occur at a greater height x = 2 in. It should be noted that this $\Delta T = 100°R$ is quite close to ΔT_{min} (ΔT corresponding to minimum heat flux—Reference 54) which is of the order of 45°-50°R for liquid nitrogen. It is possible that transition effects are beginning to show at this ΔT.

A similar h-x plot for liquid hydrogen in Figure 40 presents some interesting departures. For every value of ΔT, h reaches a minimum at a height varying from 3/8 in. to 2 in depending on the value of ΔT Here the similarity with the general trends observed with liquid nitrogen ends. The height at which h_{min} is reached progressively increases from approximately 3/8 in. at $\Delta T = 400°R$ to about 2 in. at $\Delta T = 100°R$. h_{min} is different for each ΔT, varying from a maximum of 42.5 Btu/hr $ft^2°F$ at $\Delta T = 400°R$ to a minimum of about 35.75 Btu/hr $ft^2°F$ at $\Delta T = 100°R$. Also at heights $x < 1.5$in , h increases with ΔT, in contradiction to the trend observed in liquid nitrogen.

One feature of the variation of heat transfer coefficient with height is that near the leading edge, for $\Delta T = 315°R$, 250°R, and 204°R in LN_2, it actually increases initially. This is contrary to the trend predicted by laminar analysis.

8. EFFECT OF ΔT ON HEAT FLUX

Figures 41 and 42 show plots of q' vs. ΔT at different heights for liquid nitrogen and liquid hydrogen, respectively. These curves also show an initial reduction of q' with x up to a height of approximately 7/8 in. and thereafter q' begins to increase. Data for 1 in. sphere for liquid nitrogen (54) and liquid hydrogen (64) are also shown for purposes of comparison. It may be observed that these plots show that for small values of x the reduction in q' with ΔT is much smaller than for larger values of x and that they show a trend of higher q'_{min} for low values of x. Breen and Westwater (24) also observed similar trends in their experiments with horizontal tubes.

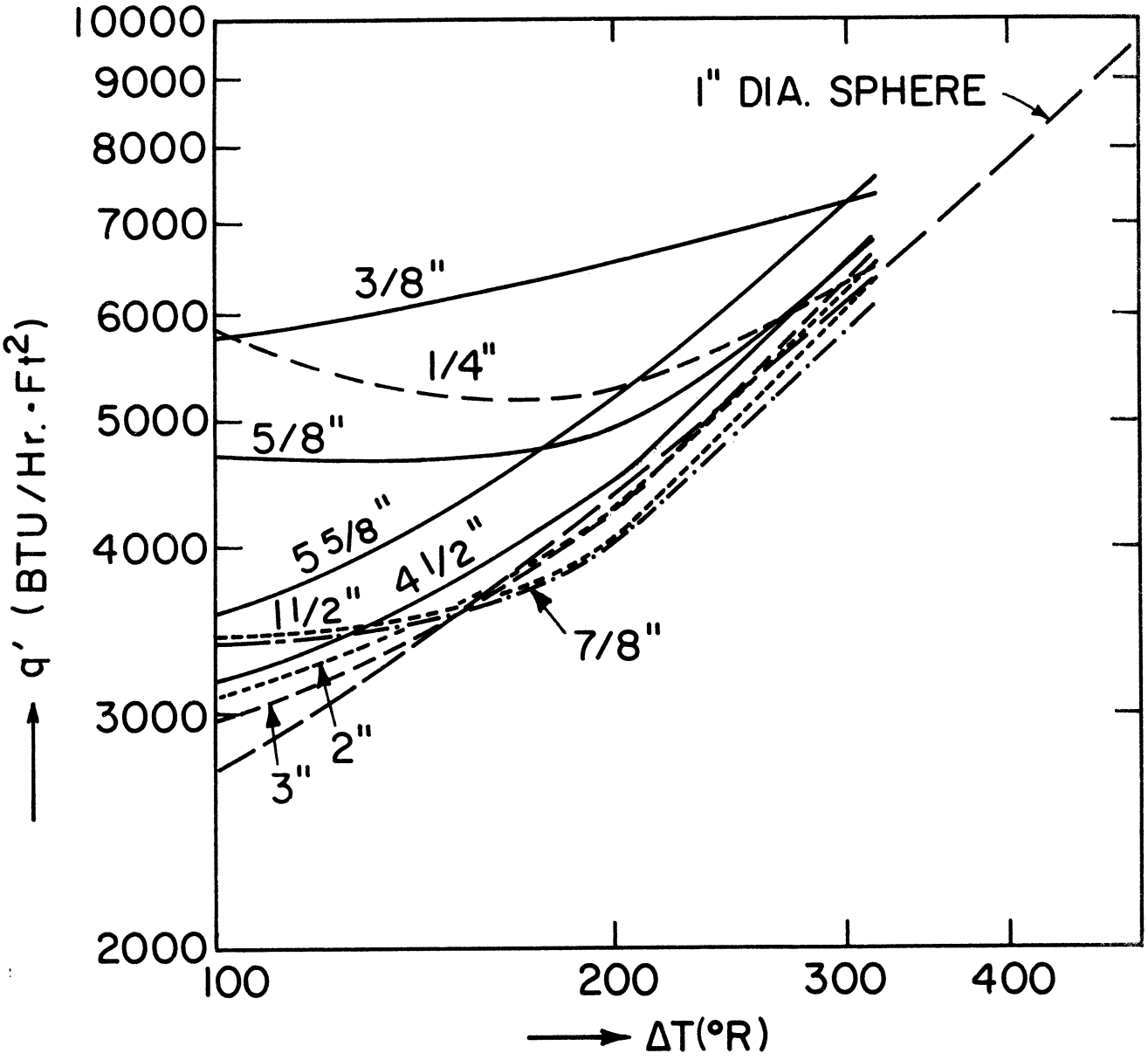

Figure 41. Effect of ΔT on heat flux. LN_2.

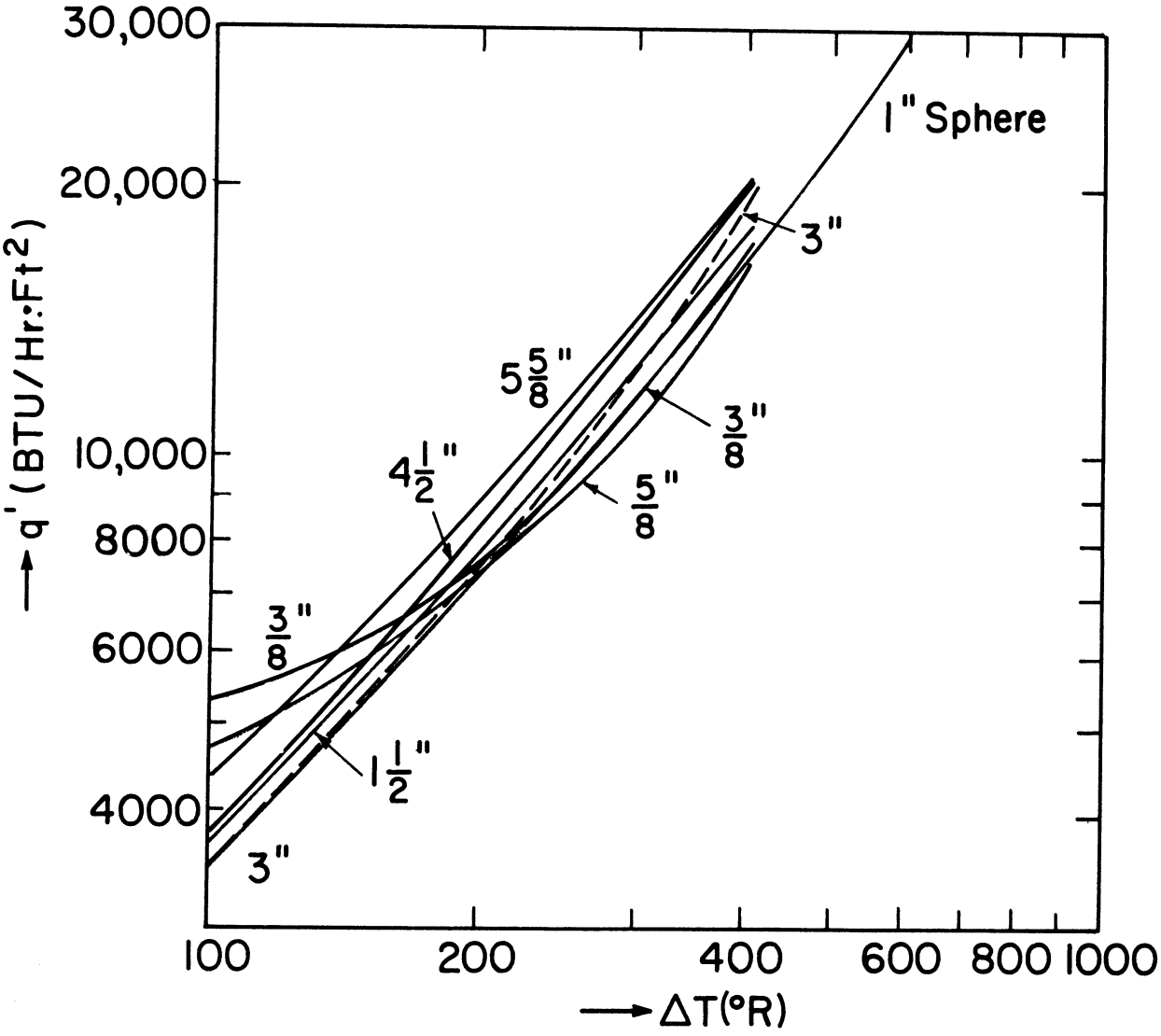

Figure 42. Effect of ΔT on heat flux. LH_2.

9. Nu-Ra CORRELATION

Figure 43 shows the local Nusselt number plotted against Rayleigh number. These are defined as

$$Nu_x = \text{Local Nusselt Number} = \frac{h_x x}{k}$$

where h_x = local heat transfer coefficient and

$$Ra_x = x^3 \frac{\rho(\rho_\ell - \rho)}{\mu^2} g \frac{C_p \mu}{k} \left[\frac{h_{fg}}{C_p \Delta T} + 0.5 \right]$$

All the data for both liquid nitrogen and liquid hydrogen have been represented in this plot. All the properties were evaluated at the film temperature, the arithmetic mean of the extreme temperatures of the vapor film. From this plot, it can be seen that the empirical correlation proposed by Frederking and Clark (57) for spheres

$$Nu = 0.14\ Ra^{1/3}$$

predicts the heat transfer values reasonably well with Nu and Ra computed on the basis of x. The Nu_x for liquid hydrogen are generally higher than this correlation particularly at low Ra. The prediction for liquid nitrogen is much better.

10. EFFECT OF HEIGHT ON HEAT TRANSFER ENHANCEMENT COEFFICIENT

Thus far, in the solution to Eqs. (5.28) a constant value of the heat transfer enhancement coefficient C was used. From an examination of Eq. (6.6)

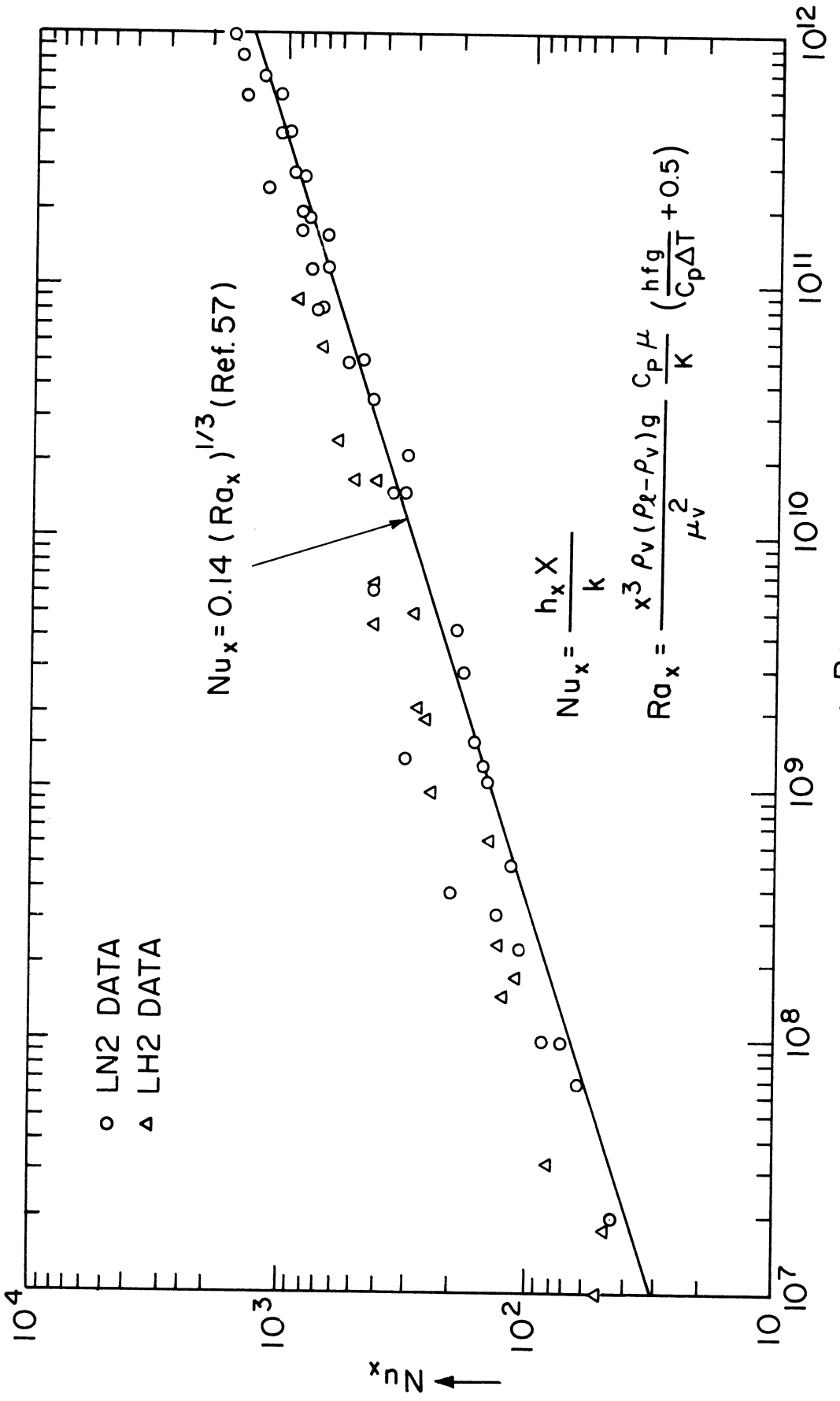

Figure 43. Nu-Ra correlation.

giving the relation between the critical wave number, velocity of the vapor, and fluid properties, it may be expected that the growth of the interfacial instabilities would also depend on these parameters. Therefore, for a given fluid, the dimensionless amplitude of the oscillations may be expected to depend on the velocity of the vapor and the vapor film thickness; these vary with height x, and as C is directly related to the dimensionless amplitude one may expect this to vary with height.

To obtain a better understanding of the variation of C with height as it relates to film thickness given by Eq. (5.5a) the motion pictures of film boiling in liquid nitrogen were analyzed.

Figures 44 and 45 show representative plots of vapor film thickness—frame number taken from such photographs as are reproduced in Figures 28-34. As the filming speed was constant (indicated as frames/sec in the plot), the frame numbers also represent time. Figure 44 shows variation of film thickness with time at heights of 0.146 in., 0.39 in., and 0.78 in. from the leading edge at a $\Delta T = 100°R$ in liquid nitrogen. All the data shown on this plot were obtained from a single film strip. Similarly, Figure 45 shows the variation of vapor film thickness at heights of 4.02 in., 4.4 in. and 4.77 in. at $\Delta T = 315°R$ in liquid nitrogen Similar plots were made for all films taken at different heights (four heights) and $\Delta T = 315°R$, 204°R, and 100°R—a total of 12 films. Figures 46, 47, and 48 are plots of film thickness against height for different ΔT, recast with data obtained from plots such as Figures 44 and 45. It may be observed from Figures 44 and 45 that the maximum and minimum vapor film thicknesses are functions of time. To

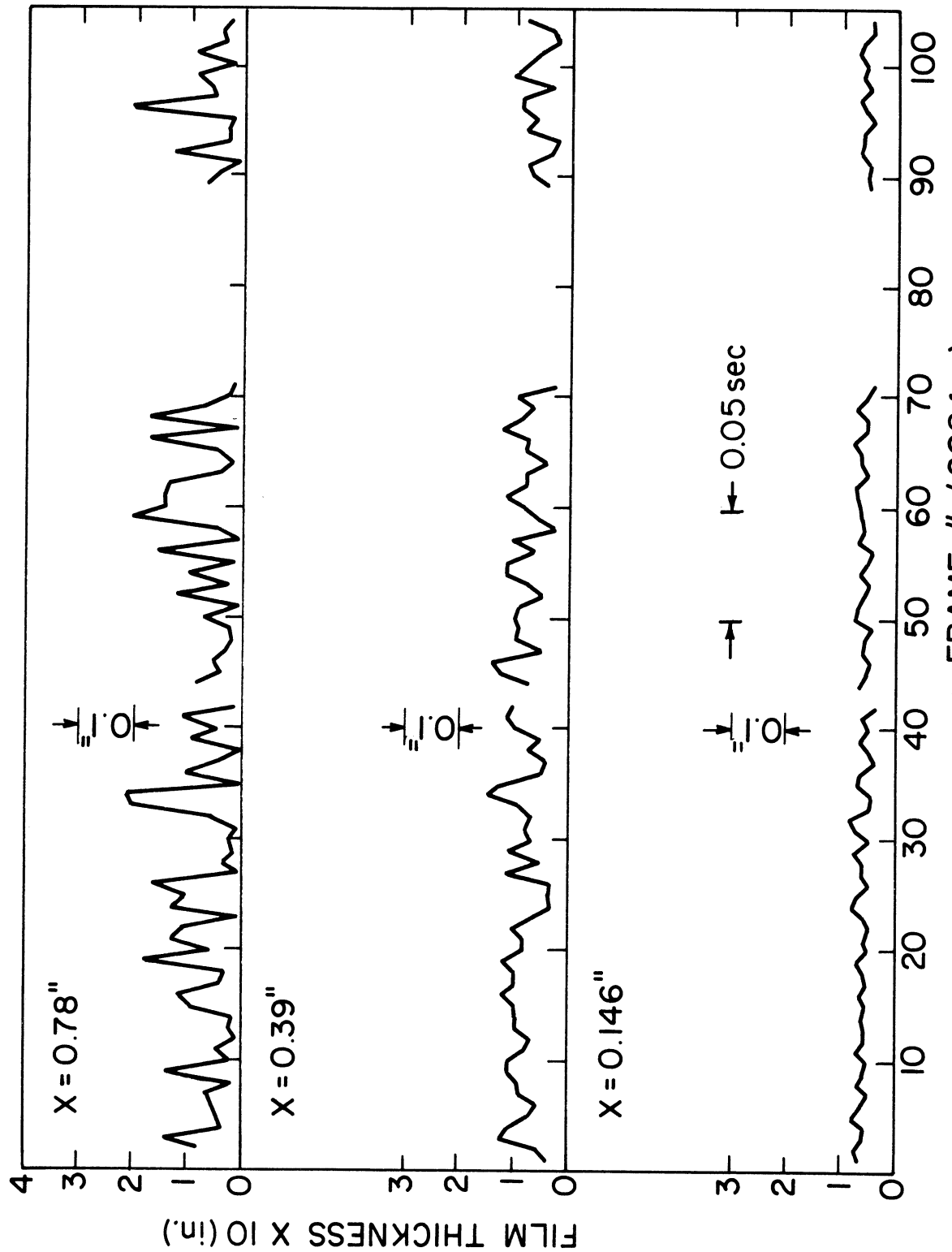

Figure 44. Variation of vapor film thickness with time. LN_2. $\Delta T = 100°R$.

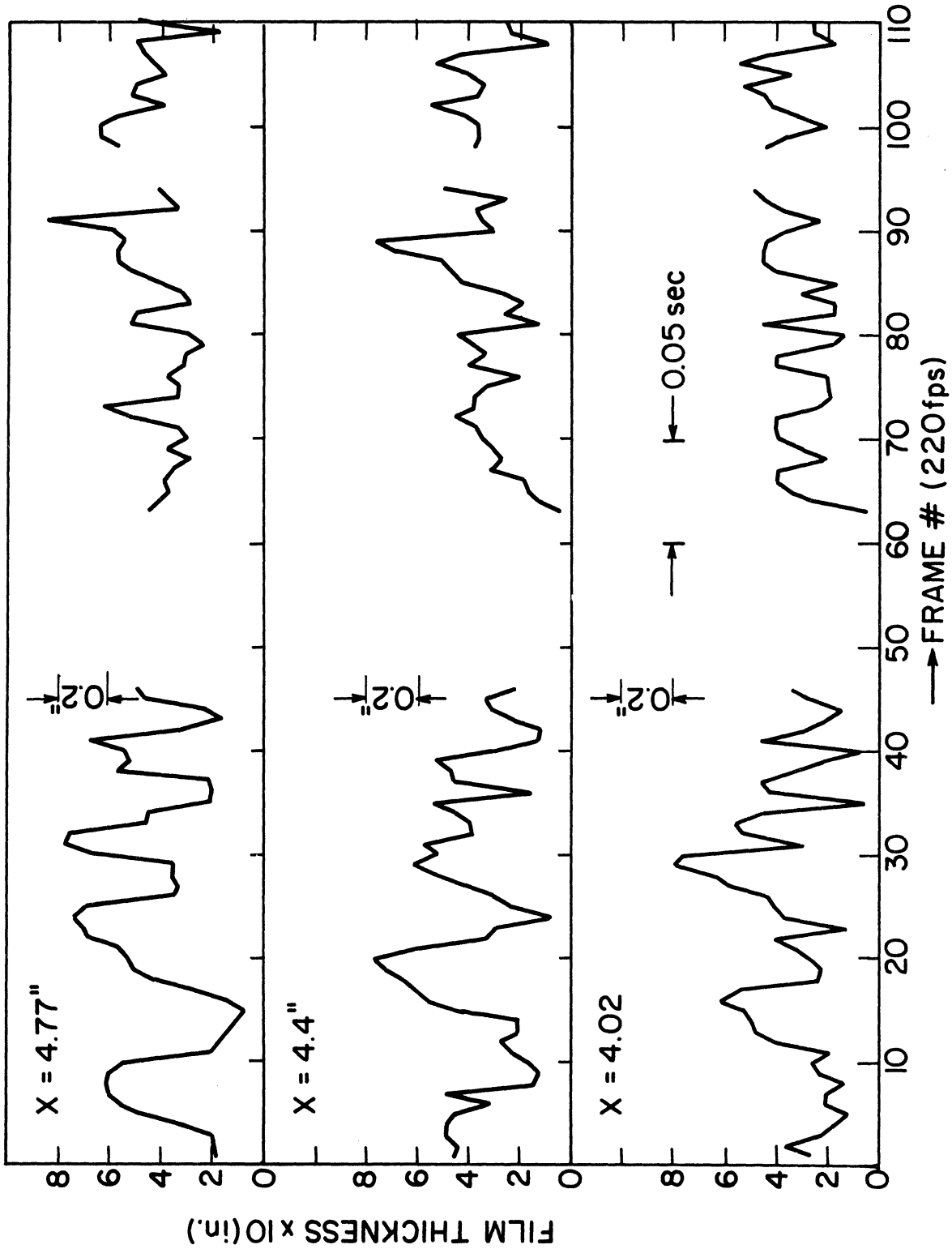

Figure 45. Variation of vapor film thickness with time. LN_2. $\Delta T = 315°R$.

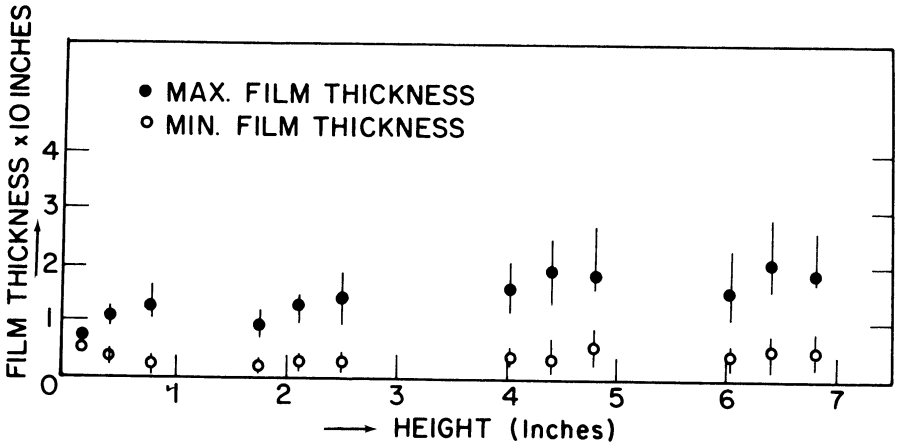

Figure 46. Variation of vapor film thickness with height. LN_2. ΔT = 100°R.

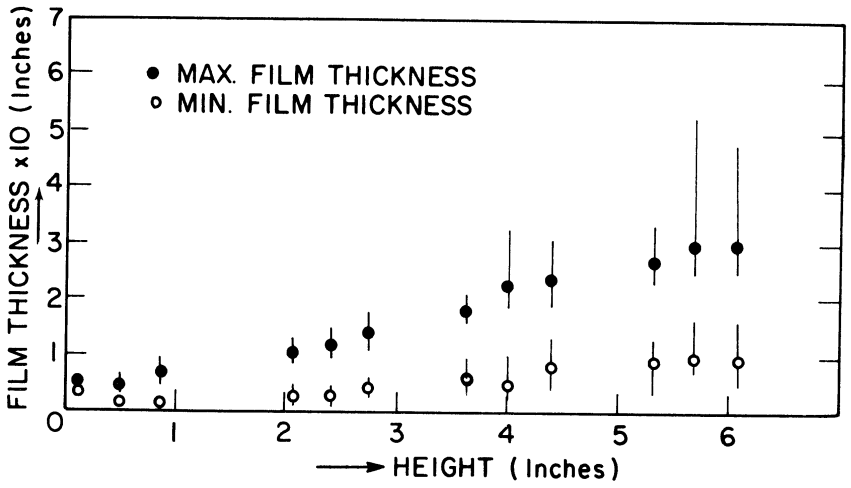

Figure 47. Variation of film thickness with height. LN_2. ΔT = 204°R.

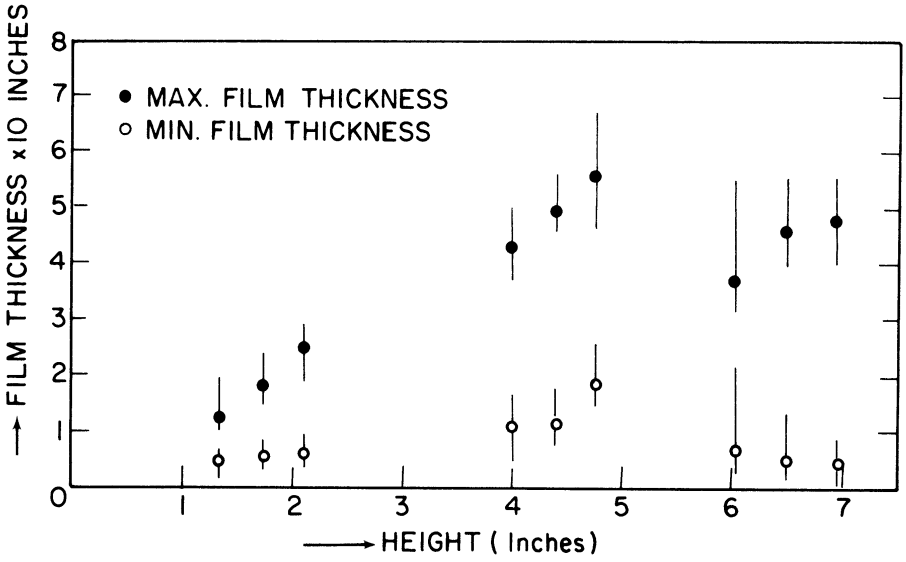

Figure 48. Variation of film thickness with height. LN_2. ΔT = 315°R.

represent all the relevant data from plots such as Figures 44 and 45, Figures 46-48 were constructed in the following manner. Each darkened circle represents the "mean maximum vapor film thickness" at a given location for one value of ΔT. A vertical line is drawn through this point to indicate the range of variation in the maximum vapor film thickness. Similarly, each blank circle represents the "mean minimum vapor film thickness," with a vertical line through it to represent the range of this "minimum thickness."

A calculation of C directly from measured values of film thickness becomes difficult because of the following:

(i) It can be observed from Figures 44 and 45 showing the variation of vapor film thickness with time, that the amplitude of oscillations is a function of time, and the heat transfer enhancement coefficient C related to the dimensionless amplitude through Eq. (5.5a) is also a function of time

(ii) The value of $C = 1/\sqrt{(1-b^2)}$ where b is the dimensionless amplitude—ratio of the amplitude of oscillations to the mean vapor film thickness—is shown plotted against b in Figure 49. From Figures 46-48 showing the minimum and maximum vapor film thickness as a function of time, it is established that the oscillations are of the same order as the vapor film thickness, so that b is close to 1.

At such high values of b, from Figure 49, the value of C is seen to be very sensitive to changes in values of b. A measurement to the degree of precision necessary is not possible, as indicated in Appendix E "Error Analysis."

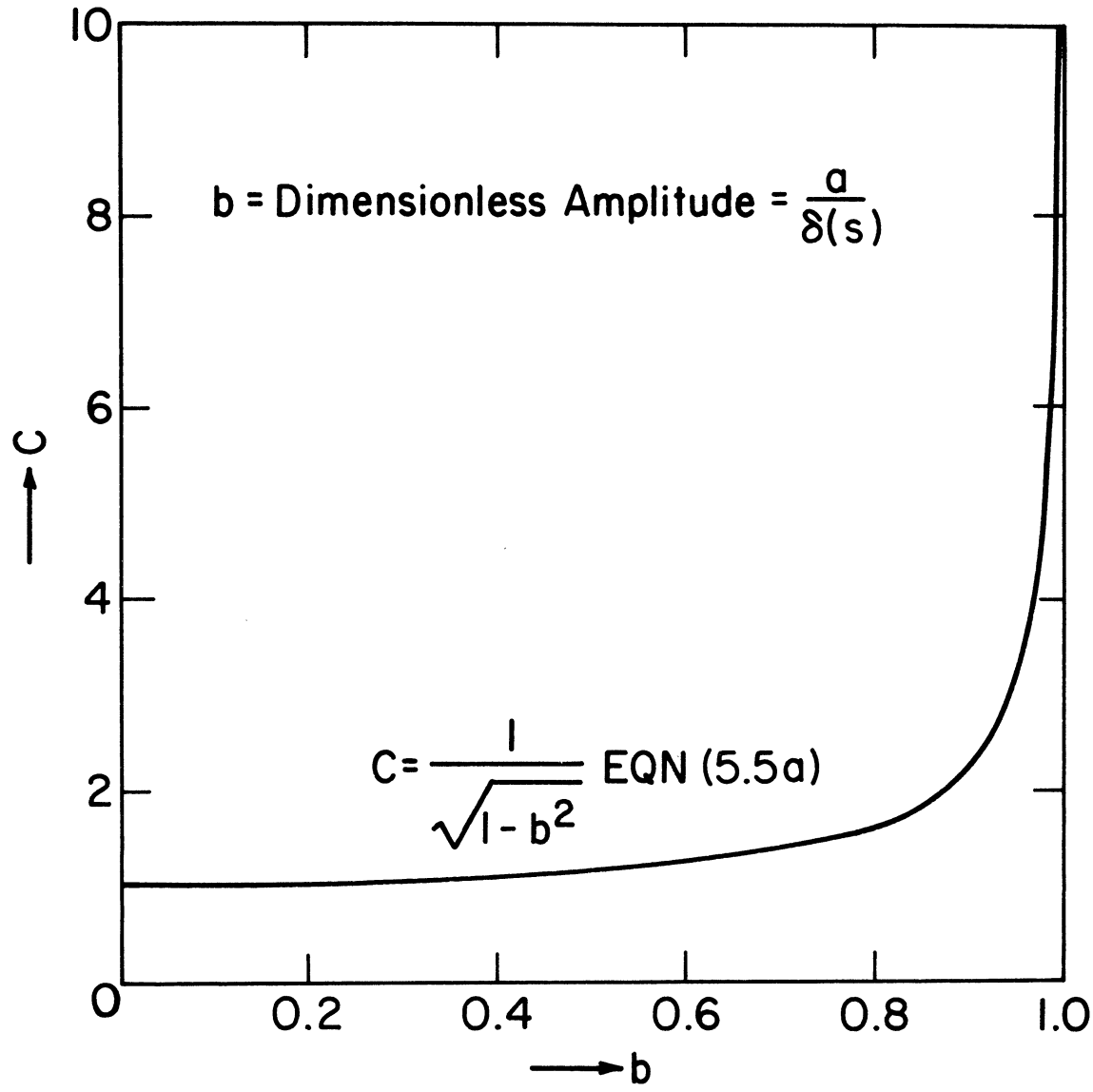

Figure 49. Variation of heat transfer enhancement coefficient C with dimensionless amplitude b.

(iii) It is also doubtful if the assumption of constant temperature profile is valid when the vapor film thickness becomes very small. In such a situation it is likely that due to the high heat transfer rates possible under such circumstances local quenching may take place leading to local suppression of surface superheat, which in turn causes a reduction in the heat transfer rates.

Keeping these factors in mind, instead of attempting to determine one value of C at a given location, three possible values were determined at each location for $\Delta T = 315°R$ and $100°R$—a maximum value obtained from the upper limit of maximum vapor film thickness and the lower limit of minimum vapor film thickness, a mean value obtained from the mean maximum and mean minimum values and a minimum value obtained from the lower limit of the maximum vapor film thickness and the upper limit of the minimum vapor film thickness. The plots of such values of C as a function of height for $\Delta T=315°R$ and $\Delta T=100°R$ are shown in Figures 50 and 51.

We may now attempt to specify a function giving the variation of C with height or another parameter associated with height, either directly or indirectly. As has been indicated earlier in this section, the value of C may be expected to be dependent on the vapor velocity, vapor and liquid density, vapor film thickness and other parameters such as surface tension and gravity. The mechanism of such oscillations is not completely understood and the precise definition of the interfacial oscillations is not possible at the present time. As a simplification, it will be hypothesized that the local Reynolds number is an indication of such oscillations. Figure 52 was constructed by replotting C_{max} from Figure 50, on a log-log scale replacing x with the corresponding Reynolds number at that location. The Reynolds number

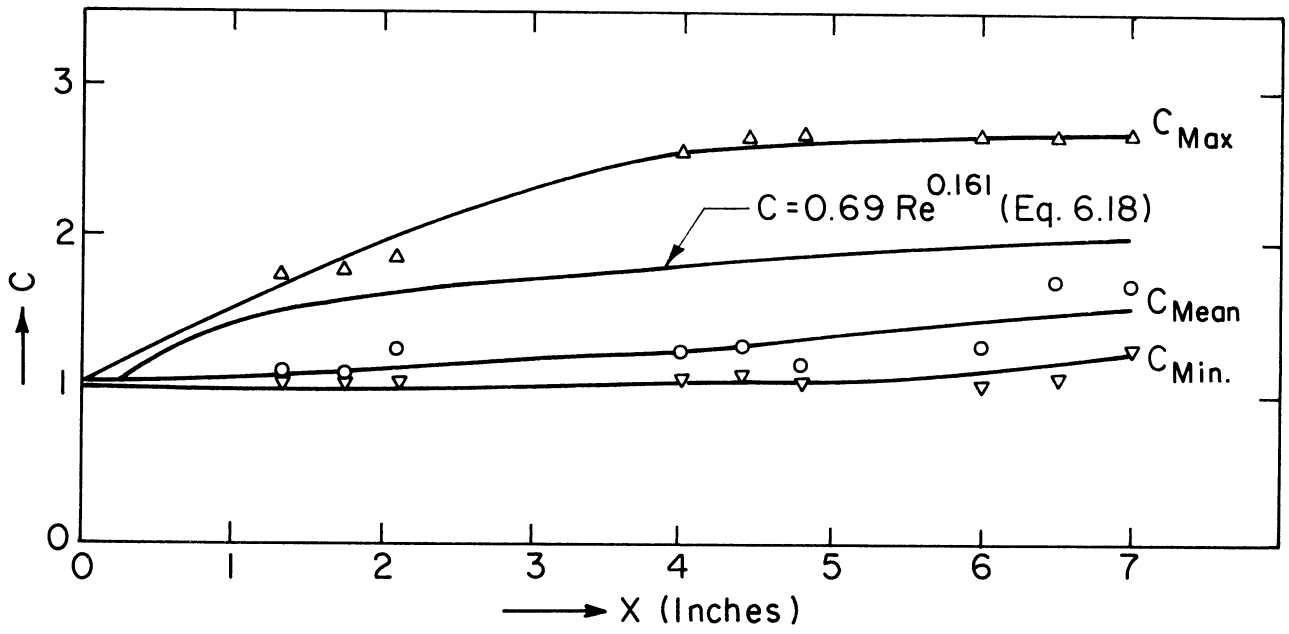

Figure 50. Variation of C with x. LN_2. ΔT = 315 °R.

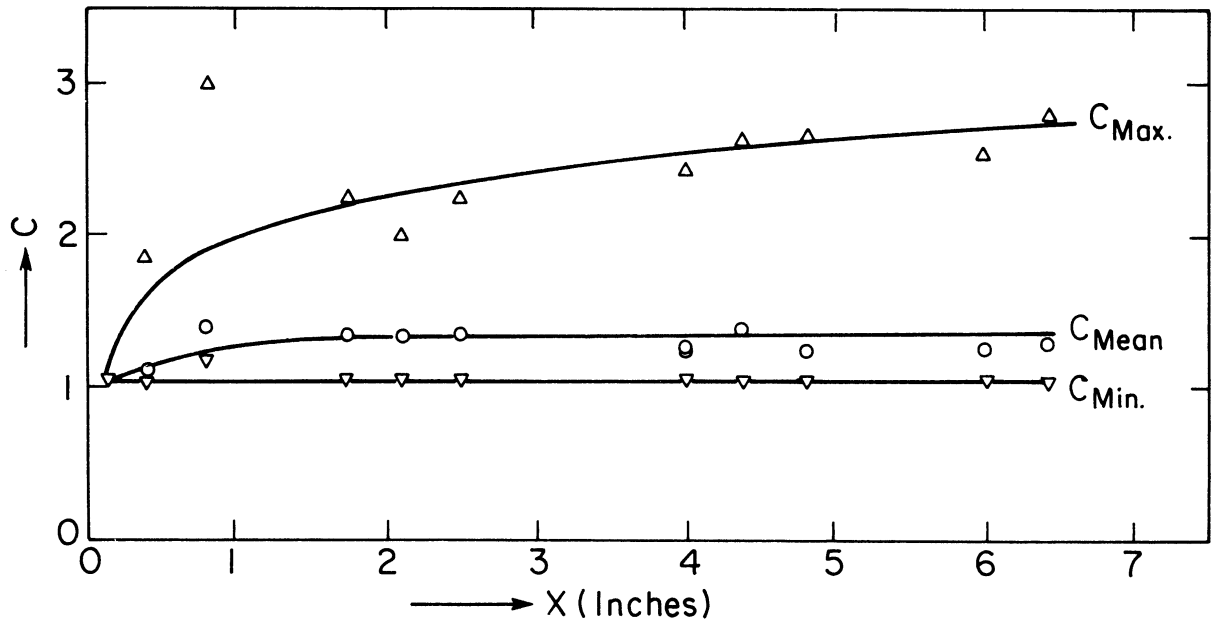

Figure 51. Variation of C with x. LN_2. ΔT = 100 °R.

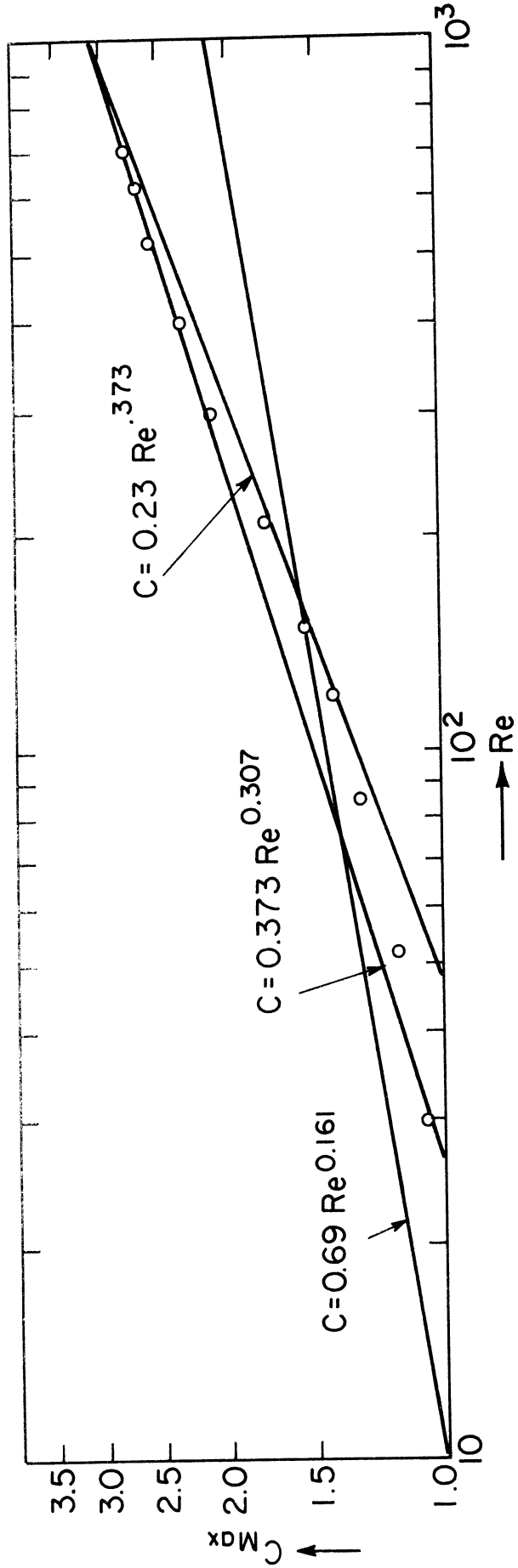

Figure 52. Variation of C_{max} with Re. IN_2. ΔT = 315°R.

was obtained from computations of turbulent film boiling using constant value of 1.78 for C.

Two lines represented by

$$C = 0.373 Re^{0.307} \tag{6.16}$$

and

$$C = 0.23 Re^{0.373} \tag{6.17}$$

are also shown on the same plot and these can be said to encompass the values of C_{max} for $\Delta T = 315°R$. From Figure 50 it can be seen that the minimum value of C is very close to 1.0, being less than 1.1 to a height of 5 in. and thereafter increasing to 1.15 at 6 in. Because of these very low values, the minimum value of C was set equal to 1. Using Eqs. (6.16) and (6.17) each to represent C_{max} and C = 1 as C_{min}, Eqs. (5.28) were solved and the resulting values of q' vs. x are shown in Figure 53. In each case, if the functional representation of C, Eqs. (6.16) and (6.17) gave a value $C < 1.0$, it was taken as C = 1, as C cannot admit a value of less than 1.0. Equation (6.16) predicts a slightly higher value for C at low Re than Eq. (6.17) and the effect of this is clearly seen in predictions close to the leading edge where Eq. (6.17) gives lower q' values. For higher values of Re, the differences in C values given by these two expressions gradually decrease, which is reflected in the similarity of q' - x behavior. q' - x plot for C = 1 is also shown in Figure 53.

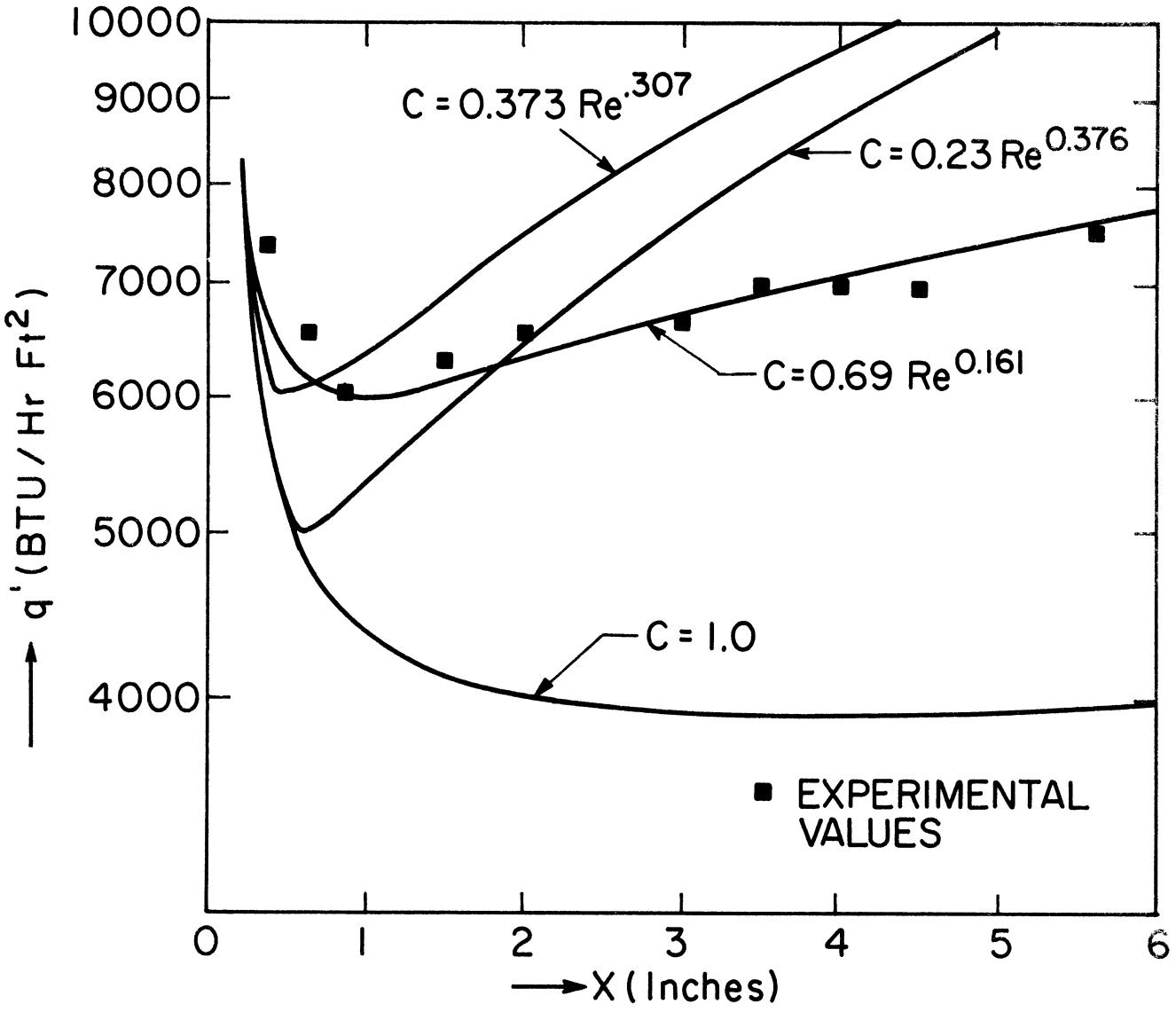

Figure 53. Effect of varying C with x. LN_2. ΔT = 315°R.

From these curves, it can be seen that the experimental values lie between the two extreme approximations in the value of C, with $C_{min} = 1.0$. Recognizing that the actual variation of C would probably lie between these two extremes, several different approximations were tried and the one giving the best fit for experimental data is shown plotted in Figure 53 with C given by

$$C = 0.69Re^{0.161} \tag{6.18}$$

This curve follows all the essential trends observed in the experimental data, the decrease in heat flux at low values of x, reaching a minimum at about 1 in. from the leading edge and then increasing with height. With this representation of C, the effects of interfacial oscillations begin to show at heights of around 0.2 in. (indicated by values of C obtained in the solution of Eqs. (5.28)) and this is consistent with the approximations in Figure 36 which indicates that the interfacial oscillations begin to appear at around 0.12 in. from the leading edge. Equation (6.18) is also shown plotted on Figure 50 showing variation of C with x.

D. Summary, Conclusions and Recommendations

1. SUMMARY

The purpose of this study was to experimentally determine the local heat transfer rates in film boiling on a vertical surface and predict such heat

transfer rates with a suitable model. Vertical cylindrical test surfaces were used to simulate vertical plane surfaces, and heat transfer rates were determined at 11 locations up to a height of 6 in. for four different values of ΔT in two cryogenic fluids—liquid nitrogen and liquid hydrogen. Supporting data were obtained with motion pictures in order to understand the nature of the vapor film. The laminar vapor regime was extended by the use of the drop tower.

2. CONCLUSIONS

From the results obtained over the range of height, ΔT and liquids covered, the following conclusion can be drawn:

(i) Under normal conditions, $a/g = 1$, laminar region with a smooth interface is confined to a very short region near the leading edge.

(ii) Initially, heat transfer rates decrease with height, reach a minimum and begin to increase gradually.

(iii) Interfacial oscillations of large amplitudes are established within a very short distance from the leading edge.

(iv) Within a short distance from the leading edge, heat transfer rates are enhanced due to the effects of interfacial oscillations and turbulence effects.

(v) The model adopted using a universal velocity profile, predicts the heat transfer rates reasonably well.

(vi) The empirical correlation suggested by Frederking and Clark (57) for spheres predict heat transfer rates reasonably well.

(vii) Even in the laminar regime, the heat transfer rates are considerably higher than predicted by laminar analysis (6).

(viii) Minimum heat flux increases with a decrease in height.

3. RECOMMENDATIONS

For further work on this problem the following suggestions are made.

(i) Extend the scope of experimental work to cover other liquids and higher ΔT and x using a flat vertical surface.

(ii) Experimentally determine the temperature and velocity profiles in the vapor film and the relation between ϵ_m and ϵ_H.

(iii) Improve the analysis by considering the effect of vaporization at the interface, both on the velocity profile and shear stress distribution and the relation between ϵ_m and ϵ_H.

APPENDIX A

DROP PACKAGE

Figure 54 shows details of the drop package. This consisted of an inner cylinder, acting as a piston, which moved in an outer cylinder. A metering pin, appropriately shaped, was attached to the bottom of the inner cylinder and passed through an orifice plate attached to the bottom of the outer cylinder. A tube with a conical wooden piece at its lower end, fixed to the outer cylinder acted as a guide for the metering pin.

The dewar itself was suspended from the cover plate of the inner cylinder. A tube screwed into the cover plate acted as the guide for the tube carrying the test piece in the dewar and had a lifting pin at the top, which could be held in a release mechanism (Figure 55). The lifting pin had a circular groove, in which balls in a cage registered. They were retained in place by a sliding ring, which had a tapered part as shown. When the ring was lowered, the balls moved out, releasing the drop package. The outer sleeve was remotely controlled by an air-cylinder piston arrangement. The drop tower (Figures 56 and 57) consisted of an enclosed chute extending from the third floor to the first floor of the laboratory, giving a free drop distance of approximately 32 ft. and a free fall drop time of approximately 1.34 sec. After the drop the package was hoisted by an air winch placed on the third floor. The package was brought to rest by a sand box at the bottom; the conical wooden piece at the end of the tube on the outer cylinder of the drop package penetrated

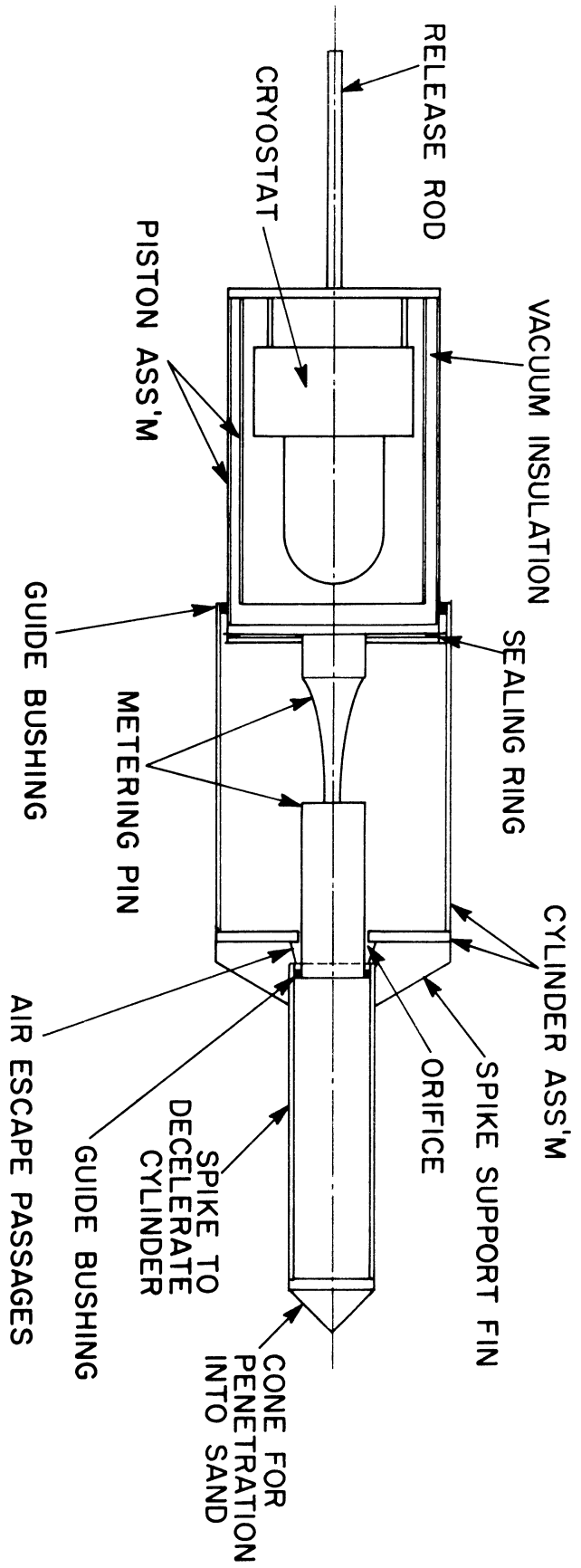

Figure 54. Drop package.

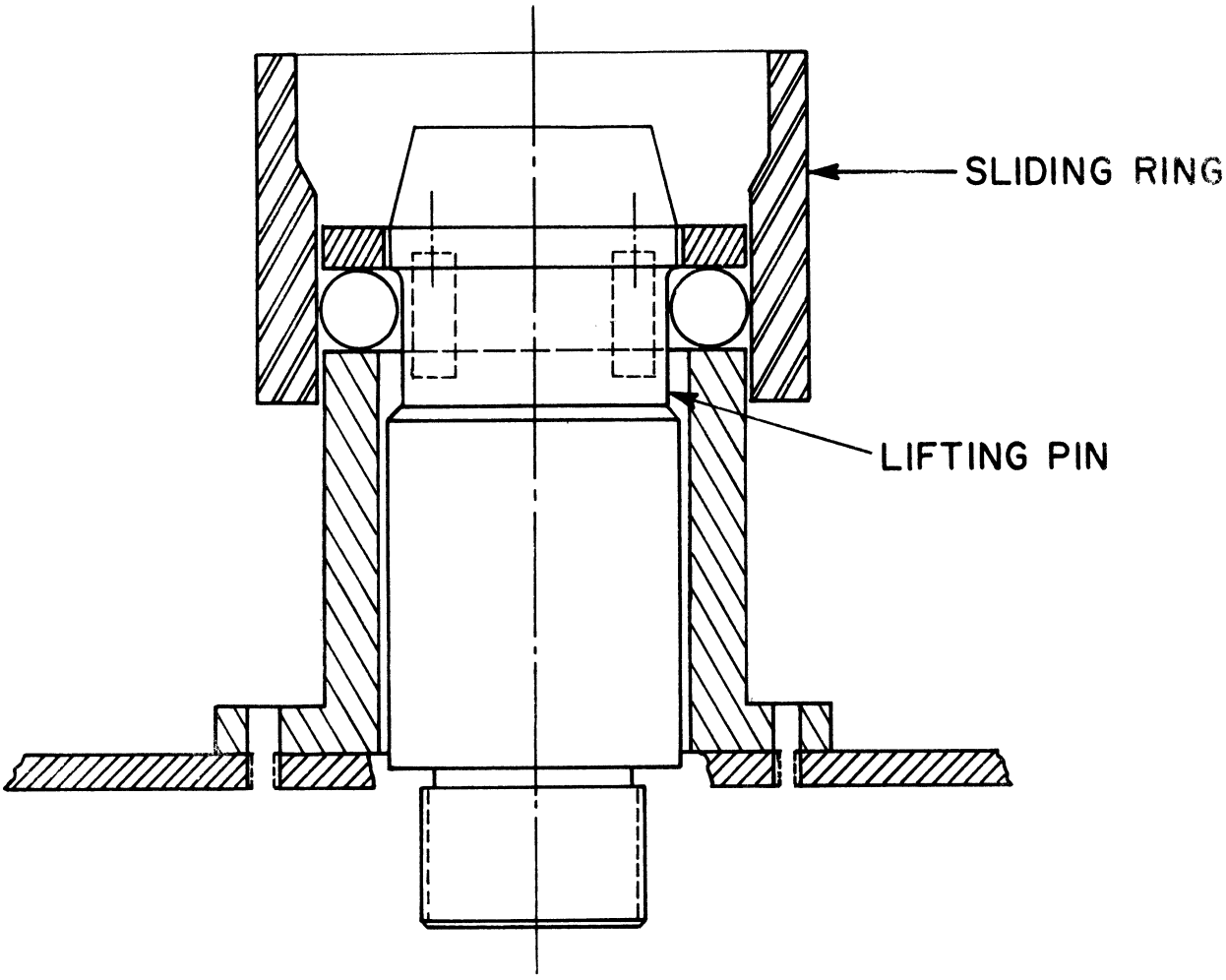

Figure 55. Release mechanism.

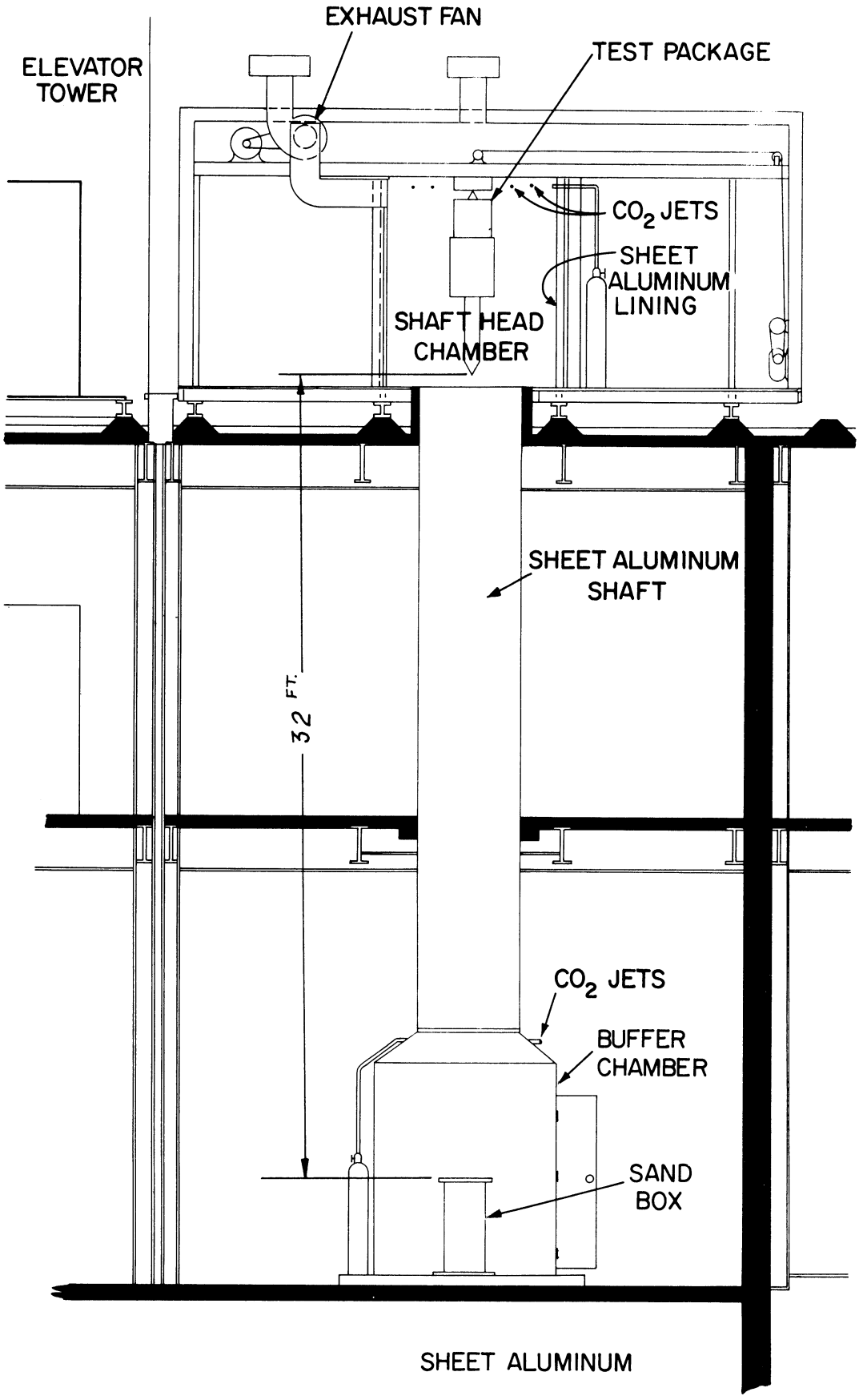

Figure 56. Drop tower—elevation.

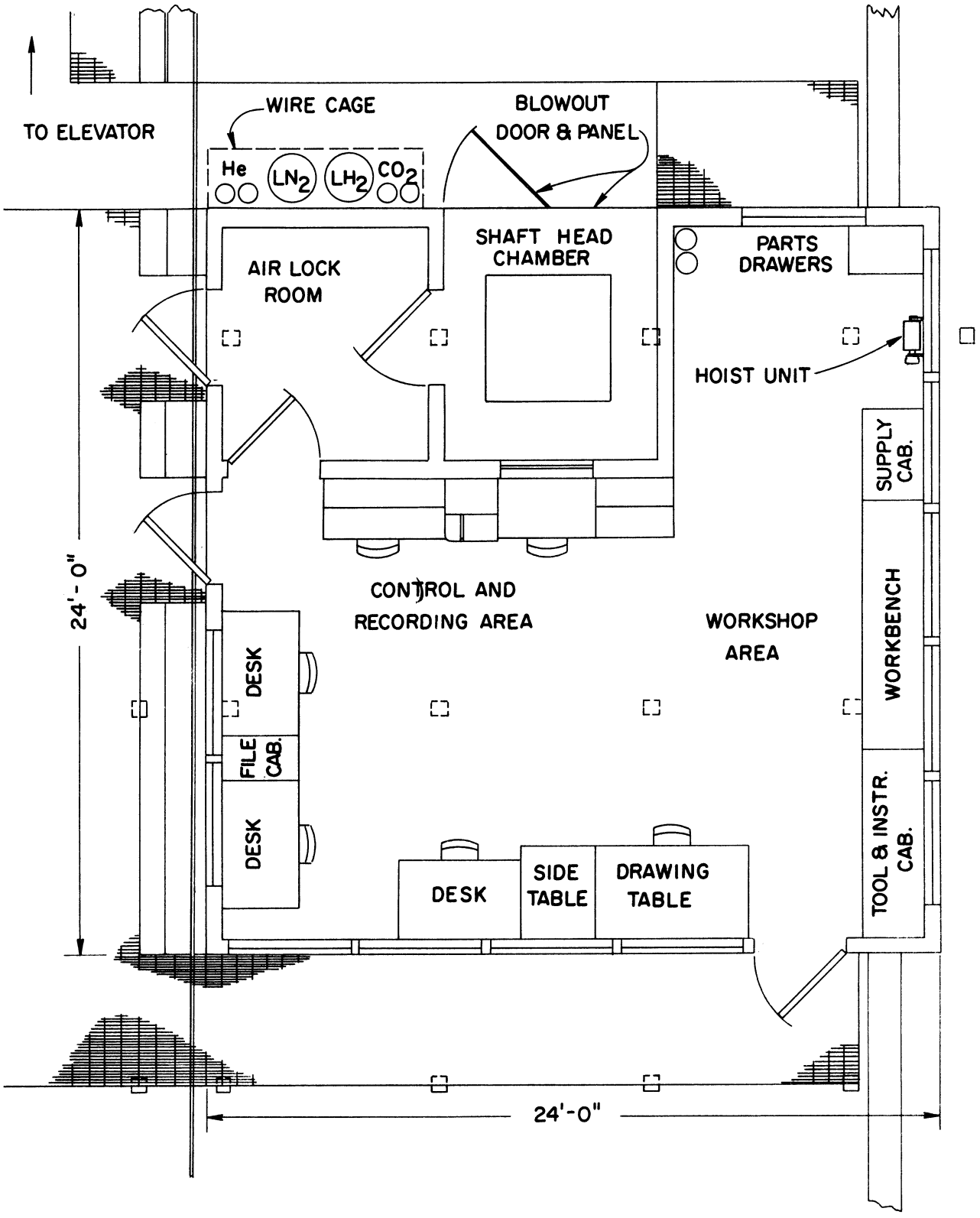

Figure 57. Drop tower—plan on third floor.

the sand approximately 17 in. under free fall conditions before the package was brought to rest.

As liquid hydrogen was used in the drop tower the following safety precautions were taken.

(i) An explosion proof ventilating fan giving two air changes per minute to remove hydrogen vapor, was continuously running.

(ii) A gas analyzer sampled the air sequentially from four stations in the drop tower and sounded an alarm whenever the hydrogen concentration in the area where a sampling station was located exceeded a preset limit.

(iii) Provision of nonsparking lead sheathed floors, grounding of all equipment, nonsparking beryllium tools and grounding leg straps for personnel in the area to prevent sparking due to discharge of static charges.

(iv) Provision for flooding the drop tower with CO_2 in case of rupture of cryostat containing liquid hydrogen, or small fires.

Before releasing the package the inner vessel was fully extended and held in that position by the release mechanism. In this position there was very little clearance between the metering pin and the orifice plate. When the outer cylinder, after release, hit the sand and came to rest, the inner cylinder continued its motion, the air trapped in the outer cylinder built up pressure till the clearance between the orifice plate and the metering pin increased venting the air until the inner vessel was within a few inches of coming to rest. The clearance between the metering pin and the orifice plate

decreased at this point allowing the trapped air in the outer cylinder to provide a cushion for the inner vessel carrying the dewar and test surface till it came to a complete rest.

The deceleration was measured by a piezoelectric crystal mounted on the top of the test package. The signal from the crystal was fed to a charge amplifier and then measured in an oscilloscope. A pressure transducer mounted on the test package monitored the air pressure in the outer cylinder. A typical oscilloscope trace is reproduced in Figure 58. The maximum deceleration was approximately 25 g and the maximum air pressure 17 psig.

The acceleration of the inner cylinder carrying the dewar and test surface was measured during free fall by a Kister model 303 accelerometer. The output was recorded on the Sanborn Recorder. The accelerometer was calibrated before use by a device which gave variable acceleration from $a/g = 1$ to $a/g = -1$. The a/g under free fall conditions is given in Figure 59. From this plot it is seen that the body force increased as the package fell, due to increasing air drag. This increase reached a maximum value of approximately 0.008. The lapsed time in free fall was approximately 1.345 sec.

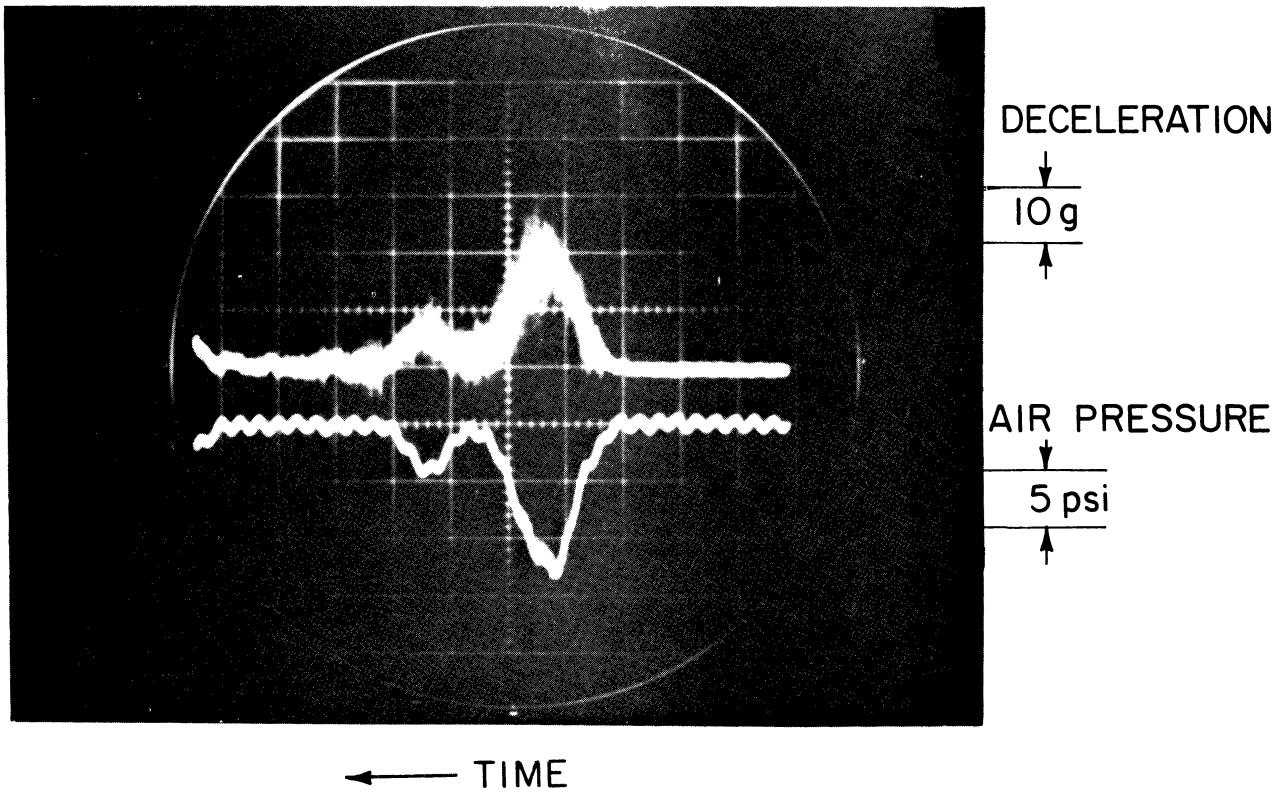

Figure 58. Drop package deceleration--inner cylinder; oscilloscope trace.

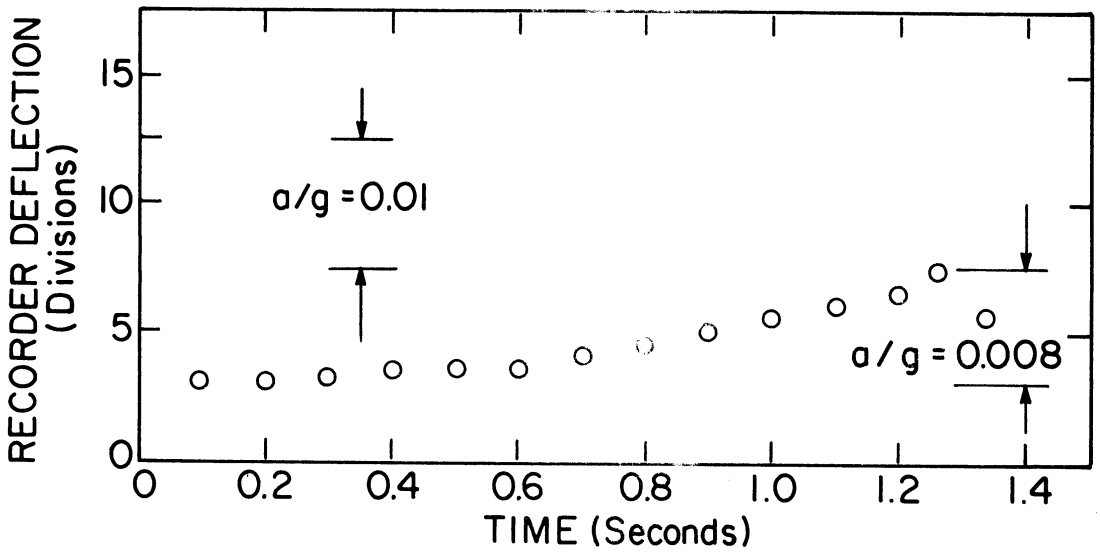

Figure 59. Drop package acceleration—free fall.

APPENDIX B

EFFECT OF INSULATION

Local heat flux measurements were made by recording the temperature of a test section as a function of time and equating the time rate of change of enthalpy of the test section to the heat transfer from the section. For this method to be valid, the test section must be thermally insulated from the adjoining spacer pieces. Attempts were made to introduce an air gap (of around 0.005 in.) between the test section and adjoining pieces but this was not practicable mainly because of difficulty in properly aligning the several pieces in the test piece.

Satisfactory results were obtained by using Teflon washers between the different sections. To minimize the area of heat leakage from the test section to the adjoining sections due to the temperature differential in the various sections during the cool down period, a recess was cut in the spacer pieces so that only a circular section of 1/16 in. radial thickness was pressed against the adjoining section, separated by a Teflon washer. In order to study the effects of introducing an insulating material, test piece 1 was constructed using different thicknesses of Teflon insulation washers (0.005 in., 0.010 in., 0.015 in., and 0.060 in.) in sequence and comparing the resulting heat flux data observed. A plot of the heat flux data from the different sections for different thicknesses of the insulating material is given in Figure 60.

From this plot it is observed that heat flux values are constant, within the limits of experimental scatter for various thicknesses of Teflon from

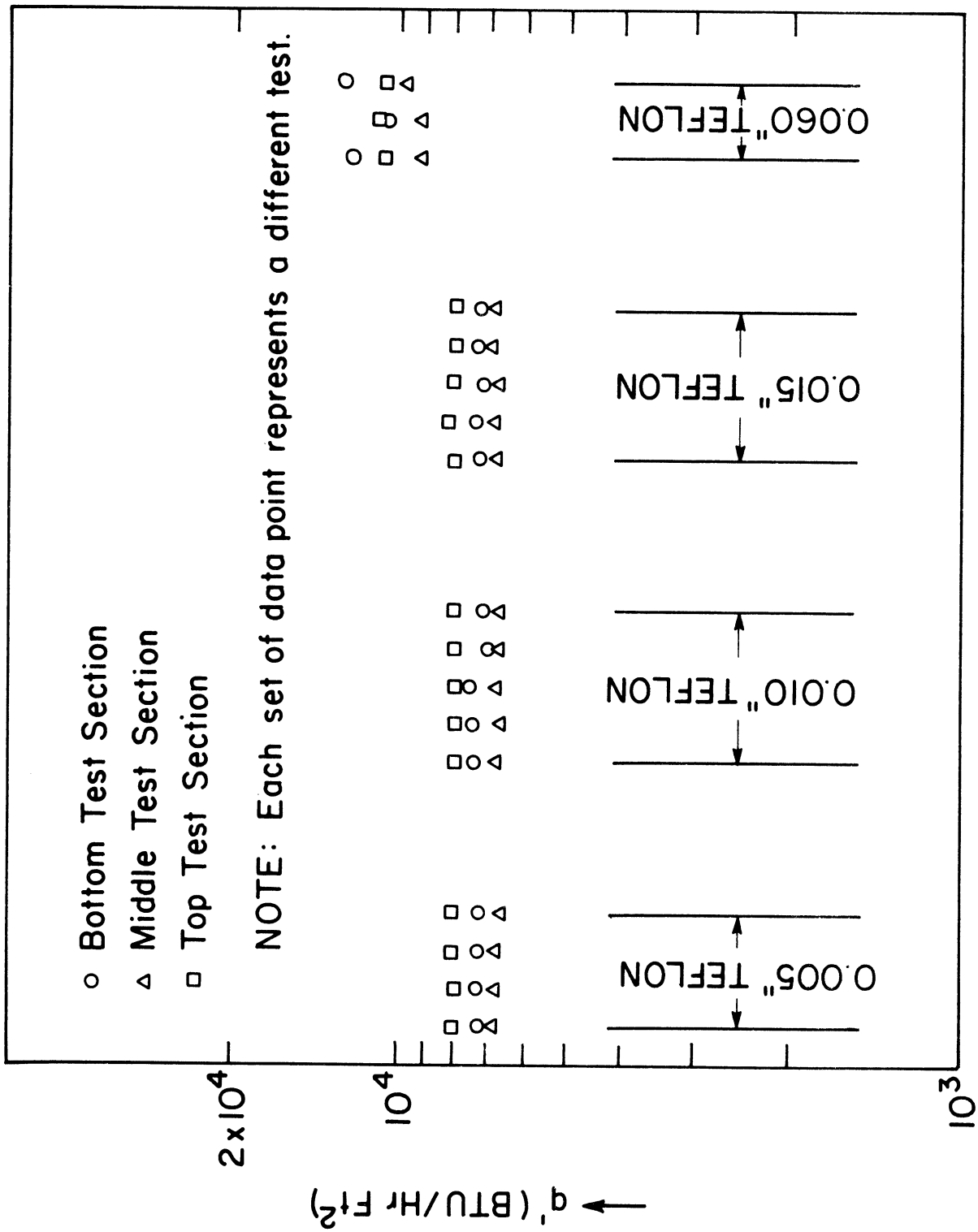

Figure 60. Effect of Teflon insulation thickness. LN_2. $\Delta T = 315°R$.

0.005 in. to 0.015 in. but there is a considerable increase in measured heat flux when the thickness is increased to 0.060 in. It is believed that this increase is due to increased heat transfer to the liquid via the larger thicknesses of Teflon. The surface temperature of the Teflon is depressed but because of the lower diffusivity of Teflon, there is no enthalpy flow to sustain the temperature at a high value, and hence nucleate boiling is quickly established with a subsequent considerable increase in the heat transfer rate. The 1/4 in. copper section is now placed between two Teflon pieces whose surface temperature is much lower than that of the section itself. Hence, in addition to the heat transfer directly to the adjacent fluid, there is a secondary heat transfer path through the Teflon pieces. This leads to an increase in the heat transfer rate from the section. But with lower thicknesses, the Teflon is blanketed by a vapor film and there is no direct liquid surface contact. It was concluded that 0.005 in. thick Teflon would provide a satisfactory insulation and was used in the test surfaces.

APPENDIX C

EFFECT OF CONTAINER SIZE

The available glass dewar had an inside diameter of 10 cm (4 in.). To find the maximum diameter of the test piece that could be used in this container without the walls of the container affecting the results, heat flux values were obtained with a 1 in. diameter test piece, first in a 6 in. diameter container, then with tubes of 2-1/2 in., 2 in., and 1-1/2 in. diameter tubes placed in the 6 in. diameter dewar. The heat flux data obtained with this test piece at three different locations—5/8 in., 3 in., and 5-5/8 in. from the leading edge at a mean temperature of 455°R—are plotted in Figure 61. This was the highest temperature of the surface used and consequently vapor generation rate was highest. From the plot it can be observed that a radial clearance of 1/2 in. is adequate to reduce the effects of the container walls to acceptable limits. Hence, test pieces were made of 1 in. and 2-1/4 in. diameter cylindrical pieces, giving a minimum radial clearance of 3/4 in. between the test surface and container walls.

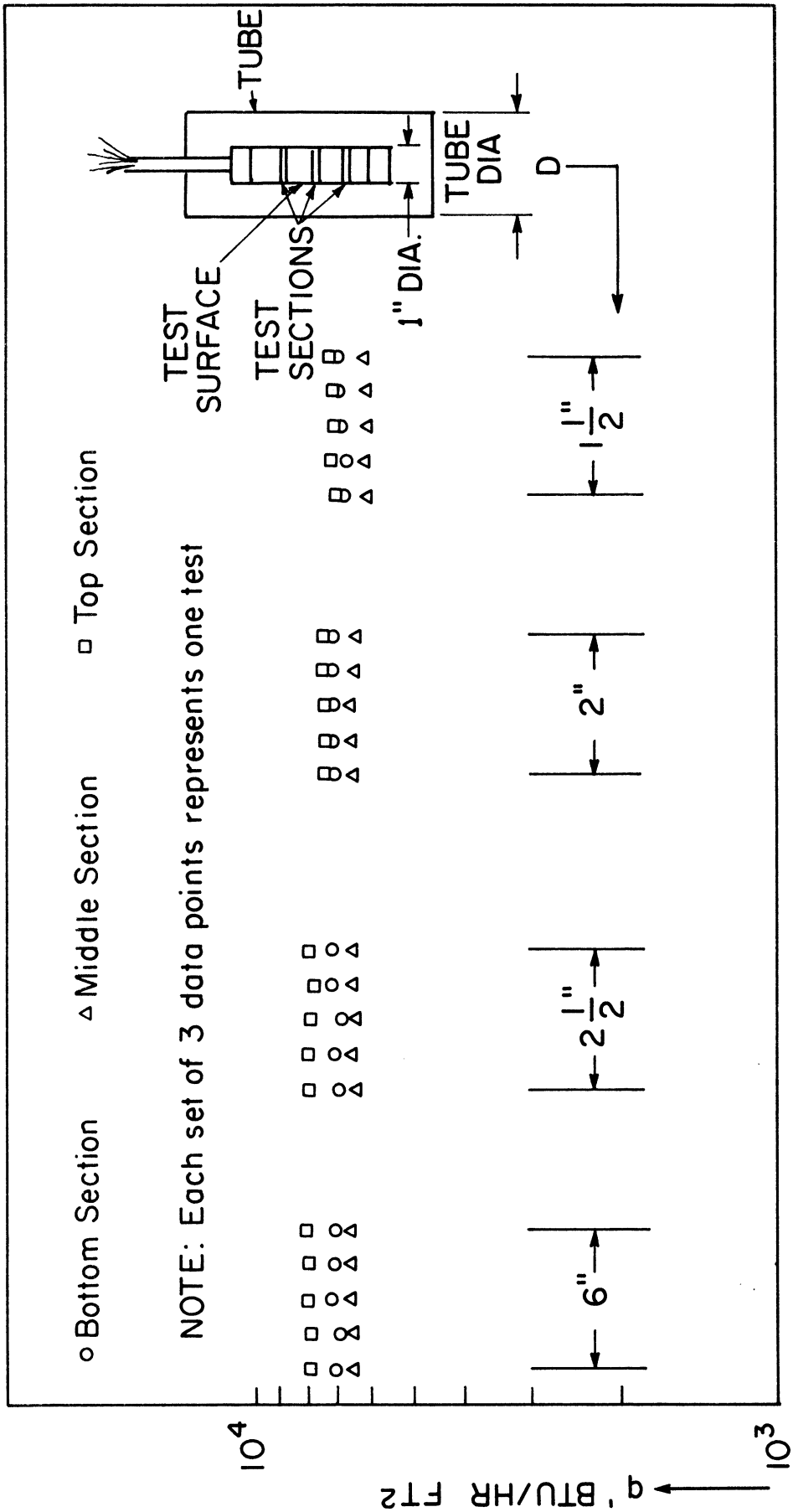

Figure 61. Effect of container size. LN_2. $\Delta T = 315°R$.

APPENDIX D

JUSTIFICATION FOR LUMPED ANALYSIS

In the experiments, the heat flux to the surrounding liquid from the test surface was calculated by measuring the rate enthalpy change of the test section. The rate enthalpy change of the test section was determined through a time-temperature chart obtained from one thermocouple installed in the test section. The validity of this procedure is dependent on the assumption that the time rate of change of temperature at every point in the test section is the same.

To test the validity of this assumption consider a semi-infinite slab of thickness 2d (Figure 62), suddenly immersed in a cryogenic fluid at its saturation temperature T_s with a heat transfer coefficient h assumed to be constant. From Figure 39 showing variation of h with ΔT, it can be seen that h is substantially constant for different values of ΔT. The initial uniform temperature of the block is T_o and is high enough to induce film boiling.

The applicable equation is

$$\frac{1}{\alpha}\frac{\partial T}{\partial t} = \frac{\partial^2 T}{\partial x^2} \tag{D.1}$$

with

$$\begin{aligned} t &= 0 \qquad T = T_o \\ x &= 0 \qquad \frac{\partial T}{\partial x} = 0 \\ x &= d \qquad k\frac{\partial T}{\partial x} + h(T_w - T_s) = 0 \end{aligned} \tag{D.2}$$

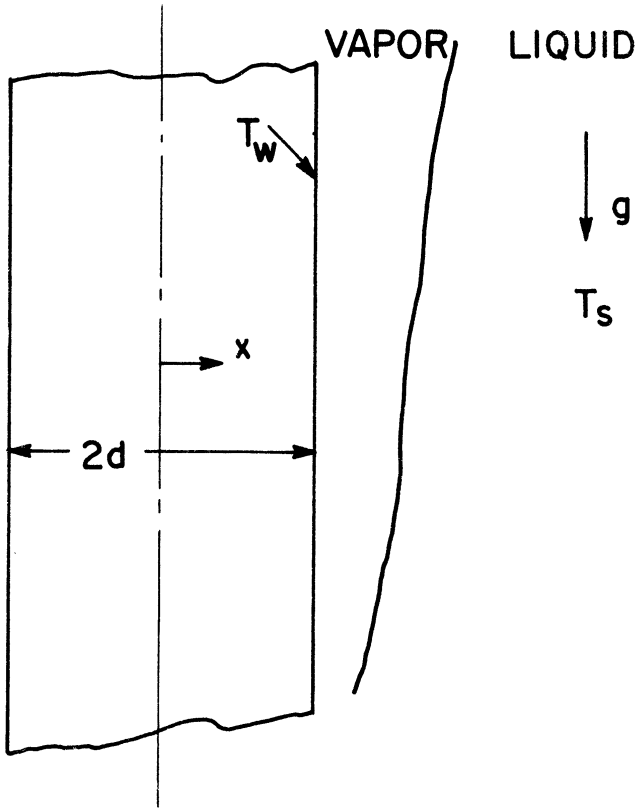

Figure 62. Model for lumped analysis.

Substituting $\theta = T - T_s$ and using the appropriate transformed boundary conditions, the solution to this is

$$\theta = \sum_{1}^{\infty} A_n e^{-\alpha \lambda_n^2 t} \cos \lambda_n x \tag{D.3}$$

The eigenvalues λ_n are given by

$$\lambda_n d \tan \lambda_n d = \frac{hd}{k} = \text{Biot Modulus} \tag{D.4}$$

and the coefficients A_n by

$$A_n = \frac{2 \theta_o \sin \lambda_n d}{\lambda_n d + \sin \lambda_n d \cos \lambda_n d} \tag{D.5}$$

The exact heat flux is then given by

$$q'_A = - k \left. \frac{\partial \theta}{\partial x} \right|_{x=d} \tag{D.6}$$

The experimental procedure can be simulated by finding the time rate of change of temperature at a given location, say $X = X_o$, from Eq. (D.3) and assuming this to be valid at every X, the time rate of change of enthalpy can be found. Thus the heat flux obtained by this simulated experiment is given by

$$q'_{ex} = - \frac{m C_p}{A} \frac{\partial \theta}{\partial t} (X = X_o) \tag{D.7}$$

If q'_{ex} and q'_A agree well, lumped analysis can be said to be valid.

Twelve eigenvalues were determined (using a computer) for typical values of h and d = 3/8 in. for liquid hydrogen and liquid nitrogen. The percent error due to the use of lumped analysis is then given by

$$\% \text{ error} = \frac{q'_{ex} - q'_A}{q'_A} \tag{D.8}$$

The maximum error in assuming the temperature at X = 0 to be the surface temperature is then given by $\theta(X = 0) - \theta(X = d)$. Representative values of percent error in heat flux calculations and determination of surface temperature due to the use of lumped analysis are given in Table IX.

TABLE XI

ERROR IN HEAT FLUX CALCULATIONS
AND SURFACE TEMPERATURE DETERMINATION
DUE TO LUMPED ANALYSIS

Liquid	$\Delta T(^\circ R)$	h, Btu/hr ft^2 $^\circ R$	$Bi = \frac{hD}{k}$	% Error in q' Eq. (D.8)	$\theta(X = 0) - \theta(X = d)$
LN_2	291	25.0	0.003397	0.057	0.50
LN_2	195	22.5	0.003057	0.051	0.30
LN_2	97	27.0	0.003375	0.057	0.16
LH_2	377	37.5	0.005095	0.086	0.96
LH_2	282	40.0	0.005435	0.092	0.76
LH_2	189	35.0	0.004557	0.077	0.43
LH_2	88	35.0	0.003125	0.058	0.14

APPENDIX E

ERROR ANALYSIS

In the experiments possible errors are associated with the determination of heat flux from the test surface, the test surface temperature, height along the test surface at which the test sections were located and the measurement of vapor film thickness from motion pictures.

1. Heat Flux

The uncertaintities in heat flux determination arise from (a) the uncertainty associated with its determination from the relation

$$q' = \frac{M}{A} C_p \frac{\partial T_w}{\partial t} \tag{E.1}$$

and (b) the heat loss from the test section.

(a) The uncertainties associated with the computation of the heat flux will be estimated following the procedure proposed by Kline and McClintock (62). According to this procedure, the uncertainty is given by

$$\Delta y = \left[\left(\frac{\partial y}{\partial x_1}\Delta x_1\right)^2 + \left(\frac{\partial y}{\partial x_2}\Delta x_2\right)^2 + \ldots + \left(\frac{\partial y}{\partial x_n}\Delta x_n\right)^2\right]^{\frac{1}{2}} \tag{E.2}$$

where Δy is the uncertainty associated with computing $y = y(x_1, x_2, \ldots x_n)$ and $\Delta x_1, \Delta x_2, \ldots \Delta x_n$ are the uncertainties associated with each of the x_i. Applying this to the determination of heat flux q', Eq. (E.1),

$$\frac{\Delta q'}{q'} = \left[\left(\frac{\Delta m}{m}\right)^2 + \left(\frac{\Delta A}{A}\right)^2 + \left(\frac{\Delta C_p}{C_p}\right)^2 + \left(\frac{\Delta(dT_w/dt)}{(dT_w/dt)}\right)^2\right]^{\frac{1}{2}} \tag{E.3}$$

The mass of the test section was determined in a chemical balance having an accuracy of ± 0.0005 gm. To find if the polishing of the test surface after final assembly made any significant difference in the mass determined, one of the test surfaces was dismantled and the mass of the test sections before and after such polishing compared. It was found that they were within - 0.01 gm. Using this value $\Delta m/m$ is estimated to be within 0.01/28 = 0.00065.

The area was computed by measuring the thickness and the diameter of the test surface sections with a vernier calipers measuring within ± 0.0005 in. The uncertainty in computing the area is given by

$$\frac{\Delta A}{A} = \left[\left(\frac{\Delta t}{t}\right)^2 + \left(\frac{\Delta d}{d}\right)^2\right]^{1/2} \qquad (E.4)$$

where t = thickness of section and d = diameter of section. For the test surfaces used, t = 0.25 in. and d = 1.0 in. and 2.25 in.

$$\frac{\Delta A}{A} = \left[\left(\frac{0.0005}{0.25}\right)^2 + \left(\frac{0.0005}{1.0}\right)^2\right]^{1/2} = 0.002$$

The uncertainty associated with the value of C_p arises from two sources (i) the uncertainty in reading the values of C_p from Ref. 58 which were used in computing these values, and (ii) the uncertainty in the data of Ref. 58 as applied to the material used for the present experiments, which is 0.01, and is considered in greater detail under Section 5, "Specific Heat of Copper." The uncertainty in reading the values from Ref. 58 is estimated to be 0.002/0.2 = 0.01.

The time rate of temperature was measured on the recorder chart, and in film boiling the trace of thermocouple output-time has a very small curvature,

and the slope can be measured with reasonable accuracy. The uncertainty in the slope is estimated to be 0.02/2 = 0.01. Combining all these, we obtain the uncertainty in computing q' to be $\Delta q'/q' = [0.00065^2 + 0.002^2 + 0.02^2 + .01^2]^{1/2} = 0.016$ or 1.6%.

(b) Heat loss from the test surface section arise from (i) loss through thermocouple wires, and (ii) leakage to adjacent sections through the Teflon insulating washer.

(i) To compute heat loss through thermocouple wires assume thermocouple junction to be at the test surface temperature and the other end coming out of the gland at the top of the test surface to be at the liquid saturation temperature. For computing heat loss the constantan wire is replaced by a copper wire. The minimum length of wire from the test surface to the gland was 4 in.; ΔT_{max} = 400°R in LH_2. Thirty gauge wires having a diameter of 0.010 in. were used for the thermocouples. Assuming an average thermal conductivity of 300 Btu/hr ft °R (58) we get

$$q_{wire} = 2KA \frac{\Delta T}{\Delta X}$$

$$= 2 \times 300 \times \frac{0.7854 \times 10^{-4}}{144} \times \frac{400}{4/12}$$

$$= 9.8 \times 10^{-2} \text{ Btu/hr}$$

On the basis of the heat transfer area from a 1 in. diameter test surface section this corresponds to

$$q'_{wires} = \frac{9.8 \times 10^{-2}}{0.5 \times 10^{-2}} = 2 \text{ Btu/hr ft}^2$$

which is negligibly small compared even with the lowest flux measured—2900 Btu/hr ft^2.

(ii) Heat loss to adjacent sections: it may be expected that the heat loss from a given test surface section to an adjacent section is compensated by the heat gain from the other adjacent section and the net loss or gain is neglibible. However, to obtain an estimate of the maximum possible error due to this heat loss (or gain), consider one adjacent section to be at a lower temperature than the test section with 0.005 in. Teflon insulating washer separating the two sections each having perfect thermal contact with the Teflon washer. The temperature differential over the different pieces of the test surfaces was a maximum of 1.5°R between the bottom piece and the top piece. There were a total of five pieces between them and hence a temperature differential of 0.5°R between two adjacent pieces may be assumed. The area of heat transfer, because of the recess in the section, was limited to a radial thickness of 1/16 in. For Teflon K = 0.1 Btu/hr °R ft (58). With these values, for 1 in. diameter test surface

$$q_{ins} = KA \frac{\Delta T}{\Delta X} = 0.1 \times \frac{\pi \times 1 \times 1/16}{144} \times \frac{0.5}{0.005/12}$$

$$= 0.1875 \text{ Btu/hr}$$

Based on the area of heat transfer of the test section this is equivalent to 37.5 Btu/hr ft^2 and is 1.3% of the lowest computed value.

Combining all the sources of uncertainties it is estimated that the uncertainty in the computed heat flux values are within $\pm$ 2.7%.

2. Temperature

The temperature of the surface was determined from the thermocouple in the sections of the test surface. The errors in its determination are due to (i) errors in measuring the output, and (ii) error due to assumption of lumped analysis.

(i) The error in reading the output is due to nonlinearity in the recorder output and the error in the potentiometer which was used to calibrate the recorder. The potentiometer had an accuracy of $\pm$ 1.3 μv in the range of values used in the experiments. The nonlinearity in the recorder output is specified at $\pm$ 0.25 div. corresponding to $\pm$ 0.5 μv at a sensitivity of 2 μv/div. Therefore, the maximum error in reading the output is estimated at $\pm$ 1.8 μv corresponding to

$$\pm \frac{1.8\ \mu v}{16.4\ \mu v/^{o}_{k}} \times \frac{1.8^{\circ}R}{^{o}_{k}} = \pm\ 0.2^{\circ}R$$

at 136.5°R—the lowest surface temperature at which data were obtained.

(ii) Error due to assumption of lumped analysis is estimated at 0.5°R at $\Delta T = 300^{\circ}R$ for LN_2 and 1°R for LH_2 at $\Delta T = 400^{\circ}R$ (see Appendix D). Hence, the uncertainty in the determination of surface superheat is $\pm$ 0.5°R in 315°R or 0.2% for LN_2 and $\pm$ 1.2°R in 400°R or 0.3% in LH_2.

3. Uncertainty in the Measurement of the Distance of Test Sections from the Leading Edge

The sources of uncertainties arise from two factors (i) the finite height of the test section leads to uncertainty in the precise location at which the heat flux was determined. The height of the test section was 0.25 in. and the heat flux was assumed to have been measured at the midheight of the test section, being the average over the height of 0.25 in. It may be assumed that the heat flux computed represents the heat flux at some point in the middle third of the test section leading to an estimated uncertainty of $\pm$ 0.041 in. in the location at which the heat flux was measured.

(ii) Because of the introduction of the stainless steel end pieces at the bottom, boiling is induced in the end piece through heat transfer by conduction from the test piece, thus shifting the leading edge from the bottom of the test surface. To estimate this shift in the leading edge, the end piece was treated as a fin with a constant heat transfer coefficient corresponding to the lowest measured in the experiments (which would give the greatest shift). The base of the fin was assumed to be at the maximum surface temperature and boiling was assumed to have ceased at a point in the fin which had the temperature corresponding to q'_{min}. The distance over which this temperature drop took place was computed as the shift in the leading edge. For liquid nitrogen T_{min} at which q'_{min} was assumed, was 40°R above saturation temperature and h=20 Btu/hr ft^2°R (54); the corresponding values for liquid hydrogen were ΔT_{min}=20°R and h=30Btu/hr ft^2°R(64) obtained in experiments with

1 in. sphere. With these values, it is estimated that the shift in leading edge is 0.037 in. for liquid nitrogen and 0.068 in. for liquid hydrogen.

Combining the two, the uncertainty in the measurement of the location of the test section is within + 0.110 in., - 0.026 in.

4. Uncertainties in the Measurement of Vapor Film Thickness by Photographic Methods

The motion pictures were projected on a ground glass sheet to give a magnification of 10 times the original size, the distances were measured by the use of a 0.040 in. diameter reference wire which established the scale of the image. The distances on the image were measured with a vernier calipers having an accuracy of $\pm$ 0.0005 in. It is estimated that the error in the measurement of the reference wire diameter on the image was within $\pm$ 0.010 in. and the uncertainty in the measurement of the vapor film thickness as $\pm$ [0.010 x 5/10] or $\pm$ 0.005 in.

5. Specific Heat of Copper

To evaluate the rate of enthalpy change of the test surface to compute the heat flux values, values for specific heat capacity of copper were taken from Ref. 58. Discrete values used from this are given in Table XII.

TABLE XII

SPECIFIC HEAT OF OFHC COPPER
(Ref. 58)

Temperature		C_p**		Temperature		C_p**	
°K	°R	J/gm°K*	$\frac{Btu}{lb°R}$VO	°K	°R	J/gm°K*	$\frac{Btu}{lb°R}$
70	126	.173	.0413	180	324	.346	.0826
80	144	.205	.04896	200	360	.356	.0850
90	162	.232	.0554	220	396	.364	.0869
100	180	.254	.0607	240	432	.371	.0886
120	216	.288	.0688	260	468	.376	.0898
140	252	.313	.0748	280	504	.381	.0910
160	288	.332	.0793	300	540	.386	.0922

*Joule/gm °K = 0.23885 Btu/lb °R.

**C_p values at intermediate temperatures were found by interpolation.

To evaluate the reliability of the values of specific heats used in the computation of rate of enthalpy change, these values were compared with those of Dockerty (60), Martin (59), and Farukawa, et al. (63). The values from these sources and from Ref. 58 (which is itself based on Ref. 60) are given in Table XIII, which also gives values of specific heats of commerically pure copper and from a comparison of these values, it can be seen that the maximum variation in the values of specific heat given by different workers is within 1% below 120°K and less than 0.5% between 120° and 300°K. It may

TABLE XIII

SPECIFIC HEAT OF COPPER—COMPARISON OF DATA FROM DIFFERENT SOURCES

Temperature		C_p (Btu/lbm °R)				
°K	°R	Ref. 59 x 10^2	Ref. 60 x 10^2	Ref. 61 x 10^2	Ref. 63 x 10^2	Ref. 60* x 10^2
70	126	4.13	4.10	4.07	4.09	4.08
80	144	4.896	4.86	4.84	4.83	4.84
90	162	5.54	5.51	5.49	5.48	5.48
100	180	6.07	6.02	6.02	6.02	5.995
120	216	6.88	6.87	6.85	6.86	6.84
140	252	7.48	7.47	7.47	7.47	7.47
160	288	7.93	7.91	7.91	7.92	7.91
180	324	8.26	8.25	8.24	8.25	8.25
200	360	8.50	8.49	8.49	8.51	8.496
220	396	8.69	8.69	8.69	8.71	8.71
240	432	8.86	8.84	8.85	8.88	8.88
260	468	8.98	8.99	8.99	9.01	9.00
280	504	9.10	9.11	9.11	9.11	9.12
300	540	9.22	9.21	9.196	9.199	9.21

*Commercially pure copper.

All other 99.99% pure copper.

also be seen that the specific heat is relatively insensitive to small amounts of impurities in copper as observed from values given in the last column of Table XIII for commerically pure copper. Martin (59) also concludes that heavily cold worked copper has a specific heat of about 0.15% higher than that of annealed copper. From these values it may be concluded that the maximum uncertainty in the value of specific heat for the machined OFHC copper used in the experiments is within $\pm$ 0.6%.

APPENDIX F

PROPERTIES OF NITROGEN AND HYDROGEN

1. Nitrogen

T_w(°R)	Film Temp. $\frac{T_w+T_s}{2}$ (°R)	ρ(61) (lbm/ft^3)	μ(58) (lbm/ft hr)	C_p(61) (Btu/lbm °R)	(h_v-h_ℓ)(61) (Btu/lbm)	k(58) (Btu/hr ft °R)
494.1	316.8	0.1217	0.04356	0.2495	130.5	0.00971
454.3	296.9	0.1323	0.0363	0.253	126.14	0.009298
390.2	264.8	0.1481	0.0242	0.2541	117.83	0.007907
343.4	241.4	0.1633	0.02226	0.2568	112.2	0.007619
239.1	189.3	0.2108	0.0176	0.2628	98.70	0.005781

Saturation pressure 14.9 psi; T_s(61) = 139.4 °R

ρ_ℓ(61) = 50.378 lbm/ft^3

h_{fg}(61) = 85.64 Btu/lbm

*Numbers in parentheses refer to references in bibliography.

2. Hydrogen

T_w(°R)	Film Temp. $\frac{T_w+T_s}{2}$ (°R)	$\rho(65)$ (lbm/ft^3)	$\mu(58)$ (lbm/ft hr)	$C_p(65)$ (Btu/lbm °R)	$(h_v-h_\ell)(65)$ (Btu/lbm)	$k(58)$ (Btu/hr ft °R)
490.3	263.6	0.0104	0.01331	2.99	798.3	0.052
436.9	236.9	0.0118	0.01226	2.89	718.47	0.050
336.9	186.9	0.0149	0.01113	2.65	578.27	0.039
236.9	136.9	0.0205	0.00847	2.54	447.22	0.031
136.9	86.9	0.0325	0.00605	2.517	321.48	0.020

Saturation pressure 14.9 psi; $T_s(65)$ = 36.9 °R

$\rho_\ell(65)$ = 4.4306 lbm/ft^3

$h_{fg}(65)$ = 191.78 Btu/lbm

*Numbers in parentheses refer to references in bibliography.

APPENDIX G

DATA

Data were reduced following the procedure outlined under Chapter IV, Section E, "Data Reduction." No datum was discarded. During a run the pressure increased by up to 0.25 psi due to vapor generation.

P = 0.5 psig: Saturated Liquid: a/g = 1

Run No.	Dia, in.	Height Above Leading Edge, in.	Test Liquid	$T_w - T_{sat}$, °R	q', Btu/hr ft^2	h, Btu/hr ft^2 °R
2001	1	3/8	LN_2	314.9	7378.5	23.43
		3		314.9	6624.8	21.04
		4-1/2		314.9	6880.7	21.85
2002	1	3/8	LN_2	314.9	7378.5	23.43
		3		314.9	6535.6	20.75
		4-1/2		314.9	6880.7	21.85
2003	1	3/8	LN_2	314.9	7378.5	23.43
		3		314.9	6506.5	20.66
		4-1/2		314.9	6815.9	21.64
2004	1	3/8	LN_2	314.9	7530.7	23.91
		3		314.9	6506.5	20.66
		4-1/2		314.9	6880.7	21.85
2005	1	3/8	LN_2	314.9	7304.8	23.2
		3		314.9	6565.0	20.8
		4-1/2		314.9	6880.7	21.85
2006	1	3/8	LN_2	250.8	6969.3	27.8
		3		250.8	5303.3	21.15
		4-1/2		250.8	5639.6	22.49
2007	1	3/8	LN_2	250.8	6969.3	27.8
		3		250.8	5303.3	21.15
		4-1/2		250.8	5588.6	22.8
2008	1	3/8	LN_2	250.8	6969.3	27.8
		3		250.8	5258.0	20.96
		4-1/2		250.8	5538.5	22.08
2009	1	3/8	LN_2	250.8	6969.3	27.79
		3		250.8	5303.3	21.15
		4-1/2		250.8	5588.6	22.28
2010	1	3/8	LN_2	250.8	6892.6	27.48
		3		250.8	5258.0	20.96
		4-1/2		250.8	5538.5	22.08
2011	1	3/8	LN_2	204.0	6525.6	31.98
		3		204.0	4297.2	21.06
		4-1/2		204.0	4526.6	22.18

P = 0.5 psig: Saturated Liquid: a/g = 1

Run No.	Dia, in.	Height Above Leading Edge, in.	Test Liquid	$T_w - T_{sat}$, °R	q', Btu/hr ft^2	h, Btu/hr ft^2 °R
2012	1	3/8	LN_2	204.0	6525.6	31.98
		3		204.0	4297.2	21.06
		4-1/2		204.0	4526.6	22.19
2013	1	3/8	LN_2	204.0	6691.4	32.79
		3		204.0	4383.1	21.48
		4-1/2		204.0	4590.3	22.50
2014	1	3/8	LN_2	204.0	6691.4	32.79
		3		204.0	4268.9	20.92
		4-1/2		204.0	4557.9	22.34
2015	1	3/8	LN_2	204.0	6525.3	31.98
		3		204.0	4311.3	22.13
		4-1/2		204.0	4574.1	22.42
2016	1	3/8	LN_2	99.7	5796.0	58.13
		3		99.7	2891.0	28.99
		4-1/2		99.7	3176.0	31.85
2017	1	3/8	LN_2	99.7	5707.0	57.24
		3		99.7	2914.0	29.22
		4-1/2		99.7	3163.0	31.73
2018	1	3/8	LN_2	99.7	5664.0	56.81
		3		99.7	3052.0	30.61
		4-1/2		99.7	3218.0	32.27
2019	1	3/8	LN_2	99.7	5796.0	58.14
		3		99.7	2961.0	29.69
		4-1/2		99.7	3218.0	32.28
2020	1	3/8	LN_2	99.7	5888.0	59.05
		3		99.7	2984.0	29.92
		4-1/2		99.7	3163.0	31.72
4001	1	5/8	LN_2	314.9	6676.5	21.20
		3		314.9	6419.6	20.39
		5-5/8		314.9	7774.0	24.69
4002	1	5/8	LN_2	314.9	6617.8	21.02
		3		314.9	6475.4	20.56
		5-5/8		314.9	7734.2	24.56

P = 0.5 psig: Saturated Liquid: a/g = 1

Run No.	Dia, in.	Height Above Leading Edge, in.	Test Liquid	T_w-T_{sat}, °R	q', Btu/hr ft^2	h, Btu/hr ft^2 °R
4003	1	5/8	LN_2	314.9	6502.3	20.65
		3		314.9	6419.6	20.39
		5-5/8		314.9	7616.7	24.18
4004	1	5/8	LN_2	314.9	6502.3	20.65
		3		314.9	6419.6	20.39
		5-5/8		314.9	7616.7	24.19
4005	1	5/8	LN_2	314.9	6559.1	20.83
		3		314.9	6475.4	20.56
		5-5/8		314.9	7648.0	24.29
4006	1	5/8	LN_2	350.8	5632.9	22.46
		3		250.8	5327.9	21.24
		5-5/8		250.8	6226.3	24.83
4007	1	5/8	LN_2	250.8	5632.9	22.46
		3		250.8	5241.3	20.90
		5-5/8		250.8	6226.3	24.82
4008	1	5/8	LN_2	250.8	5733.3	22.86
		3		250.8	5241.3	20.89
		5-5/8		250.8	6348.4	25.31
4009	1	5/8	LN_2	250.8	5632.9	22.46
		3		250.8	5241.3	20.90
		5-5/8		250.8	6348.4	25.31
4010	1	5/8	LN_2	250.8	5632.9	22.46
		3		250.8	5284.6	21.07
		5-5/8		250.8	6286.4	25.06
4011	1	5/8	LN_2	204.0	5035.0	24.67
		3		204.0	4306.3	21.10
		5-5/8		204.0	5345.9	26.06
4012	1	5/8	LN_2	204.0	4997.6	24.49
		3		204.0	4306.3	21.11
		5-5/8		204.0	5077.4	24.88
4013	1	5/8	LN_2	204.0	4961.2	22.99
		3		204.0	4306.3	21.10
		5-5/8		204.0	5077.4	24.88

P = 0.5 psig: Saturated Liquid: a/g = 1

Run No.	Dia, in.	Height Above Leading Edge, in.	Test Liquid	T_w-T_{sat}, °R	q', Btu/hr ft^2	h, Btu/hr ft^2 °R
4014	1	5/8	LN_2	204.0	4819.7	23.62
		3		204.0	4251.7	20.84
		5-5/8		204.0	5002.6	24.52
4015	1	5/8	LN_2	204.0	4889.4	23.96
		3		204.0	4251.7	20.84
		5-5/8		204.0	5077.4	24.88
4016	1	5/8	LN_2	99.7	4747.0	47.61
		3		99.7	2921.0	29.29
		5-5/8		99.7	3481.0	34.91
4017	1	5/8	LN_2	99.7	4932.0	49.46
		3		99.7	2966.0	29.75
		5-5/8		99.7	3613.0	36.26
4018	1	5/8	LN_2	99.7	4631.0	46.45
		3		99.7	2921.0	29.29
		5-5/8		99.7	3545.7	35.56
4019	1	5/8	LN_2	99.7	4747.0	47.61
		3		99.7	2954.0	29.63
		5-5/8		99.7	3481.0	34.91
4020	1	5/8	LN_2	99.7	4575.0	45.88
		3		99.7	2822.0	28.30
		5-5/8		99.7	3579.0	35.89
5001	1	1/4	LN_2	314.9	6189.6	19.65
		1-1/2		314.9	6268.3	19.90
		3		314.9	6609.3	20.99
5002	1	1/4	LN_2	314.9	7191.5	22.84
		1-1/2		314.9	6401.7	20.33
		3		314.9	6609.3	20.99
5003	1	1/4	LN_2	314.9	6292.2	21.98
		1-1/2		314.9	6294.2	19.98
		3		314.9	6496.3	20.63
5004	1	1/4	LN_2	314.9	6398.7	20.32
		1-1/2		314.9	6268.3	19.91
		3		314.9	6726.4	21.36

P = 0.5 psig: Saturated Liquid: a/g = 1

Run No.	Dia, in.	Height Above Leading Edge, in.	Test Liquid	$T_w - T_{sat}$, °R	q', Btu/hr ft^2	h, Btu/hr ft^2 °R
5005	1	1/4	LN_2	314.9	6509.3	20.67
		1-1/2		314.9	6294.2	19.99
		3		314.9	6726.4	21.36
5006	1	1/4	LN_2	250.8	5896.3	23.50
		1-1/2		250.8	5126.1	20.44
		3		250.8	5349.5	21.33
5007	1	1/4	LN_2	250.8	5589.4	22.28
		1-1/2		250.8	5126.1	20.44
		3		250.8	5306.0	21.56
5008	1	1/4	LN_2	250.8	5894.3	23.50
		1-1/2		250.8	5046.0	20.11
		3		250.8	5349.5	21.33
5009	1	1/4	LN_2	250.8	5894.3	23.5
		1-1/2		250.8	5046.0	20.12
		3		250.8	5349.5	21.33
5010	1	1/4	LN_2	250.8	5789.0	23.08
		1-1/2		250.8	5004.0	19.95
		3		250.8	5306.0	21.16
5011	1	1/4	LN_2	204.0	5200.6	25.49
		1-1/2		204.0	4112.5	20.16
		3		204.0	4340.3	21.27
5012	1	1/4	LN_2	204.0	5450.0	26.71
		1-1/2		204.0	4138.2	20.28
		3		204.0	4340.3	21.27
5013	1	1/4	LN_2	204.0	5450.0	26.71
		1-1/2		204.0	4396.1	21.54
		3		204.0	4340.3	21.27
5014	1	1/4	LN_2	204.0	5009.2	24.55
		1-1/2		204.0	4112.5	20.16
		3		204.0	4340.3	21.27
5015	1	1/4	LN_2	204.0	5240.5	25.73
		1-1/2		204.0	4138.2	20.28
		3		204.0	4340.3	21.27

P = 0.5 psig: Saturated Liquid: a/g = 1

Run No.	Dia, in.	Height Above Leading Edge, in.	Test Liquid	T_w-T_{sat}, °R	q', Btu/hr ft^2	h, Btu/hr ft^2 °R
5016	1	1/4	LN_2	99.7	5810.0	58.27
		1-1/2		99.7	3441.3	34.51
		3		99.7	3190.0	31.99
5017	1	1/4	LN_2	99.7	5899.3	59.1
		1-1/2		99.7	3553.4	35.64
		3		99.7	3299.1	33.09
5018	1	1/4	LN_2	99.7	5899.3	59.17
		1-1/2		99.7	3441.3	34.52
		3		99.7	3112.8	31.22
5019	1	1/4	LN_2	99.7	5945.1	59.62
		1-1/2		99.7	3520.7	35.31
		3		99.7	3216.6	32.26
5020	1	1/4	LN_2	99.7	6184.8	62.32
		1-1/2		99.7	3536.9	35.47
		3		99.7	3216.6	32.26
6001	2-1/4	7/8	LN_2	314.9	6391.4	20.29
		3		314.9	6930.5	22.0
		3-1/2		314.9	7404.2	23.51
6002	2-1/4	7/8	LN_2	314.9	6311.9	20.04
		3		314.9	6954.5	22.08
		3-1/2		314.9	7194.1	22.85
6003	2-1/4	7/8	LN_2	314.9	6067.0	19.26
		3		314.9	6722.6	21.35
		3-1/2		314.9	6995.7	22.21
6004	2-1/4	7/8	LN_2	314.9	6048.9	19.20
		3		314.9	6722.6	21.34
		3-1/2		314.9	6807.9	21.62
6005	2-1/4	7/8	LN_2	314.9	6048.9	19.20
		3		314.9	6722.6	21.34
		3-1/2		314.9	6947.6	22.0
6006	2-1/4	7/8	LN_2	250.8	5015.0	19.99
		3		250.8	5445.6	21.72
		3-1/2		250.8	5443.6	21.70

P = 0.5 psig: Saturated Liquid: a/g = 1

Run No.	Dia, in.	Height Above Leading Edge, in.	Test Liquid	T_w-T_{sat}, °R	q', Btu/hr ft^2	h, Btu/hr ft^2 °R
6007	2-1/4	7/8	LN_2	250.8	5015.0	19.99
		3		250.8	5411.6	21.57
		3-1/2		250.8	5443.6	21.70
6008	2-1/4	7/8	LN_2	250.8	5015.0	19.99
		3		250.8	5445.6	21.72
		3-1/2		250.8	5512.5	21.97
6009	2-1/4	7/8	LN_2	204.0	4111.5	17.12
		3		204.0	4598.1	19.15
		3-1/2		204.0	4492.0	18.71
6010	2-1/4	7/8	LN_2	204.0	4093.3	17.05
		3		204.0	4598.1	19.15
		3-1/2		204.0	4628.2	19.28
6011	2-1/4	7/8	LN_2	204.0	4093.3	17.05
		3		204.0	4598.1	19.15
		3-1/2		204.0	4536.5	18.89
6012	2-1/4	7/8	LN_2	99.7	3739.8	37.51
		3		99.7	3161.0	31.70
		3-1/2		99.7	3012.4	30.21
6013	2-1/4	7/8	LN_2	99.7	3440.5	34.50
		3		99.7	3368.9	33.79
		3-1/2		99.7	3323.3	33.33
6014	2-1/4	7/8	LN_2	99.7	3583.9	35.94
		3		99.7	3325.2	33.35
		3-1/2		99.7	3302.1	33.12
7001	2-1/4	2	LN_2	314.9	6509.6	20.67
		3		314.9	6767.4	21.49
		4		314.9	6951.9	22.07
7002	2-1/4	2	LN_2	314.9	6468.4	20.54
		3		314.9	6835.6	21.70
		4		314.9	7072.9	22.46
7003	2-1/4	2	LN_2	314.9	6593.5	20.93
		3		314.9	6789.9	21.56
		4		314.9	6905.0	21.93

P = 0.5 psig: Saturated Liquid: a/g = 1

Run No.	Dia, in.	Height Above Leading Edge, in.	Test Liquid	T_w-T_{sat}, °R	q', Btu/hr ft^2	h, Btu/hr ft^2 °R
7004	2-1/4	2	LN_2	250.8	5223.8	20.82
		3		250.8	5466.1	21.79
		4		250.8	5365.3	21.39
7005	2-1/4	2	LN_2	250.8	5223.8	20.83
		3		250.8	5332.7	21.26
		4		250.8	5466.0	21.79
7006	2-1/4	2	LN_2	250.8	6223.8	20.82
		3		250.8	5398.6	21.52
		4		250.8	5466.0	21.79
7007	2-1/4	2	LN_2	204.0	4433.2	21.72
		3		204.0	4460.8	21.86
		4		204.0	4594.7	22.49
7008	2-1/4	2	LN_2	204.0	4269.0	20.92
		3		204.0	4334.7	21.24
		4		204.0	4549.2	22.29
7009	2-1/4	2	LN_2	204.0	4269.0	20.92
		3		204.0	4334.7	21.24
		4		204.0	4596.7	22.57
7010	2-1/4	2	LN_2	99.7	3107.8	31.17
		3		99.7	3097.1	31.06
		4		99.7	3078.7	30.87
7011	2-1/4	2	LN_2	99.7	3053.0	30.62
		3		99.7	3273.5	32.83
		4		99.7	3173.1	31.82
7012	2-1/4	2	LN_2	99.7	3145.6	31.55
		3		99.7	3232.7	32.43
		4		99.7	3173.1	31.83
4021	1	5/8	LH_2	400	16354.7	40.9
		3		400	19625.8	49.1
		5-5/8		400	20398.0	50.99
4022	1	5/8	LH_2	300	11045.7	36.8
		3		300	12373.7	41.2
		5-5/8		300	14201.6	47.3

P = 0.5 psig: Saturated Liquid: a/g = 1

Run No.	Dia, in.	Height Above Leading Edge, in.	Test Liquid	T_w-T_{sat}, °R	q', Btu/hr ft^2	h, Btu/hr ft^2 °R
4023	1	5/8	LH_2	200	6991.7	34.96
		3		200	7658.1	38.3
		5-5/8		200	8914.3	44.6
4024	1	5/8	LH_2	100	4601.8	46.0
		3		100	3504.1	35.0
		5-5/8		100	4334.7	43.3
4025	1	Runs made in nucleate boiling				
4026	1					
4027	1	5/8	LH_2	100	4754.2	47.5
		3		100	3486.9	34.9
		5-5/8		100	4308.9	43.1
4028	1	5/8	LH_2	200	7466.8	37.8
		3		200	7658.1	38.3
		5-5/8		200	8914.3	44.6
2021	1	3/8	LH_2	100	5795.4	57.95
		3		100	3606.1	36.1
		4-1/2		100	3852.2	38.5
2022	1	3/8	LH_2	100	5233.2	52.3
		3		100	3606.1	36.1
		4-1/2		100	3728.9	37.3
2023	1	3/8	LH_2	200	7666.0	38.3
		3		200	7807.1	39.04
		4-1/2		200	8845.6	44.3
2024	1	3/8	LH_2	200	7666.0	38.3
		3		200	7807.1	39.04
		4-1/2		200	8540.5	42.7
2025	1	3/8	LH_2	300	12319.9	41.1
		3		300	13281.8	44.2
		4-1/2		300	13493.9	45.0
2026	1	3/8	LH_2	300	11625.8	38.8
		3		300	12668.7	42.2
		4-1/2		300	13274.5	44.2

P = 0.5 psig: Saturated Liquid: a/g = 1

Run No.	Dia, in.	Height Above Leading Edge, in.	Test Liquid	T_w-T_{sat}, °R	q', Btu/hr ft^2	h, Btu/hr ft^2 °R
2027 2028	]	Runs made in nucleate boiling				
2029	1	3/8	LH_2	400	17261.4	43.2
		3		400	19456.9	48.6
		4-1/2		400	20207.8	50.6
2030	1	3/8	LH_2	400	17065.2	42.7
		3		400	19712.9	49.3
		4-1/2		400	20071.2	50.2
2031	1	3/8	LH_2	300	11625.8	38.8
		3		300	12866.7	42.2
		4-1/2		300	13167.5	43.9
2032	1	3/8	LH_2	200	7365.4	36.8
		3		200	7973.2	39.4
		4-1/2		200	8845.6	44.2
2033	1	3/8	LH_2	100	5156.3	51.6
		3		100	3606.1	36.1
		4-1/2		100	3853.2	38.5
5023	1	1/4	LH_2	100	5176.1	51.8
		1-1/2		100	3684.2	36.8
		3		100	3780.6	37.8
5024	1	1/4	LH_2	100	5251.2	52.5
		1-1/2		100	3703.1	37.0
		3		100	3840.3	38.4
5025	1	1/4	LH_2	200	7842.0	39.2
		1-1/2		200	7438.5	37.2
		3		200	8142.6	40.7
5026	1	1/4	LH_2	200	7611.4	38.1
		1-1/2		200	7163.0	35.8
		3		200	7237.9	36.6
5027	1	1/4	LH_2	300	12544.0	41.8
		1-1/2		300	12142.5	40.4
		3		300	13213.2	44.0

P = 0.5 psig: Saturated Liquid: a/g = 1

Run No.	Dia, in.	Height Above Leading Edge, in.	Test Liquid	T_w-T_{sat}, °R	q', Btu/hr ft^2	h, Btu/hr ft^2 °R
5028	1	1/4	LH_2	300	12452.5	41.1
		1-1/2		300	12499.6	41.3
		3		300	13315.7	44.3
5029	1	1/4	LH_2	400	16868.3	42.1
		1-1/2		400	17572.6	43.9
		3		400	19055.5	47.6
5030	1	1/4	LH_2	400	17635.0	44.1
		1-1/2		400	18192.8	45.5
		3		400	19290.7	48.2
5031	1	1/4	LH_2	400	17243.1	43.1
		1-1/2		400	17981.3	44.9
		3		400	19290.7	48.2
5032	1	1/4	LH_2	300	12185.7	40.6
		1-1/2		300	12384.4	41.3
		3		300	13013.0	43.4
5033	1	1/4	LH_2	200	8531.4	42.6
		1-1/2		200	7438.5	37.2
		3		200	8142.6	40.7

Run No.	Test Liquid	T_w, °R	Pressure psig	T_w-T_s, °R	a/g	Subcooling, °R	Height Above Leading Edge, in.	q', Btu/hr ft^2	h, Btu/hr ft^2 °R
8003	LN_2	494.1	0.5	354.7	0	0	3/8	2818	7.94
							2	2122	5.99
8003	LN_2	497.5	0.5	358.1	1	0	3/8	8385	23.4
							2	8133	22.7
8004	LN_2	497.5	0.5	337.0	1	21.1	3/8	16844	50.1
							2	14719	42.5
8004	LN_2	494.1	0.5	333.6	1	21.1	3/8	19250	57.2
							2	14680	43.6
8005	LN_2	494.1	0.5	333.6	1	21.1	3/8	16365	48.7
							2	15855	46.6
8005	LN_2	497.5	0.5	337.0	1	21.1	3/8	16421	48.7
							2	15906	47.4
8006	LN_2	494.1	0.5	354.7	1	0	3/8	8110	22.87
							2	8940	25.19
8006	LN_2	497.5	0.5	358.1	1	0	3/8	8143	22.75
							2	8358	23.39
8007	LN_2	494.1	0.5	356.7	0	0	3/8	3385	9.55
							2	2180	6.15
8007	LN_2	497.5	0.5	358.1	1	0	3/8	8279	23.15
							2	8150	22.8
8010	LH_2	490.3	0.5	453.6	1	0	3/8	23390	51.6
							2	24800	54.6
8010	LH_2	494.1	0.5	451.4	1	0	3/8	23350	51.0
							2	25080	56.4
8011	LH_2	490.3	32.5	445.5	1	8.1	3/8	27990	62.9
							2	32000	72.0
8011	LH_2	494.1	32.5	449.3	1	8.1	3/8	27890	62.1
							2	30990	69.0
8012	LH_2	490.3	0.5	453.6	0	0	3/8	7707.8	16.99
							2	5975.0	13.17

Run No.	Test Liquid	T_w, °R	Pressure psig	T_w-T_s, °R	a/g	Subcooling, °R	Height Above Leading Edge, in.	q', Btu/hr ft^2	h, Btu/hr ft^2 °R
8012	LH_2	494.1	0.5	457.4	1	0	3/8	23980	52.6
							2	22500	49.4
9001	LN_2	494.0	0.5	354.7	1	0	5/8	8842	24.9
							3	7928	22.4
9001	LN_2	497.5	0.5	358.1	1	0	5/8	8367	23.4
							3	7950	22.2
9002	LN_2	494.0	0.5	354.7	1	0	5/8	8350	23.5
							3	7920	22.3
9002	LN_2	497.5	0.5	358.1	1	0	5/8	7991	22.3
							3	7880	22.0
9003	LN_2	494.1	32.5	333.6	1	21.1	5/8	14200	42.6
							3	11850	37.6
9003	LN_2	497.5	32.5	337.1	1	21.1	5/8	13990	41.5
							3	11250	33.4
9004	LN_2	494.1	32.5	333.6	1	21.1	5/8	14261	42.7
							3	11600	34
9004	LN_2	497.0	32.5	337.0	1	21.1	5/8	14211	42.2
							3	11600	34.0
9005	LN_2	494.0	0.5	356.7	0	0	5/8	2060	5.86
							3	1455	3.64
9005	LN_2	497.5	0.5	358.1	1	0	5/8	8158	22.8
							3	7367	20.6
9005	LN_2	494.0	0.5	354.7	1	0	5/8	8187	23.1
							3	7807	22.0
9006	LN_2	494.0	0.5	354.7	0	0	5/8	2120	5.95
							3	2040	5.75
9006	LN_2	497.5	0.5	358.1	1	0	5/8	8074	22.5
							3	7240	20.1
9010	LH_2	494.1	0.5	457.4	1	0	5/8	22432	49.1
							3	24208	53.0

Run No.	Test Liquid	T_w, °R	Pressure psig	T_w-T_s, °R	a/g	Subcooling, °R	Height Above Leading Edge, in.	q', Btu/hr ft^2	h, Btu/hr ft^2 °R
9010	LH_2	490.3	0.5	453.6	1	0	5/8	23275	51.4
							3	25325	55.9
9011	LH_2	490.3	34	445.5	1	8.1	5/8	27556	61.5
							3	31309	69.9
9011	LH_2	494.1	34	449.3	1	8.1	5/8	27495	61.4
							3	30588	68.3
9012	LH_2	494.1	0.5	451.4	1	0	5/8	22432	49.1
							3	23677	51.8
9012	LH_2	488.9	0.5	452.2	0	0	5/8	5910	13.1
							3	5150	11.5
10001	LN_2	497.5	0.5	358.1	1	0	1-1/8	7710	21.5
							3-1/2	8150	22.8
10001	LN_2	494.1	0.5	354.7	1	0	1-1/8	7861	22.2
							3-1/2	8150	22.8
10002	LN_2	497.5	0.5	358.1	1	0	1-1/8	7672	21.42
							3-1/2	8170	22.8
10002	LN_2	494.1	0.5	354.7	1	0	1-1/8	7641	21.5
							3-1/2	8550	24.1
10003	LN_2	494.1	34	333.6	1	21.1	1-1/8	13550	40.5
							3-1/2	13872	41.5
10003	LN_2	497.5	34	337.0	1	21.1	1-1/8	12802	38.1
							3-1/2	12012	35.7
10004	LN_2	494.1	0.5	354.7	0	0	1-1/8	2320	6.6
							3-1/2	2090	5.9
10004	LN_2	497.5	0.5	358.1	1	0	1-1/8	7549	21.1
							3-1/2	7811	21.8
10010	LH_2	490.3	0.5	453.6	1	0	1-1/8	22809	50.5
							3-1/2	26825	59.1
10010	LH_2	494.1	0.5	457.4	1	0	1-1/8	22007	48.1
							3-1/2	27350	59.8

Run No.	Test Liquid	T_w, °R	Pressure psig	T_w-T_s, °R	a/g	Subcooling, °R	Height Above Leading Edge, in.	q', Btu/hr ft^2	h, Btu/hr ft^2 °R
10011	LH_2	490.3	32.5	445.5	1	8.1	1-1/8	29189	65.3
							3-1/2	34715	77.6
10011	LH_2	494.1	32.5	449.3	1	8.1	1-1/8	28282	63.0
							3-1/2	33602	74.9
10012	LH_2	490.3	0.5	453.6	0	0	1-1/8	9518	21.0
							3-1/2	4260	9.4
10012	LH_2	494.1	0.5	457.4	1	0	1-1/8	23569	51.5
							3-1/2	23443	51.3

BIBLIOGRAPHY

1. Kreith, F., "Principles of Heat Transfer," International Text Book (1958).

2. Roshenow, W. M., "Heat Transfer and Temperature Distribution in Laminar Film Condensation," Trans. ASME 78 (1956), pp. 1645-1648.

3. Sparrow, E. M., and Gregg, J. L., "A Boundary Layer Treatment of Laminar Film Condensation," Trans. ASME Series C, J. Heat Transfer 81 (1959), pp. 13-18.

4. Koh, J.C.Y., "An Integral Treatment of Two-Phase Boundary Layer in Film Condensation," Trans. ASME 83 Series C, J. Heat Transfer (1961), pp. 359-362.

5. Koh, J.C.Y., Sparrow, E. M., and Hartnett, J. P., "The Two-Phase Boundary Layer In Film Condensation," International J. of Heat and Mass Transfer 2 (1961), pp. 69-82.

6. Bromley, L. A., "Heat Transfer In Stable Film Boiling," Chem. Eng. Progr. 46 (1950), p. 221.

7. Bromley, L. A., "Effect of Heat Capacity of Condensate," Ind. Eng. Chem. 44 (1952), pp. 2966-2968.

8. McFadden, P. W., and Grosh, R. J., "High Heat Flux Heat Transfer Studies—An Analytical Investigation of Laminar Film Boiling," AEC Res. and Dev. Rep. ANL-6060, 1959.

9. Koh, J.C.Y., "Analysis of Film Boiling on Vertical Surfaces," Trans. ASME 84 Series C., J. Heat Transfer (1962), pp. 55-62.

10. Cess, R. D., "Analysis of Laminar Film Boiling From a Vertical Plate," Research Report 405 FF 340-R2-X, Westinghouse Research Lab. (1959).

11. Sparrow, E. M., and Cess, R. D., "The Effect of Subcooled Liquid on Laminar Film Boiling," Trans. ASME 84 Series C, J. Heat Transfer (1962), pp. 149-156.

12. Nishikawa, K., and Ito, T., "Two-Phase Boundary Layer Treatment of Free Convective Film Boiling," International J. Heat and Mass Transfer 9 (1966), pp. 103-115.

13. Frederking, T.H.K., "Laminar Two-Phase Boundary Layers in Natural Convection Film Boiling," ZAMP 14 (1963), pp. 207-218.

14. Frederking, T.H.K., and Hopenfield, J., "Laminar Two-Phase Boundary Layers In Natural Convection Film Boiling of Subcooled Liquids," ZAMP 15 (1964), pp. 388-399.

15. McFadden, P. W., and Grosh, R. J., "An Analysis of Laminar Film Boiling with Variable Properties," Int. J. Heat and Mass Transfer 1 (1961), pp. 325-335.

16. Tachinaba, F., and Fukaui, S., "Heat Transfer In Film Boiling to Subcooled Liquids," Int. Dev. in Heat Transfer—Proc. Int. Heat Transfer Conf. Boulder, Col., 1961, Part II.

17. Lubin, B. T., "Analytical Derivation for Total Heat Transfer Coefficient in Stable Film Boiling From Vertical Plate," Trans. ASME, Series C, J. Heat Transfer (1969), pp. 452-453.

18. Merte, H., Jr., and Clark, J. A., "Boiling Heat Transfer with Cryogenic Fluids at Standard, Fractional and Near Zero Gravity," ASME Paper #63-HT-28.

19. Rhea, L. G., and Nevins, R. G., "Film Boiling Heat Transfer From an Oscillating Sphere," Trans. ASME, Series C, J. Heat Transfer (1969), pp. 267-272.

20. Hendricks, Robert C., and Baumeister, K. J., "Film Boiling From Submerged Spheres," NASA TN-D5124.

21. Chang, Y. P., "A Theoretical Analysis of Heat Transfer In Natural Convection In Film Boiling," Trans. ASME 79 (1957), pp. 1501-1510.

22. Chang, Y. P., "Wave Theory of Heat Transfer in Film Boiling," Trans. ASME 81 (1959), pp. 1-12.

23. Berenson, P. J., "Film Boiling Heat Transfer From a Horizeontal Surface," Trans. ASME 83 (1961), pp. 351-358.

24. Breem, B. P., and Westwater, J. W., "Effect of Diameter of Horizontal Tubes on Film Boiling Heat Transfer," Chem. Eng. Progr. 58 #7 (1962), pp. 67-72.

25. Hosler, E. R., and Westwater, J. W., "Film Boiling on a Horizontal Plate," ARS J., April 1962, pp. 553-558.

26. Pomerantz, M. L., "Film Boiling on a Horizontal Tube in Increased Gravity Fields," J. Heat Transfer 86 (1964), pp. 213-219.

27. Baumeister, K. J., and Hamill, Thomas D., "Laminar Flow Analysis of Film Boiling From a Horizontal Wire," NASA TN-D-4035.

28. Cess, R. D., and Sparrow, E. M., "Film Boiling in a Forced Convection Boundary Layer Flow," ASME Paper #60-WA-148.

29. Kays, W. M., Convective Heat and Mass Transfer, McGraw-Hill Book Co., (1966).

30. Laverty, W. F., and Rohsenow, W. M., "Film Boiling of Saturated Nitrogen Flowing In a Vertical Tube," ASME Paper 65-WA/HT-26.

31. Chi, J.W.H., "Slug Flow and Film Boiling of Hydrogen," ASME Paper 65-WA/HT-32.

32. Frederking, T.H.K., Wu, Y. C., and Clement, B. W., "Effects of Interfacial Instability on Film Boiling of Saturated Liquid Helium 1 Above a Horizontal Surface," A.I.Ch.E., 1966, pp. 238-244.

33. Sparrow, E. M., "The Effect of Radiation On Film Boiling Heat Transfer," Int. J. Heat and Mass Transfer 7 64 (19__), pp. 229-238.

34. Yeh, H. C. and Yang, W. J., "Radiation Effects On Film Boiling in Natural and Forced Convection Boundary Layer Flow," ASME Paper 66-WA/HT-6.

35. Frederking, T.H.K., "Stability of Film Boiling Two-Phase Flow in Cryogenic Systems," Report NSG-237-62, Dept. of Engineering, U.C.L.A., California.

36. Rohsenow, W. M., Webber, J. H., and Ling, A. T., "Effect of Vapor Velocity On Laminar and Turbulent Film Condensation," Trans. ASME 18 (1956), pp. 1637-1643.

37. McAdams, W. H., Heat Transmission, McGraw-Hill Book Co., 3rd edition.

38. Lee, John, "Turbulent Film Condensation," A.I.Ch.E.J. 10 (1964), pp. 540-544.

39. Hsu, Y. Y., and Westwater, J. W., "Film Boiling From a Vertical Surface," A.I.Ch.E.J. 4 (1958), pp. 58-62.

40. McFadden, P. W., and Grosh, R. J., "An Analysis of Laminar Film Boiling With Variable Properties," Int. J. of Heat and Mass Transfer Vol. 1, 1961, pp. 325-335.

41. Borishanskry, V. M., and Fokin, B. S., "Correlation of Heat Transfer Data On Stable Film Boiling On Vertical Surfaces Under Free Convection in a Large Volume," J. Engineering Physics 8 (1965), pp. 197-199.

42. Bradfield, W. S., Barkdoll, R. O., and Byrme, J. T., "Film Boiling On Hydrodynamic Bodies," Convair Scientific Research Lab. Research Note #37.

43. Arpaci, Vedat S., Conduction Heat Transfer, Addison-Wesley Publishing Co. (1966).

44. Spalding, D. B., "Heat Transfer To a Turbulent Stream From a Surface With a Stepwise Discontinuity In Wall Temperature," Int. Dev. In Heat Transfer, Int. Heat Transfer Conference, Boulder, Col., Part III (ASME).

45. Marxman, G. A., and Gilbert M., "Turbulent Boundary Layer Combustion In the Hybrid Rocket," Ninth Symp. (Int.) On Combustion, p. 371, Academic Press, 1963.

46. Marxman, Gerald A., "Combustion In the Turbulent Boundary Layer On a Vaporizing Surface," Tenth Symp.(Int.) On Combustion, Pittsburgh.

47. Woolridge, C. E., and Muzzy, R. J., "Measurements In a Turbulent Boundary Layer with Porous Wall Injection and Combustion," Tenth Symp. (Int.) On Combustion, pp. 1351-1362.

48. Schilichting, H., Boundary Layer Theory, McGraw-Hill Book Co., (4th edition).

49. Lees, L., "Combustion and Propulsion," Third AGARD Colloquium, Pergamon (1958), p. 451.

50. Coury, G. E., and Dukler, A. E., "Turbulent Film Boiling On Vertical Surface—A Study Including the Influence of Interfacial Waves," Int. Heat Transfer Conf., Paris, 1970.

51. Benjamin, T. B., "Wave Formation in Laminar Flow Down an Inclined Plane," JFM 2 (1957), pp. 554-574.

52. Chandrasekhar, S., "Hydrodynamic and Hydromagnetic Stability," Oxford, The International Series of Monographs in Physics.

53. Deissler, Robert G., "Analysis of Turbulent Heat Transfer, Mass Transfer and Friction in Smooth Tubes At High Prandtl and Schmidt Numbers," NACA Report #1210.

54. Lewis, Eugene W., "Boiling of Liquid Nitrogen In Reduced Gravity Fields With Subcooling," Ph.D. Thesis, University of Mich., 1967.

55. Sparks, Larry L., Powell, Robert L., and Hall, William J., "Cryogenic Thermocouple Tables," NBS Report No. 9712 (1968).

56. Dougall, R. P., and Rohsenow, W. H., "Film Boiling On the Inside of Vertical Tubes With Upward Flow of the Fluid At Low Qualities," Tech. Rep. #9079-26, Dept. of Mech. Eng. M.I.T., Cambridge, Mass.

57. Frederking, T.H.K., and Clark, J. A., "Natural Convection Film Boiling On a Sphere," Advances In Cryogenic Engineering 8 (1963), pp. 501-506.

58. Johnson, V. J. (General Editor), "A Compendium of the Properties of Materials At Low Temperatures (Phase I) Part II—Properties of Solids," NBS, 1960, WADD Tech. Report 60-56.

59. Martin, Douglas L., "The Specific Heat of Copper From 20° to 300°K," Canadian J. Physics 38 (1960), pp. 17-24.

60. Dockerty, S. M., "Specific Heat of Copper From 20°K to 200°K," Canadian J. Research 15A (1937), pp. 59-66.

61. Bloomer, O. T., and Rao, K. N., "Thermodynamic Properties of Nitrogen," Institute of Gas Technology Research Report 18.

62. Kline, S. J., and McClintock, F. A., "The Descriptions of Uncertainties in Single Sample Experiments," Mechanical Engineering 75 (1953).

63. Farukawa, G. T., et al., "Critical Analysis of the Heat Capacity Data of the Literature and Evaluation of Thermodynamic Properties of Copper, Silver, and Gold From 0°K to 300°K," NSRDS-NBS 18 (1968).

64. Clark, J. A., et al., "Study of Transient Heat Transfer," Prog. Report 40, Oct. 1968, The University of Michigan, Contract No. NAS 8-20228.

65. Dean, John W., "A Tabulation of the Thermodynamic Properties of Hydrogen from Low Temperature to 540°R from 10 to 1500 PSIA—Supplement A (British Units)," NBS Technical Notes 120 A.